

THE HYDROGENOLYSIS OF SIMPLE ALKANES  
OVER SUPPORTED PLATINUM AND NICKEL CATALYSTS

By

GORDON JAMES KELLY

A THESIS SUBMITTED FOR THE DEGREE OF  
DOCTOR OF PHILOSOPHY  
OF THE UNIVERSITY OF GLASGOW

DEPARTMENT OF CHEMISTRY, NOVEMBER 1992

ProQuest Number: 13818573

All rights reserved

INFORMATION TO ALL USERS

The quality of this reproduction is dependent upon the quality of the copy submitted.

In the unlikely event that the author did not send a complete manuscript and there are missing pages, these will be noted. Also, if material had to be removed, a note will indicate the deletion.



ProQuest 13818573

Published by ProQuest LLC (2018). Copyright of the Dissertation is held by the Author.

All rights reserved.

This work is protected against unauthorized copying under Title 17, United States Code  
Microform Edition © ProQuest LLC.

ProQuest LLC.  
789 East Eisenhower Parkway  
P.O. Box 1346  
Ann Arbor, MI 48106 – 1346

Thesis  
9378  
copy 1

GLASGOW  
UNIVERSITY  
LIBRARY

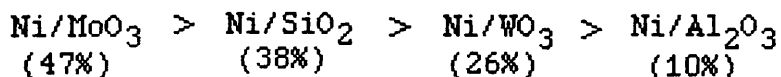
## SUMMARY

A series of supported platinum and nickel catalysts were prepared and extensively characterised by the Glasgow-Hull-ICI group. The catalysts were prepared using impregnation, co-crystallisation and metal-vapour deposition methods using silica, alumina, tungstia and molybdena as supports.

The seven catalysts that were used in this study were prepared by the impregnation method. They were as follows.

Pt/Al <sub>2</sub> O <sub>3</sub>	Ni/Al <sub>2</sub> O <sub>3</sub>
Pt/SiO <sub>2</sub>	Ni/SiO <sub>2</sub>
Pt/MoO <sub>3</sub>	Ni/MoO <sub>3</sub>
	Ni/WO <sub>3</sub>

To complete the characterisation of the nickel catalysts, carbon monoxide chemisorption and high resolution transmission electron microscopy (HRTEM) experiments were carried out. From the carbon monoxide chemisorption experiments the nickel catalyst dispersions were found to lie in the order,



The HRTEM studies were unsuccessful in producing particle size distributions for the nickel catalysts due to the low loadings, fairly high dispersions and the difficulty of contrasting the nickel particles from the support.

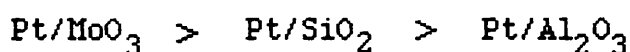
The hydrogenolysis of ethane, propane, n-butane and iso-butane was carried out over the series of catalysts. The following apparent activation energies were observed.

Catalyst	Ea (kJ mol <sup>-1</sup> )			
	C <sub>2</sub> H <sub>6</sub>	C <sub>3</sub> H <sub>8</sub>	n-C <sub>4</sub> H <sub>10</sub>	iso-C <sub>4</sub> H <sub>10</sub>
Pt/Al <sub>2</sub> O <sub>3</sub>	219	147	130	92
Pt/SiO <sub>2</sub>	203	157	96	125
Pt/MoO <sub>3</sub>	253	310	53	136
-----				
Ni/Al <sub>2</sub> O <sub>3</sub>	185	171	154	152
Ni/SiO <sub>2</sub>	237	243	234	183
Ni/MoO <sub>3</sub>	199	257	271	228
Ni/WO <sub>3</sub>	175	218	-	-

The metal function of the catalysts was the determining factor for the selectivity of the hydrogenolysis reactions; the platinum catalysts showed a high selectivity towards single hydrogenolysis whereas the nickel catalysts strongly favoured multiple hydrogenolysis.

The isomerisation reactions of n-butane and iso-butane over the nickel and platinum catalysts were strongly influenced by the metal and the support. The isomerisation selectivities for the reactions of both n-butane and iso-butane over the platinum catalysts were

found to lie in the order,



For the nickel catalysts the isomerisation selectivities were found to lie in the order,



The multiple hydrogenolysis activities of the platinum catalysts followed the same order as the isomerisation selectivities, suggesting a relation between isomerisation and multiple hydrogenolysis.

The activation energies for the isomerisation reactions of n-butane and iso-butane over the platinum and nickel catalysts were as follows.

Catalyst	Ea (kJ mol <sup>-1</sup> )	
	n-C <sub>4</sub> H <sub>10</sub>	iso-C <sub>4</sub> H <sub>10</sub>
Pt/Al <sub>2</sub> O <sub>3</sub>	161	116
Pt/SiO <sub>2</sub>	102	148
Pt/MoO <sub>3</sub>	274	176
Ni/MoO <sub>3</sub>	252	274

The high activation energies for the isomerisation reactions of n-butane and iso-butane over the Ni/MoO<sub>3</sub> catalyst and n-butane over the Pt/MoO<sub>3</sub> catalyst are consistent with reactions taking place directly on the support. The similarity between the

hydrogenolysis and isomerisation activation energies for the reactions of n-butane and iso-butane over the Pt/Al<sub>2</sub>O<sub>3</sub> and Pt/SiO<sub>2</sub> catalysts and iso-butane over the Pt/MoO<sub>3</sub> catalyst suggests that these isomerisation reactions are metal-only catalysed rearrangements.

The hydrogen pressure rate coefficients (m) were calculated for the reactions of ethane, ethene, propane and propene over the Pt/Al<sub>2</sub>O<sub>3</sub> and Ni/Al<sub>2</sub>O<sub>3</sub> catalysts, as follows.

Feed Gas	Pt/Al <sub>2</sub> O <sub>3</sub> m values	Ni/Al <sub>2</sub> O <sub>3</sub> m values
C <sub>2</sub> H <sub>6</sub>	-0.71	-0.82
C <sub>2</sub> H <sub>4</sub>	-0.68	-1.59
C <sub>3</sub> H <sub>8</sub>	-0.79	-0.88
C <sub>3</sub> H <sub>6</sub>	+1.58	-1.09

The positive order with respect to hydrogen pressure for the reaction of propene over the Pt/Al<sub>2</sub>O<sub>3</sub> catalyst was accompanied by an increase of multiple hydrogenolysis with increasing hydrogen pressure. This suggests a different reaction mechanism for alkene hydrogenolysis over platinum catalysts than that operative in the hydrogenolysis of alkanes.

The hydrogenolysis of ethane, propane, n-butane and iso-butane was carried out over the MoO<sub>3</sub> support. The MoO<sub>3</sub> was shown to readily isomerise n-butane to iso-butane but not iso-butane to n-butane.

### Acknowledgements

I should like to thank my supervisor, Professor G. Webb, for his advice during the preparation of this thesis. I should like to express my thanks to the technical staff in the Chemistry Department, particularly Rose Millar for the great help she gave me during the latter stages of my practical work.

I would like to thank my friends and colleagues, both past and present, for their help, advice and encouragement.

I would also like to thank Catherine Edgar for her patience in deciphering my handwriting and typing this thesis, and all the Edgar family, for the use of their computer and the many lunches supplied.

Finally, I would like to give a big thank you to my parents, Nan and Dougie, for supporting me through my many years at university.

## TABLE OF CONTENTS

	Page	
<u>CHAPTER ONE: INTRODUCTION</u>		
1.1	Catalysis	1
1.2	Hydrogenolysis	4
1.3	Reforming	5
1.4	Mechanism of Hydrogenolysis	7
1.5	Influence of Metal on Hydrogenolysis	20
1.6	Influence of Support on Hydrogenolysis - Bifunctional Catalysts	24
1.7	Metal Catalysed Rearrangements	29
1.8	Structure Sensitivity	43
1.9	Chemisorption Complexes of Hydrocarbons	50
1.10	Support Materials	59
1.11	Alumina	62
1.12	Silica	67
1.13	Molybdenum Trioxide and Tungsten Trioxide	72
1.14	Hydrogen Spillover	74
1.15	Hydrogen Metal Bronzes	82
 <u>CHAPTER TWO: OBJECTIVES OF THE PRESENT STUDY</u>		
2	Objectives of the Present Study	88
 <u>CHAPTER THREE: EXPERIMENTAL</u>		
3.1	Introduction	90
3.2	Catalyst Preparation	91
3.2.1	Materials	91
3.2.2	Preparation	91

3.3	Catalyst Characterisation	92
3.3.1	Gas Chemisorption Apparatus	92
3.3.2	Standard Reduction	98
3.3.3	Carbon Monoxide Chemisorption Procedure	98
3.3.4	Transmission Electron Microscopy	99
3.4	Microreactor System	100
3.4.1	Gas Supply	100
3.4.2	Microreactor	100
3.4.3	Mass Flow Control	106
3.4.4	Reactor Tube	110
3.4.5	Diffusion Limitation	111
3.4.6	Microreactor Experimental Procedures	114
3.4.7	Microreactor Analytical System	116

#### CHAPTER FOUR: TREATMENT OF RESULTS

4.1	Carbon Monoxide Chemisorption Experiments	119
4.1.1	Molecules of CO Chemisorbed on Catalyst	119
4.1.2	Dispersion	120
4.1.3	Mean Surface Average Diameter	121
4.1.4	Metal Surface Area	123
4.2	Transmission Electron Microscopy	124
4.3	Hydrogenolysis Reaction	125
4.3.1	Number of Moles	125
4.3.2	Moles Converted	125
4.3.3	Fractional Conversion	126
4.3.4	Selectivity	128
4.3.5	Reaction Rate and Turnover	129
4.3.6	Activation Energies	129

4.3.7	Rate Law	130
4.3.8	Kempling-Anderson Reaction Network	131

#### CHAPTER FIVE: RESULTS

5.1	Summary of Results from Glasgow-Hull-ICI Group	135
5.1.1	Characterisation of Support Materials	135
5.1.2	Microanalytical Data	136
5.1.3	Temperature Programmed Reduction	137
5.1.4	Hydrogen Bronze Formation	137
5.1.5	Gas Chemisorption Studies	138
5.1.6	Pt catalysts - Particle Size Distributions	139
5.2	Characterisation of Nickel Catalysts	140
5.2.1	Carbon Monoxide Chemisorption	140
5.2.2	Transmission Microscopy	142
5.3	Hydrogenolysis Reactions	143
5.3.1	Ethane Hydrogenolysis	143
5.3.2	Propane Hydrogenolysis	150
5.3.3	n-Butane Hydrogenolysis	157
5.3.4	iso-Butane Hydrogenolysis	175
5.4	Hydrogen Pressure Rate Coefficient	191
5.5	Reactions on the MoO <sub>3</sub> Support	200

#### CHAPTER SIX: DISCUSSION

6.1	Glasgow-Hull-ICI Characterisations	203
6.2	Nickel Catalyst Characterisations	205
6.3	Hydrogenolysis Reactions	205
6.4	Ethane Hydrogenolysis	206

6.5	Propane Hydrogenolysis	208
6.6	n-Butane Hydrogenolysis	213
6.7	iso-Butane Hydrogenolysis	220
6.8	Hydrogen Pressure Effect	225
6.9	Conclusions	229
	References	234

## CHAPTER ONE

## CHAPTER 1

### INTRODUCTION

#### 1.1 CATALYSIS

The earliest purely chemical description of a catalytic process was given by Charles Bernard Désormes and Nicolas Clément in 1806 (1). They suggested a theory for the formation of sulphuric acid in the lead chamber process (2). Later, in 1822, Döberiner discovered that oxygen and hydrogen combined in the presence of finely divided platinum (3).

From these and similar disparate observations on chemical transformations the term catalysis (from the Greek for decomposition) was coined by Berzelius in 1835. At about the same time Mitscherlich introduced perhaps the more appropriate term, contact action, for a similar group of phenomena. It was not until 1894, however, that Ostwald gave us the modern concept of catalysis as a method of controlling the rate and direction of a chemical reaction (4).

The best definition of a catalyst is, "a catalyst is a substance which increases the rate of

attainment of equilibrium of a reacting system without causing any great alteration to the free energy changes involved" (5).

Catalysis is a purely kinetic process in which the rates of both forward and backward reactions are equally affected. A catalyst, therefore, can only alter the rate of a chemical reaction which is thermodynamically feasible, that is, a reaction which involves a decrease in free energy. It is incorrect to say that the catalyst should remain unchanged at the end of the reaction as in practice catalysts are sintered, eroded, etched or covered with residues left behind by the reacting molecules. The rate enhancement by catalysis is realised by a lowering of the activation energy of the reaction, achieved through the transitory adsorption (almost always chemisorption) of one or more reactants onto the surface of the catalyst.

The catalytic effect is "classically" described in many texts by three theories, geometric, electronic or the chemical approach. The geometric theory emphasises the importance between the geometrical configuration of the active atom at the surface of the catalyst and the arrangement of atoms in the portion of the reacting molecule that adsorbs on the catalyst. The electronic theories proceed from the fact that the chemisorption involves the distortion or displacement of

electron clouds and they attempt to relate activity to the electronic properties of the catalyst. These two theories reflect a primarily physical approach in that the catalyst is regarded as essentially a static material. The chemical approach, on the other hand, regards the catalyst as a chemical intermediate that forms an unstable, surface, transitory complex with the reactants. This theory leads to the concept that the maximum rate is obtained when the bonds between the adsorbed complex and the catalyst are neither too strong nor too weak (Sabatier effect (6)).

Metals are good catalysts for reactions involving the addition or subtraction of hydrogen, for example, hydrogenation, dehydrogenation and hydrogenolysis. Metals are used in catalysts in a variety of physical forms, wires, gauzes, finely divided metal powders or most commonly when supported on a carrier.

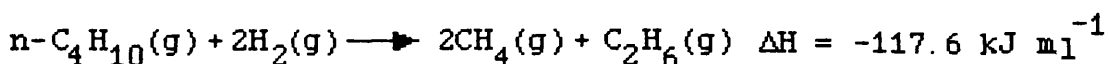
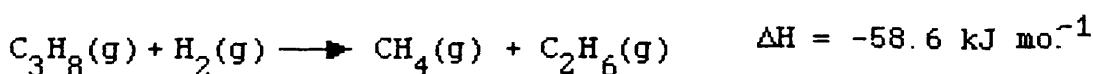
A supported metal carrier usually contains more than 80% w/w carrier. The purpose of the carrier is to act as a means of increasing the dispersion of the supported metal, giving the resulting catalyst physical and mechanical properties superior to those of the unsupported metal (7). The use of a carrier, or support, also gives added stability by allowing small crystallites to be sufficiently separated to prevent

sintering and gives greater resistance to poisoning.

## 1.2 HYDROGENOLYSIS

The hydrogenolysis reaction of simple alkanes over metal catalysts has been known for many years (8-13) and has been incorporated into many reviews of hydrocarbon reactions (14-18). Hydrogenolysis can be defined as, "the breakage of carbon-carbon bonds with the uptake of hydrogen". As each hydrogenolysis reaction involves the rupture of one carbon-carbon bond and the formation of two carbon-hydrogen bonds they are always exothermic.

e.g.



Although greatly studied the hydrogenolysis of alkanes is still of great interest for many reasons. These include the uncertainty over its mechanism, the roles of the support and metallic functions and its structure sensitivity as defined by Boudart (19). These topics are covered more fully in the appropriate sections.

Industrially an understanding of the hydrogenolysis reaction is important as it occurs as an unwanted side reaction in the reforming of naphthas (Section 1.3). As the mechanism for hydrogenolysis reactions involves the formation of hydrogen deficient intermediates (20) the hydrogenolysis reaction is also associated with the coking and lifetimes of reforming catalysts.

Simple alkanes such as ethane, propane, iso-butane and n-butane can be used as "archetype" molecules for studying hydrogenolysis reactions as they allow the comparison between possible 1,2, 1,3 and 1,4 adsorptions of hydrocarbons on the catalyst surface (14). Iso-butane and n-butane are also useful molecules for studying bond shift isomerisation reactions (section 1.7).

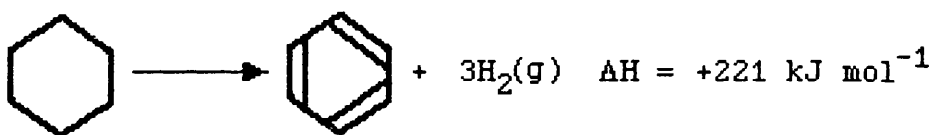
### 1.3 REFORMING

Reforming using a molybdena/alumina catalyst to increase the octane rating of naphthas was introduced in the United States and Germany prior to World War II. In the early 1950's this was superseded by a catalytic reforming process using a supported platinum/alumina catalyst (21).

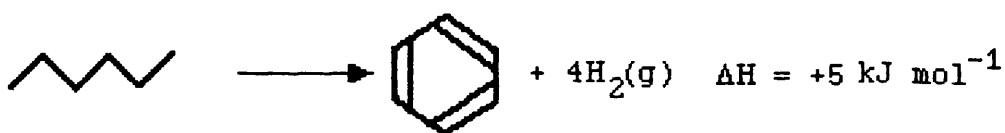
More recent reforming catalysts incorporate a second metal into the system such as rhenium, iridium or

tin to act as a promoter to improve the stability and lifetime of the catalyst. This promotion by rhenium has been variously explained by ensemble effects (22), the sulphidation of rhenium from sulphur containing compounds in the feed (23) and the prevention of the formation of graphitic species on the catalyst surface (24).

The reforming of naphthas increases the octane rating mainly by the dehydrogenation of naphthenes to aromatics,



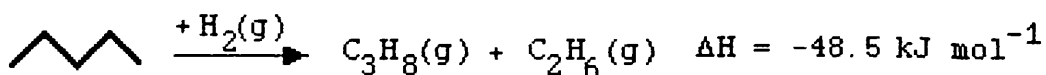
and by the dehydrocyclisation of paraffins.



Under reforming conditions (700-800K, 10-33 atm.) several other catalytic reactions can take place. These include the isomerisation of n-alkanes to branched alkanes,



and the hydrogenolysis of alkanes.

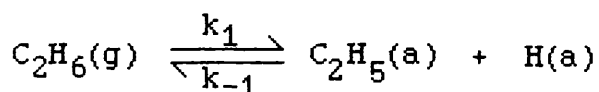


In the reforming of light hydrocarbons (in the range C<sub>5</sub>-C<sub>11</sub>) hydrogenolysis has to be minimised to achieve a better selectivity of production of aromatics. In practice this is achieved by carrying out the reaction in a large excess of hydrogen as it has been shown that the rate of alkane hydrogenolysis has a strong inverse dependence of hydrogen pressure (20).

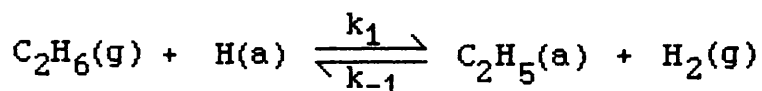
#### 1.4 MECHANISM OF HYDROGENOLYSIS

In discussing the mechanism of hydrogenolysis of saturated hydrocarbons it is logical to begin by considering the mode of chemisorption of the hydrocarbon reactant. This mode of chemisorption is simplified greatly by the absence of any functional groups on saturated alkanes.

The chemisorption of alkanes on metals is accompanied by the evolution of hydrogen (25) and hydrogen-deuterium exchange (26-29) can be carried out at temperatures that are much lower than those for hydrogenolysis. The carbon-hydrogen bonds of the alkanes are therefore activated much more easily than the carbon-carbon bonds. Dissociative chemisorption at a site where C-H bond scission occurs is therefore the initial step in hydrogenolysis. For ethane this can be represented as

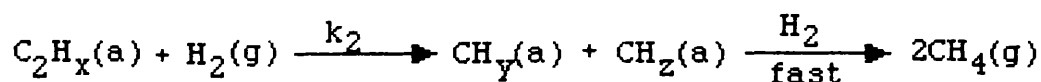
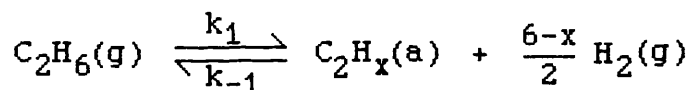


or following the proposals by Frennet and Lienard (30-32) as



The next steps in the reaction sequence are not so straightforward and rely heavily on kinetic interpretations of the reaction. The most important kinetic features for alkane hydrogenolysis were first identified by Cimino et al. (20), particularly the strong inverse dependence of hydrogen pressure on the reaction rates for ethane and propane over iron, nickel and cobalt catalysts. This led to a proposed mechanism for ethane hydrogenolysis as follows.

Scheme 1



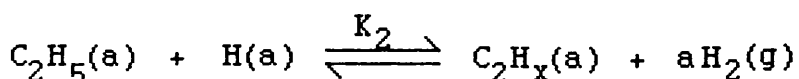
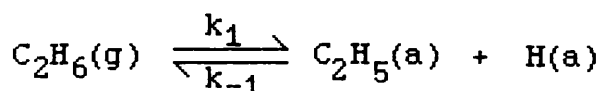
The cleavage of the carbon-carbon bond in the dehydrogenated intermediate  $\text{C}_2\text{H}_x(\text{a})$  was taken as the rate determining step. The  $\text{CH}_y(\text{a})$  and  $\text{CH}_z(\text{a})$  fragments were rapidly removed to the gas phase as methane. From a classical Langmuir kinetic treatment this gave the following rate equation.

$$\text{rate} = k' P_{\text{C}_2\text{H}_6}^n P_{\text{H}_2} \left( 1 - n \frac{6-x}{2} \right)$$

where  $P_{\text{C}_2\text{H}_6}$  and  $P_{\text{H}_2}$  were the partial pressures of ethane and hydrogen respectively and  $k'$  a rate constant.

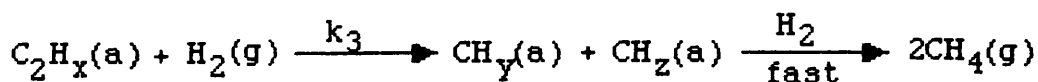
From a study of ethane hydrogenolysis over the supported group VIII metals Sinfelt found (14,33) that the reaction order with respect to the hydrocarbon was always positive and in the range 0 - 1, while the order with respect to hydrogen varied from slightly positive for Fe and Re to about -1 for Co, Ru and Os and about -1 to -2 for Ni, Rh, Pd and Pt (see table 1). From this study Sinfelt extended Cimino's mechanism to the following sequence of reaction steps.

SCHEME 2



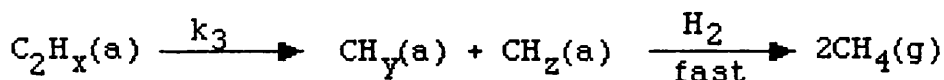
and a choice of third steps. Either a reaction of the  $\text{C}_2\text{H}_x(\text{a})$  intermediate with molecular hydrogen in accord with Cimino

SCHEME 2(a)



or a unimolecular carbon-carbon bond rupture.

SCHEME 2(b)



Provided that the coverage of adsorbed species was low and that equilibrium was effectively maintained between  $\text{C}_2\text{H}_5(\text{a})$ ,  $\text{C}_2\text{H}_x(\text{a})$  and  $\text{H}_2$  in the gas phase, Sinfelt's kinetic analysis led to the following rate expressions.

For scheme 2(a)  $\text{rate} = \frac{k_1 P_{\text{C}_2\text{H}_6}}{1 + b P_{\text{H}_2}^{a-1}}$

and for scheme 2(b)  $\text{rate} = \frac{k_1 P_{\text{C}_2\text{H}_6}}{1 + b P_{\text{H}_2}^a}$

where  $b = \frac{k_{-1}}{k_3 K_2}$  and  $a = \frac{6-x}{2}$

When these equations were compared with the data on ethane hydrogenolysis on the group VIII metals Scheme 2(a) led to values of x in the dehydrogenated species  $\text{C}_2\text{H}_x(\text{a})$  for most of the metals, of equal to zero, that is, surface intermediate species totally

devoid of hydrogen (34). As this seemed rather severe Scheme 2(b) was favoured and produced the following values for x and a.

Table 1 Hydrogenolysis of ethane over group VIII metals

Catalyst	x	a	exponent on H <sub>2</sub> pressure
Fe	-	-	+0.5
Co	4	1	-0.8
Ni	2	2	-2.4
Ru	2	2	-1.3
Rh	0	3	-2.2
Pd	0	3	-2.5
Re	-	-	+0.3
Os	2	2	-1.2
Ir	2	2	-1.6
Pt	0	3	-2.5

Again this mechanism suggested very highly dehydrogenated species with x values in C<sub>2</sub>H<sub>x</sub>(a) as low as zero for Rh, Pd and Pt. Sinfelt explained the positive orders of the reaction with respect to hydrogen with Fe and Re as due to the rate determining step being the rehydrogenation of the chemisorbed species.

Neither this model by Sinfelt nor the original model of Cimino, however, takes into account the competition between H<sub>2</sub> and C<sub>2</sub>H<sub>6</sub> adsorptions in contradiction with observed data (35).

For instance, the work on the hydrogenolysis of ethane, propane and iso-butane over a Pt/Al<sub>2</sub>O<sub>3</sub> catalyst by Leclercq et al. (36) showed that the exponent of hydrogen pressure was positive at low hydrogen pressures (<0.5 atm.) and rose to a maximum before becoming increasingly negative at higher hydrogen pressures. This agreed with earlier work carried out on butanes and pentanes over platinum films (37) and platinum black (38).

As the exponent of the hydrogen pressure changes with pressure a simple power rate law cannot be used to describe the hydrogenolysis reaction and the kinetic data can only have a limited use in its prediction of the dehydrogenated state C<sub>2</sub>H<sub>x</sub>(a) using the simple models of Cimino and Sinfelt.

It is clear, however, that the negative reaction order, at high hydrogen pressures, arises naturally if the carbon-carbon bond breakage is preceded by a dehydrogenative chemisorption step leading to a highly unsaturated intermediate. Multiple carbon-carbon bond formation in the dehydrogenated species is unlikely as it is this carbon-carbon bond that is broken during hydrogenolysis. The unsaturated intermediates formed therefore possess high metal-organic bond multiplicities, indicative of carbene and carbyne type

chemistry (see section 1.9).

The basic mechanism for ethane hydrogenolysis at high hydrogen pressures, as originally proposed by Cimino, still then holds as follows.

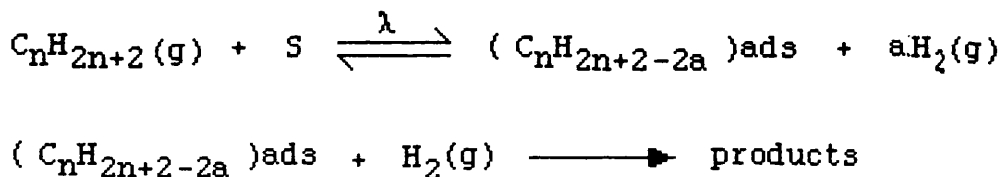
- (i) Dissociative chemisorption of ethane.
- (ii) Formation of a dehydrogenated intermediate  $C_2H_x(a)$ .
- (iii) Fragmentation and desorption of methane.

Other evidence for this type of mechanism comes from data on apparent activation energies for hydrogenolysis. As all the dehydrogenation steps are endothermic one expects the apparent activation energy to be higher the more numerous the dehydrogenation steps that are involved. Consequently the more negative the order versus hydrogen, the higher the apparent activation energy should be. Such a correlation between orders and apparent activation energies have been found for the isomerisation and hydrogenolysis of  $C_5$ -hydrocarbons on  $Pt/Al_2O_3$  catalysts (39,40) and for ethane hydrogenolysis on various metals (41).

To explain the change in order with changing hydrogen pressure and extending the ethane mechanism of Cimino and Sinfelt to higher alkanes, Leclercq and his

co-workers proposed the following mechanism (36,42).

SCHEME 3



They supposed that the rate determining step involved molecular hydrogen and they replaced all the equilibrated dehydrogenated steps with an overall equilibrium, with an equilibrium constant  $\lambda$ .

Assuming that the reactive species  $C_n H_{2n+2-2a}$  was by far the most abundant radical, a rate equation which accounted satisfactorily for the results was derived.

$$\text{rate} = \frac{K \lambda P_{HC} P_{H_2}}{P_{H_2}^a + \lambda P_{HC}}$$

Where  $P_{HC}$  is the partial pressure of the hydrocarbon.

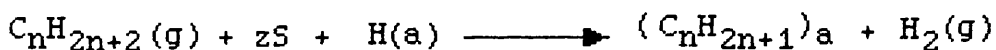
This mechanism was also used very effectively to correlate increasing reaction rates with increasing hydrocarbon equilibrium constants (42).

One limitation of this model is that if the isomerisation of  $C_4$ 's and  $C_5$ 's proceed by a similar

mechanism to hydrogenolysis (see section 1.7), then the positive orders that are found for the isomerisation of C<sub>4</sub>'s and C<sub>5</sub>'s at low hydrogen pressures (37) would only be accounted for if hydrogen were involved in the rate determining step, which is unlikely.

Frennet and his co-workers (43) proposed that the hydrocarbon adsorption involved not a single site but an ensemble of several (z), contiguous sites (seven or eight) on the surface. This led to the following first step.

SCHEME 4



The adsorbed species (C<sub>n</sub>H<sub>2n+1</sub>)<sub>a</sub> then undergoes stepwise dehydrogenative adsorption, as in the previous schemes, before fragmentation. Assuming that both H<sub>2</sub> and the hydrocarbon are adsorbed on the same sites and there is competition for adsorption this leads to the following rate equation.

$$\text{rate} = k \prod_i K_i \frac{P_{HC} \theta_H^m}{P_{H_2}^n} \theta_S^z \quad (i)$$

where K<sub>i</sub> is the equilibrium constant for the ith

dehydrogenation step.

$m$  is the number of these steps

$k$  is the rate constant

$z$  is the number of atoms involved in the adsorption ensemble

$\theta_H$  is the surface hydrogen coverage

$\theta_S$  is the concentration of free sites

As  $\theta_H$  is mainly dependent upon the surface coverage in hydrocarbon radicals,  $\theta_C$ , it remains practically constant i.e.

$$\theta_H = \theta_H^0 (1 - \theta_C) \quad (ii)$$

$\theta_S$ , the concentration of free sites, is equal to

$$\theta_S = (1 - \theta_H^0)(1 - \theta_C) \quad (iii)$$

Combining equations (i), (ii) and (iii), the rate can be expressed by

$$\text{rate} = k \prod_i K_i \frac{P_{HC} (\theta_H^0)^m (1 - \theta_H^0)^z}{P_{H_2}^m} (1 - \theta_C)^{m+z}$$

This includes two terms  $f(\theta_H^0, P_{H_2})$  and  $g(\theta_C) = (1 - \theta_C)^{m+z}$  whose formal orders versus hydrogen are negative and positive respectively.

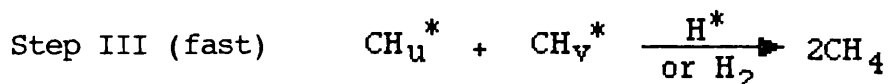
At high hydrogen pressures and low  $\theta_C$ ,  $(1 - \theta_H^0)^z$  is an inhibiting term that contributes to negative



number of hydrogen atoms remaining on the two-carbon surface compound.



Where B is either a free site (\*) adsorbed hydrogen (H\*) or gas phase molecular hydrogen (H<sub>2</sub>).



Assuming that the third step is fast and the coverage of CH<sub>u</sub>\* and CH<sub>v</sub>\* is negligible, so that steady state approximations can be applied, the rate of hydrogenolysis will be proportional to the concentration of the bond-splitting agent, B, and the coverage of the two-carbon surface compound.

$$\text{rate} = k[\text{B}][\text{C}_2\text{H}_m^*]$$

From this scheme Kristyán and Szamosi concluded that the bond-splitting agent was gaseous hydrogen (H<sub>2</sub>) and produced m values, for the number of hydrogens on C<sub>2</sub>H<sub>m</sub>\* , for Ni and Pd catalysts (45) as follows.

catalyst	Temp(K)	m
Ni	523	2.36 ± 0.1
Pd	623	3.33 ± 0.1

From the above treatments it ensues that no straightforward conclusion can be drawn from any kinetic study. The kinetic models suggest, however, a general mechanism for the hydrogenolysis of alkanes which is as follows.

- (i) dissociative chemisorption of the alkane and hydrogen on to suitable vacant sites of the catalyst surface.
- (ii) formation of a dehydrogenated intermediate  $C_xH_y(a)$  with a high degree of metal-organic bond multiplicity.
- (iii) fragmentation or skeletal rearrangement of this dehydrogenated species.
- (iv) rehydrogenation and desorption of the products, restoring vacant surface sites to complete the catalytic cycle.

In principle any of these four steps can be rate limiting. However, hydrogen adsorption at high temperatures is expected to be more rapid than any of the other steps. The rate of ethane adsorption has been assumed to be the rate limiting step by Martin (46) while studying the kinetics of ethane hydrogenolysis

over a nickel catalyst. The formation of a strongly adsorbed dehydrogenated intermediate, step(ii), has been suggested to be the rate determining step for the hydrogenolysis of n-butane over Pt/Al<sub>2</sub>O<sub>3</sub> (47) by Bond and Gelsthorpe. Steps (iii) and (iv), C-C bond rupture and hydrogenation of methyl fragments have also been reported as rate limiting steps (34,20,48).

In practice it can be shown that significant results can be drawn from hydrogenolysis reactions when the coverage of the alkanes does not interfere in the rate equation, that is, for which negative orders versus hydrogen have been found. In this case large differences in activation energies most probably mean different reaction mechanisms (16).

### 1.5 INFLUENCE OF METAL ON HYDROGENOLYSIS

The group VIII metals show a clear tendency for hydrogenolysis activity to decrease when proceeding from left to right across a period (14). Within the 4d series (Ru, Rh, Pd) maximum activity is found at Ru, for the 5d series (Os, Ir, Pt) at Os i.e. in the first subgroup of group VIII. From Ru to Pd and Os to Pt the activity decreases by 6-9 orders of magnitude. In the first transition series Co and Ni both exhibit comparably high activity (18). This pattern of reactivity does not depend appreciably on the alkane, the catalyst surface structure or catalyst type.

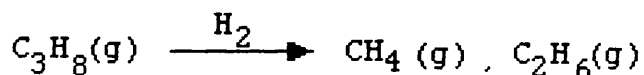
The apparent activation energies for hydrogenolysis reactions also show a tendency to increase in proceeding from right to left across a period. This is not surprising as the apparent activation energies contain heat of adsorption terms, and the heat of adsorption generally decreases in going from left to right across the periodic table (49). Unfortunately there is very little heat of adsorption data available for critical comparison with data on activation energies.

In his review (18) Sinfelt related the hydrogenolysis activity to the percentage d character of the metal, as defined by Pauling's Valence bond theory (50) of metals, representing the extent of participation of d orbitals in the bonding between atoms in a metal lattice.

Although there was a degree of correlation between hydrogenolysis and percentage d character with the second and third transition group VIII metals (Ru, Rh, Pd, Os, Ir, Pt) the metals of the first transition series (Fe, Co, Ni) showed higher hydrogenolysis activities than would have been expected from their percentage d character values. It was clear therefore that this parameter alone was not adequate for characterising the catalytic activity of the transition

metals for hydrogenolysis (34).

The metals also vary in their depth of hydrogenolysis, that is, in how many carbon-carbon bonds that are broken per visit of a reactant hydrocarbon to the catalyst surface. Single hydrogenolysis is defined as the breakage of a single carbon-carbon bond per visit to the catalyst surface. Multiple hydrogenolysis involves the breakage of more than one bond per visit. The depth of hydrogenolysis, or the extent of multiple hydrogenolysis can be followed from the product distributions (42). e.g. for the hydrogenolysis of propane



If the ratio of the products  $\frac{\text{CH}_4(\text{g})}{\text{C}_2\text{H}_6(\text{g})} > 1$  then

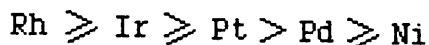
multiple hydrogenolysis is taking place.

The metals Pt and Pd have a high selectivity for single hydrogenolysis. On the other hand W, Ta, Fe and Co all have a high tendency for total degradation to methane. The metals Ir, Rh, Os, Re, Ru, and Ni all lie somewhere between these two extremes. When single hydrogenolysis takes place it is possible to express product distributions in terms of relative bond rupture

probabilities (18).

This depth of hydrogenolysis, however, has no relation to the selectivity of the reaction, that is, the tendency for particular bonds to be broken. Ni, Pd and Rh show high selectivity for terminal carbon-carbon bond splitting (demethylation). Other 4d and 5d Group VIII metals (particularly Pt and Ir) show less selective cracking leading to a largely statistical spectrum of primary products.

Under hydrogenolysis conditions isomerisation of alkanes can also take place. Most of the group VIII transition metals exhibit activity, in at least one alkane isomerisation reaction. The order of activities usually follows the sequence



with a  $10^2$  to  $10^4$  fold variation in rate between the least and most active metals (18). Among pure metals only Pt and to a lesser extent Pd, exhibit very high selectivities for isomerisation over hydrogenolysis, as shown by reactions on evaporated Pt (51) and Pd (52) films.

The hydrogenolysis activities of the group VIII metals can also be classified according to their

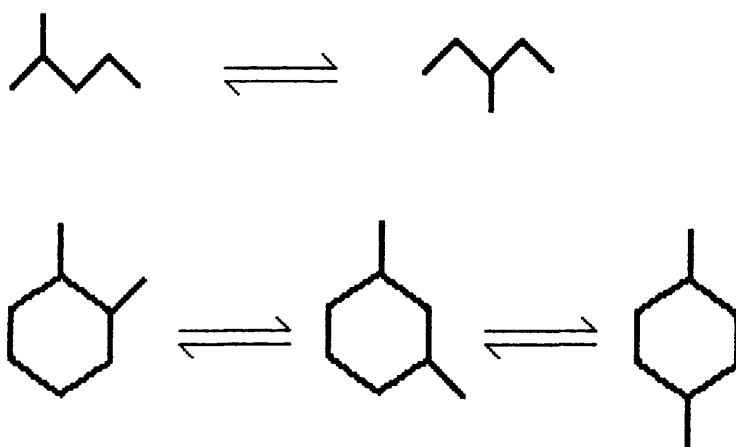
increasing capacities to form metallocarbenes, as suggested by the multiple exchange of methane for adsorbed methylene formation which follows the order (53),



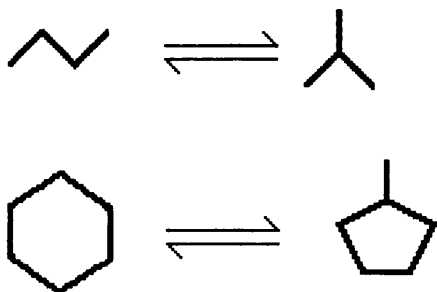
### 1.6 INFLUENCE OF SUPPORT ON HYDROGENOLYSIS - BIFUNCTIONAL CATALYSTS

It has long been established, from catalytic cracking reactions, that acidic catalysts (e.g.  $\text{AlCl}_3$ ,  $\text{H}_2\text{SO}_4$ ,  $\text{SiO}_2\text{-Al}_2\text{O}_3$ ) can be used to carry out isomerisation reactions. On these acidic catalysts the following reactions have been reported.

(a) Interconversions between isomers with at least one tertiary carbon (54,55,56).

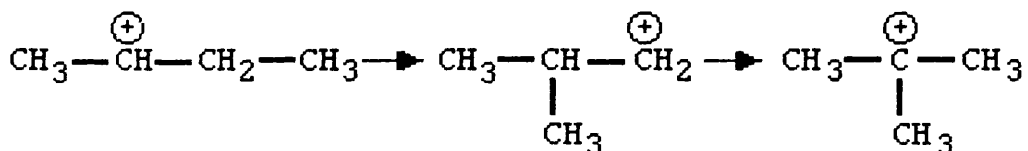


(b) Isomerisations of hydrocarbons without a tertiary carbon (57).



The reactions take place at temperatures below that required for the cracking of alkanes over these catalysts. The type (a) reactions take place more readily than the type (b) reactions.

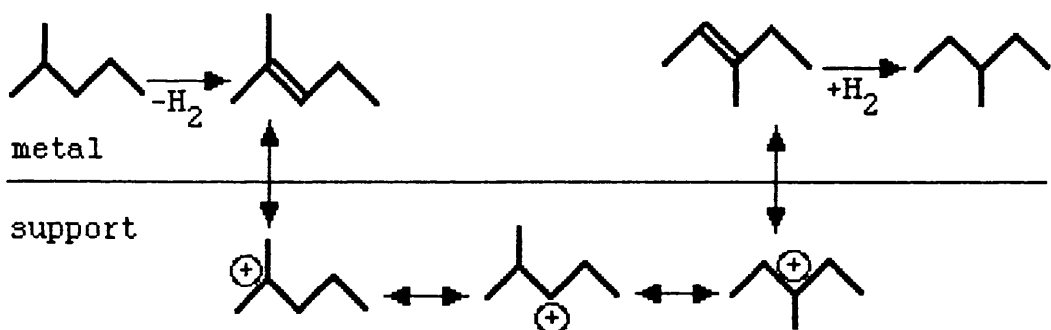
All these reactions have been interpreted according to mechanisms which include carbonium ions as reaction intermediates, for example for n-butane (58).



It was found that the addition of a transition metal to an acidic catalyst increased considerably the rate of isomerisation reactions. Among the different transition metals it was rapidly established that platinum was the most efficient co-catalyst. Platinum

supported on an acidic support, such as acidic alumina or silica-alumina, was therefore used as a basis for reforming catalysts (see section 1.3).

It is generally accepted that on reforming catalysts skeletal isomerisation occurs according to a bifunctional mechanism. On the metallic function (usually platinum), alkanes and cycloalkanes undergo dehydrogenation to alkenes plus hydrogen. The alkene then migrates, probably through the gas phase to an acidic site where it becomes a carbonium ion and undergoes either skeletal rearrangement or ring closure, or ring enlargement. It can then lose a proton, become an alkene again and migrate back to the metal where it can be rehydrogenated, for example for the isomerisation of 2-methyl pentane (59).

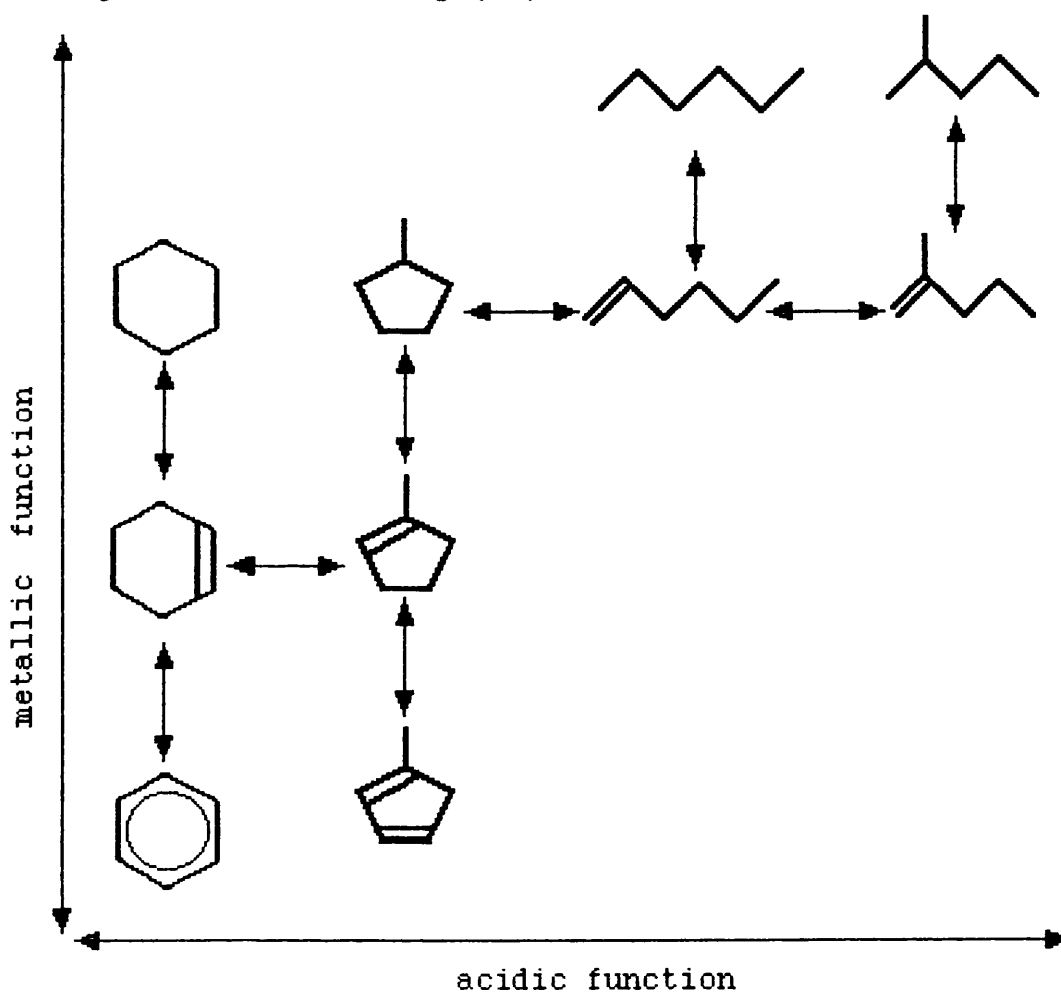


This concept of a dual function catalyst with two distinctly different kinds of sites was introduced by Mills et al. (60) through his work with catalysts containing only an acidic function, only a

dehydrogenation function, or both.

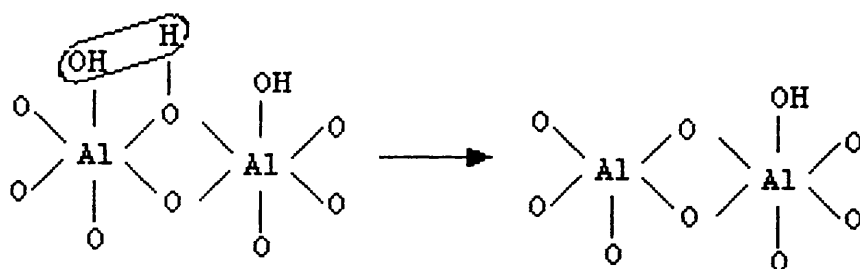
Later Wiesz (61) showed by studies with mechanical mixtures that the intermediates were true gas phase species that were transported by gaseous diffusion between the different sites.

The reaction pathway for n-hexane on a bifunctional reforming catalyst is shown below, with the reactions on the metal (involving hydrogen addition or subtraction) occurring vertically, while those on the acidic support (involving isomerisation or ring closure) being shown horizontally (62).



The nature of the acidic sites on alumina has been the subject of much discussion. The surface is characterised by the presence of hydroxyl groups which could conceivably be a source of Brönsted acidity.

However, it has been concluded that the hydroxyl sites do not contribute significantly as a source of protonic acid sites (63), on the basis that infrared spectra obtained after adsorption of ammonia or pyridine on the surface do not exhibit bands due to ammonium or pyridinium ions. However the surface of aluminas in a reforming catalyst usually contain chloride ions which can interact with the hydroxyl groups to enhance their acidity (64). Since the aluminas employed in reforming catalysts are normally heated to high temperatures (770-870K) in their preparation, there are Lewis acid sites present as a result of dehydroxylation reactions (65)



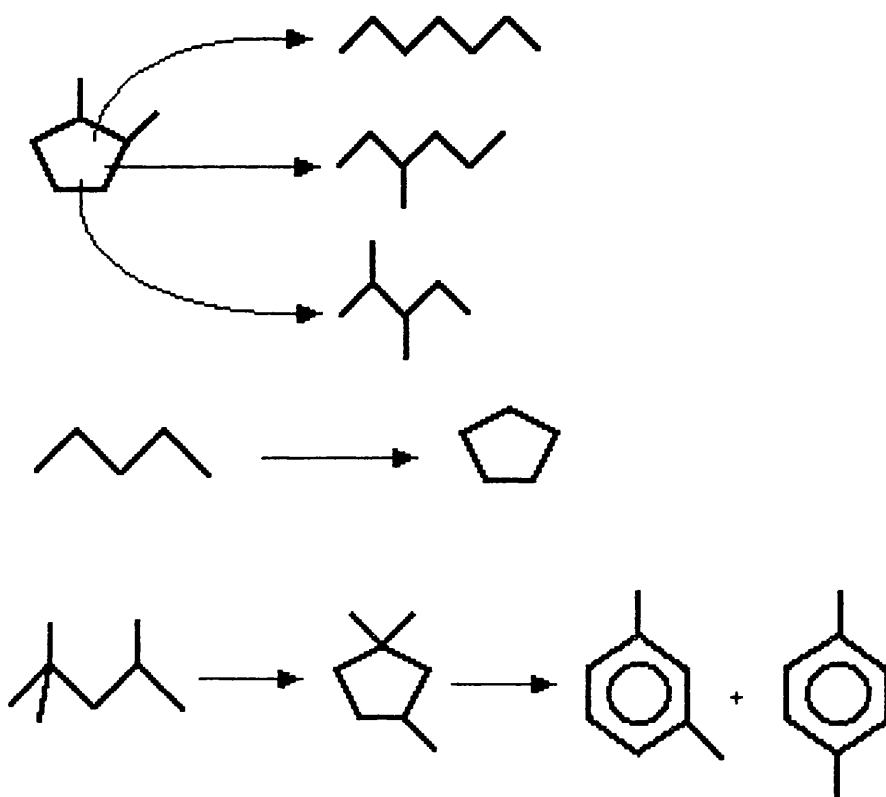
where incompletely coordinated aluminium atoms are formed which could serve as electron acceptors.

## 1.7 METAL CATALYSED REARRANGEMENTS

It is generally accepted that on reforming catalysts, Pt dispersed on an acidic support, skeletal isomerisation necessarily occurs according to a bifunctional mechanism which involves three consecutive steps, dehydrogenation on the metal, isomerisation of the resulting olefin on the acidic support by a carbonium ion mechanism and rehydrogenation of the isomerised olefin (see section 1.6).

However, in the absence of an acidic function, Pt alone is able to effect skeletal rearrangements of alkanes or cycloalkanes, as discussed below. Under reforming conditions such Pt-only catalysed skeletal reactions probably make only a minor contribution to the overall reaction on a bifunctional catalyst system, since the presence of an acidic function is essential in order to obtain the necessary activity and selectivity for the reforming conversion (17).

Using non-acidic charcoal as a support, it has been shown (66, 67, 68) that Pt catalyses reactions such as the hydrogenolysis of polymethylcyclopentane, the dehydrocyclisation of alkanes and the aromatisation of substituted alkanes. e.g.



Skeletal isomerisations have also been demonstrated on various metal films (48), particularly Pt and Pd and on supported platinum (69,70) under conditions (200-300°C) such that the support (glass or alumina) was catalytically inactive. This clearly shows that the metal itself can catalyse the reaction.

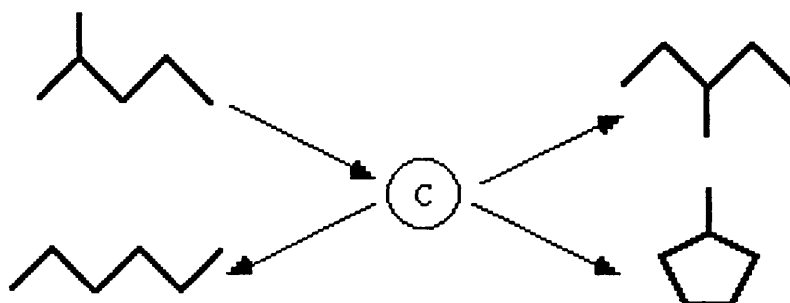
Two basic mechanisms have been proposed for the skeletal isomerisation of hydrocarbon on metals.

(1) The bond shift mechanism which corresponds to a simple carbon-carbon bond displacement, accounting for the isomerisation of short chain paraffins (37).



The various metals act specifically for this reaction since platinum isomerises neo-pentane to iso-pentane whereas palladium does not (37,71) except under special experimental conditions (oriented films of palladium and rather low partial pressure of hydrocarbon) (52).

(2) The cyclic mechanism, which involves dehydrocyclisation to an adsorbed intermediate, C, followed by ring cleavage and desorption of the products, accounting for the isomerisation of alkanes large enough to form 5 membered rings (69, 70).



Evidence in support of this cyclic mechanism is based on the facts that isomerisation product distributions closely parallel those displayed in methylcyclopentane ring opening (72) and that cyclopentane formation from dehydrocyclisation always

accompanies skeletal rearrangement.

Since cyclic type isomerisation first involves carbon-carbon bond formation and then carbon-carbon bond rupture, one does not expect hydrogenolysis to occur by this mechanism. In contrast, as suggested from early work (70), if bond shift isomerisation involves first carbon-carbon bond rupture and then carbon-carbon bond recombination a common intermediate should exist leading to both hydrogenolysis and isomerisation.

Anderson and Avery (37) demonstrated that bond shift isomerisations of n-butane, iso-butane and neo-pentane over Pt films were accompanied by hydrogenolysis and the activation energies for the two processes were identical.

Isomerisation reactions also show a strong inverse dependence of hydrogen pressure on the reaction rate (17), similar to hydrogenolysis reactions, suggesting partially dehydrogenated species are also reaction intermediates.

To further elucidate this mechanism Anderson and Avery (37) compared hydrogenolysis reactions of ethane, iso-butane, n-butane and neo-pentane. Over a Pt film neo-pentane reacted with an activation energy and frequency factor very similar to those for the butanes,

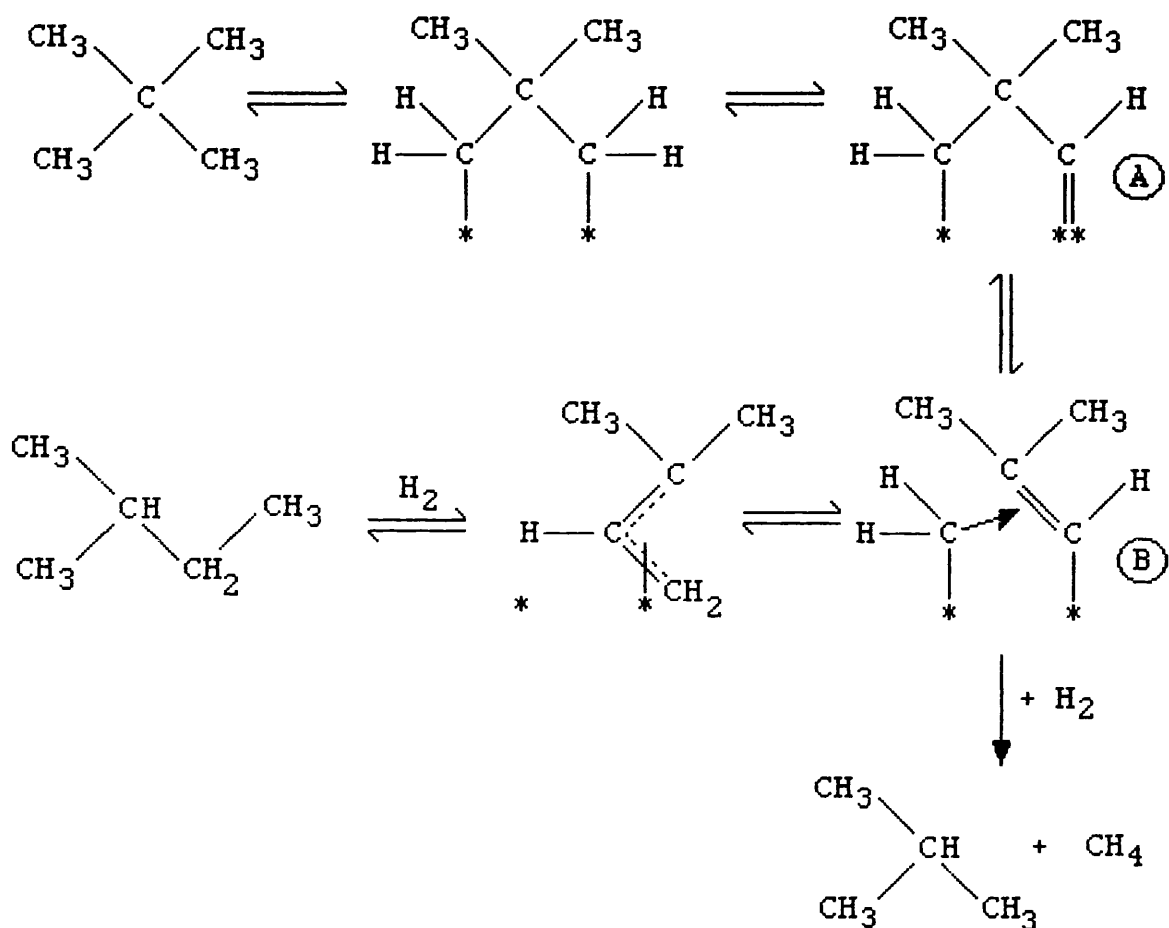
and since neo-pentane cannot form a 1,2-diadsorbed intermediate, it was concluded that a 1,2-diadsorbed intermediate was not primarily involved in the butane reactions. Ethane which can only be diadsorbed in the 1,2- mode, reacted with a much higher activation energy than the other hydrocarbons. It was concluded that the surface precursor to the reaction of butanes was a 1,3-diadsorbed species.

This agrees with the known propensity of Pt to promote  $\alpha,\gamma$ - exchange of paraffins with deuterium (73).

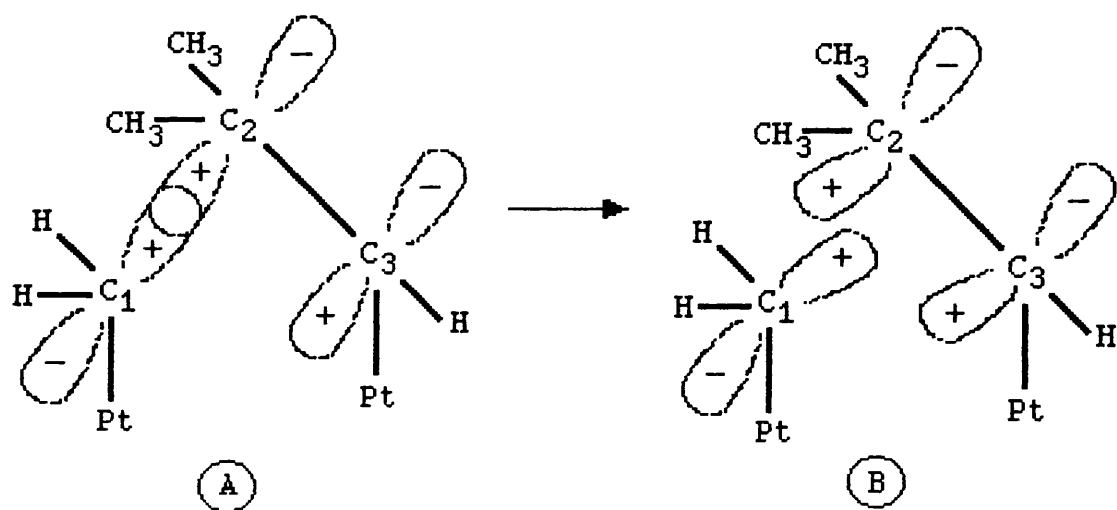
As a consequence of this work, Anderson and Avery (74) proposed a mechanism for the hydrogenolysis and isomerisation of aliphatic hydrocarbons at a Pt surface as follows:

The model proposed that the surface precursor was a 1,3-diadsorbed species with a double bond to the surface at one carbon atom (structure A), and that isomerisation and hydrogenolysis occurred by the transformation of this to a bridged structure B, a  $\pi$ -complex of the Dewar type (75).

### Anderson and Avery mechanism

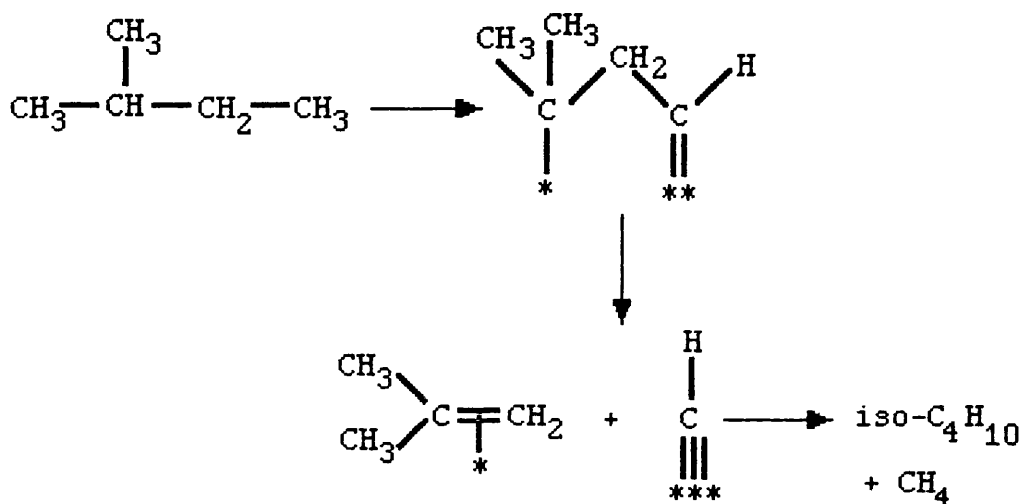


### Dewar Complexes

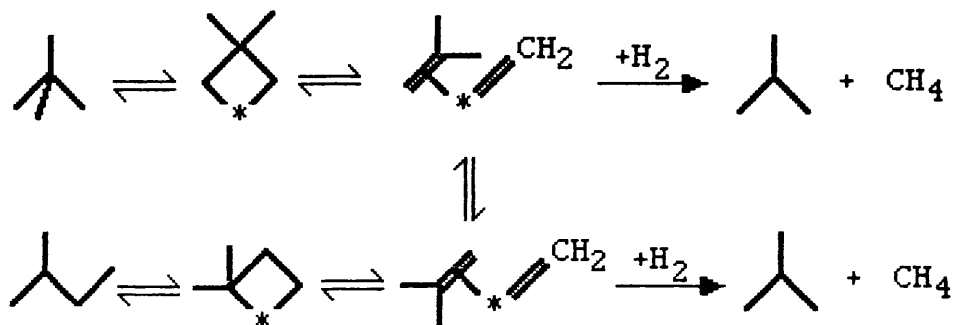




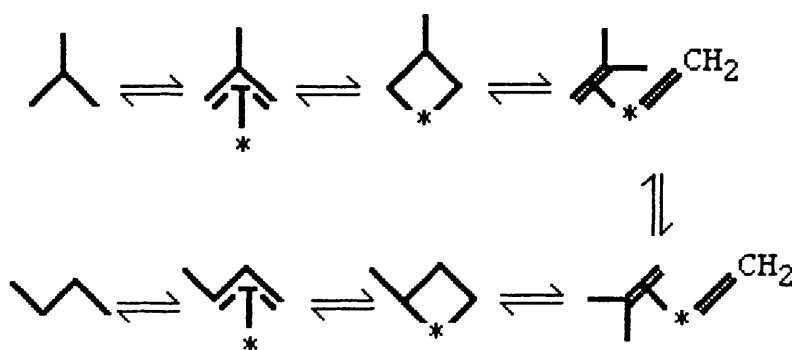
This led Leclercq to suggest the following mechanism for hydrogenolysis, also involving a 1,1,3-triadsorbed species in which the rupture occurred at the carbon atom in the  $\alpha$ -position to the metal atom double bond.



Garin and Gault (77,78) put forward the existence of an  $\alpha,\alpha,\gamma$ -intermediate triadsorbed on one metal atom. Since many platinocyclobutanes have been characterised (79), the direct formation of a metallocyclobutane in the case of Pt could explain the unique propensity of Pt to promote the isomerisation of neo-pentane to iso-pentane.



As previously mentioned, while iso-butane is isomerised on both Pt and Pd, Pt, but not Pd, catalyses the isomerisation of neo-pentane to iso-pentane. The easiest way to explain this is to assume that in the case of Pd the precursor species is attached by three adjacent carbon atoms and only two in the  $\alpha,\gamma$  positions in the case of Pt. This assumption based on the known propensity of Pd to form  $\pi$ -allyl complexes (80) led Gault to suggest the following mechanism (16) for the isomerisation of iso-butane over Pd.

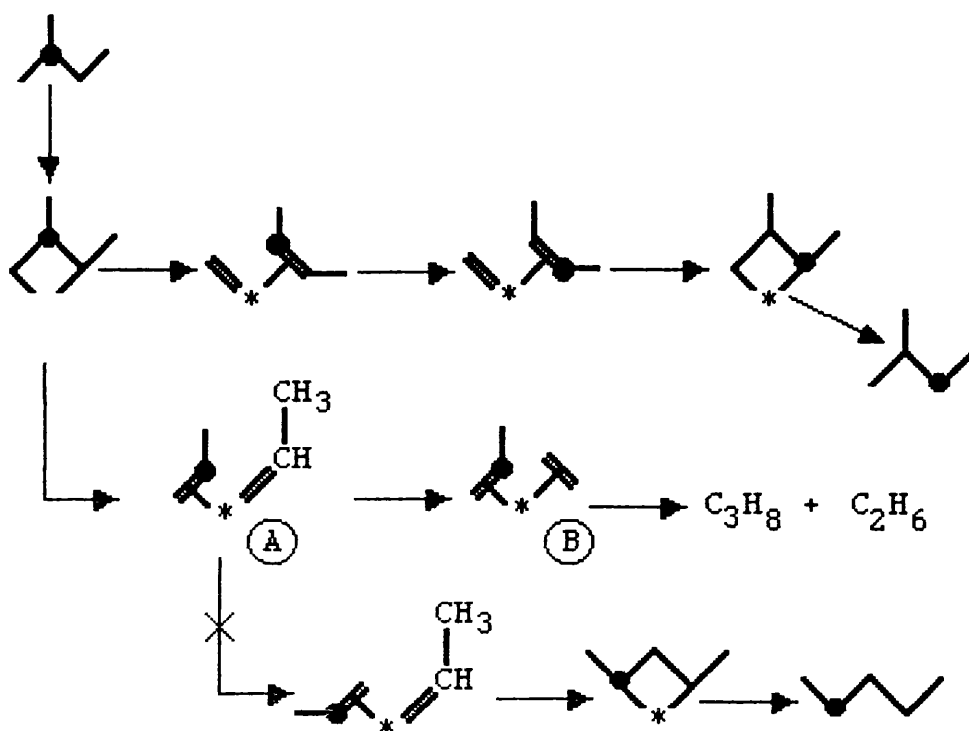


Garin and Gault found further evidence for the metallocyclobutane mechanism for Pt from the kinetic data for the skeletal rearrangement and hydrogenolysis of pentanes over a 10% Pt/Al<sub>2</sub>O<sub>3</sub> catalyst (16). Following the reactions with <sup>13</sup>C-labels they classified the possible reactions into four groups according to their apparent activation energies.

			activation energy kcalmol <sup>-1</sup>	order w.r.t. hydrogen	
Group I		→		71.4	-3.4
Group II		→		55.3	-1.8
		→		54.3	-2.3
Group III		→		45.3	-1.9
		→		45	-1.65
		→	C <sub>3</sub> H <sub>8</sub> + C <sub>2</sub> H <sub>6</sub>	45	-1.65
		→	C <sub>3</sub> H <sub>8</sub> + C <sub>2</sub> H <sub>6</sub>	44.5	-1.3
Group IV		→	 + CH <sub>4</sub>	38.5	-0.6
		→	 + CH <sub>4</sub>	35	-0.7

The reaction with the highest activation energy, Group I, was the cyclic type isomerisation of n-pentane which led to the complete scrambling of the label. Group II included the isomerisation of 2-methylbutane to n-pentane and the reverse reaction. The reactions in Group III included the isomerisation of 2-methylbutane-2-<sup>13</sup>C to 2-methylbutane-3-<sup>13</sup>C and to neo-pentane and the hydrogenolysis of the internal carbon-carbon bond in n-pentane and 2-methylbutane. Demethylation reactions in Group IV were the least activated. It was noticeable that the bond shift reactions were split into two groups, one of these groups (Group III) being associated with hydrogenolysis and the other (Group II) not. There was also a distinction, among the hydrogenolysis reactions, between internal fission and demethylation.

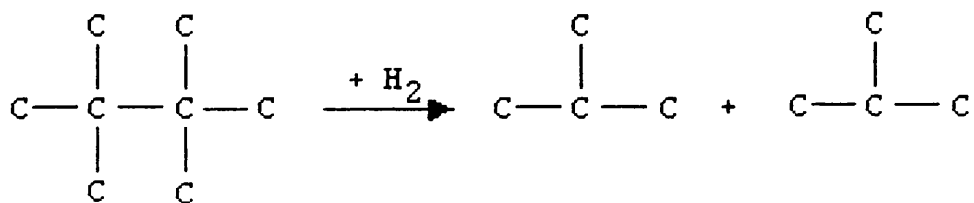
Both Anderson's mechanism involving a triadsorbed precursor and Gault's mechanism involving a metallocyclobutane intermediate could account for the reactions of Group III where isomerisation and hydrogenolysis were associated. The fact that all these reactions are almost negligible on palladium (internal fission, methyl shift and neo-pentane isomerisation) is the first argument in favour of the metallocyclobutane mechanism for Pt. Moreover, if the mechanism was operative in the isomerisation of 2-methylbutane to n-pentane. e.g.



then the adsorbed ethylidene (A) formed would be rapidly isomerised by a hydrogen shift to an adsorbed olefin (B) (81).

The metallocyclobutane then cannot be reformed and isomerisation is replaced by the hydrogenolysis of the internal carbon-carbon bond. Thus at the same time it is explained why internal fission has the same activation energy as methyl shift (Group III) and why chain lengthening does not take place by this mechanism but requires a more activated process (Group II). In contrast the Anderson-Avery mechanism does not discriminate among the various isomerisation reactions.

None of these mechanisms including 1,3-diadsorbed species, however, can account for Leclercq and his co-workers results for the hydrogenolysis of 2,2,3,3-tetramethylbutane over a Pt/Al<sub>2</sub>O<sub>3</sub> catalyst (76). They showed that the initial hydrogenolysis product was iso-butane in almost total absence of methane. e.g.



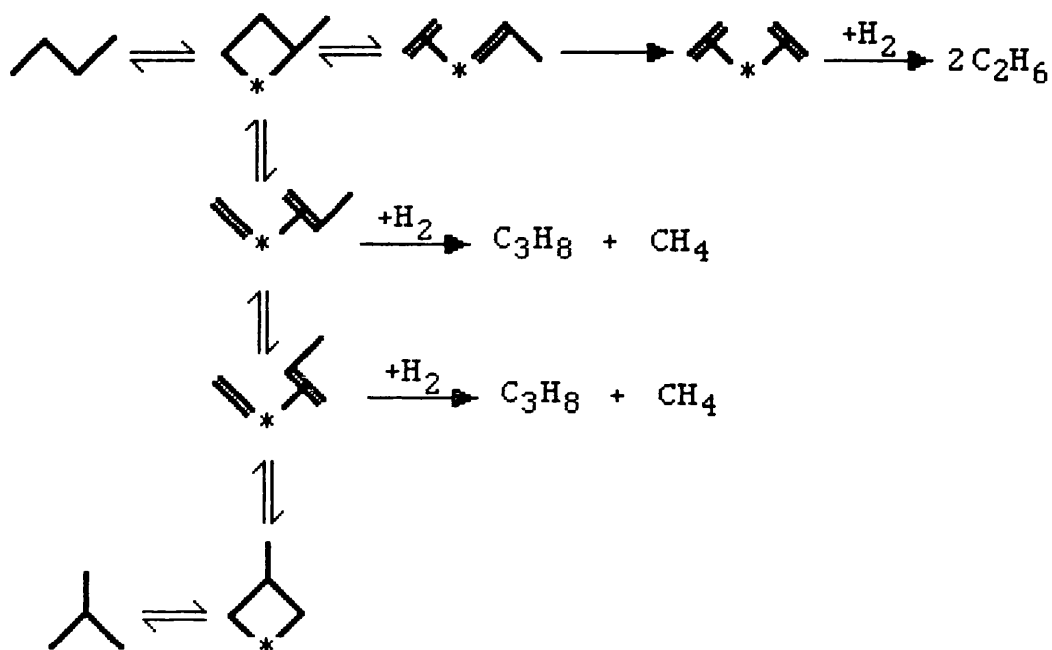
The breakage of the central carbon-carbon bond cannot be accounted for by a 1,3-diadsorbed mechanism and suggests that  $\alpha, \delta$ -intermediates can also be formed on Pt catalysts.

Although no conclusive proof can be offered for any of the mechanisms, the metallocyclobutane mechanism for hydrogenolysis and isomerisation proposed by Garin and Gault best accounts for

- (i) the difference between Pt and Pd catalysts.
- (ii) the possible breakage of bonds  $\beta$  to a tertiary carbon atom.
- (iii) the relation between the activation energies of

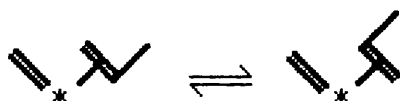
certain bond shift and isomerisation reactions.

Using this mechanism the isomerisation and hydrogenolysis reactions of iso-butane and n-butane can be represented as follows.

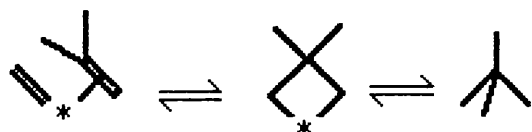


One corollary of this mechanism is that the isomerisation of n-butane is related to the breakage of the C<sub>1</sub>-C<sub>2</sub> bond and not the central C<sub>2</sub>-C<sub>3</sub> bond of n-butane.

The isomerisation step in this mechanism involves the rotation of the olefin. e.g.



a process which requires an activation energy of 40-60  $\text{kJmol}^{-1}$  (82) on Pt depending on the substituents. The ease of the reformation of the metallocyclobutane may explain, for instance, the difficulty of isomerising iso-pentane to neo-pentane (83), where this step would be



with the bond reforming hindered by the presence of the methyl groups on the olefin.

### 1.8 STRUCTURE SENSITIVITY

The first reported case of a reaction which had a large dependence of specific rate on the catalyst structure was that of neo-pentane on platinum (84).

This result led Boudart to classify reactions on metals as:

- (a) facile or structure insensitive reactions for which the specific rate does not depend on the particle size and
- (b) demanding or structure sensitive reactions for which the specific rate is highly dependent on the particle size (19).

Structure insensitive reactions, reactions which

do not depend on the dispersion of the metal, include the dehydrocyclisation of cyclohexane (85), hydrogenolysis of cyclopentane (86), hydrogenation of cyclohexane and allyl alcohol (87, 88), hydrogenation of cyclopropane (89) and the dehydrogenation of 1,1,3-trimethylcyclohexane (90).

Surface sensitive reactions such as alkane hydrogenolysis (91-94, 72), the exchange of benzene on iridium and nickel (95) and the dehydrocyclisation of n-heptane on platinum catalysts (96), all show a high dependence of the specific rate on the metal dispersion.

Alkane hydrogenolysis reactions are the best examples of structure sensitive hydrocarbon reactions. The reactions of ethane over nickel (91) and rhodium (92), n-pentane over rhodium (93) and iridium (94), neopentane (84), n-hexane, 2-methylpentane and 3-methylpentane (13) over platinum are all examples in which the activity decreases by about 5-fold when the average particle size increases from about 1.5 to 6nm.

Structure sensitive reactions are also often structure sensitive for selectivity as the product distributions can vary widely with the particle size. For instance, for the hydrogenolysis of methylcyclopentane, non-selective hydrogenolysis takes place on a highly dispersed Pt/Al<sub>2</sub>O<sub>3</sub> catalyst with a

loading smaller than 0.6%, while selective rupture of the bissecondary C-C bonds occurs on heavily loaded catalysts (more than 6% platinum on alumina) (97).

Boudart suggested that specific sites with special geometric requirements were involved in structure sensitive reactions (19), while all the atoms of the surface were available for structure insensitive reactions. These sites with special geometric requirements could be surface irregularities such as steps or kinks which have both been shown to have a decisive role in breaking C-C , and to a lesser extent, C-H bonds (98, 99). The concentration of active corner and kink microfacets decreases markedly with increasing crystallite size. A sharp decrease in these sites also accompanies alloying with group IB metals, where C-C bond breaking reactions are always suppressed more strongly than reactions involving C-H bond scission (100). Metallocyclobutane and metallocarbenes, which have been proposed as reaction intermediates in isomerisation and hydrogenolysis reactions (sections 1.4, 1.7) could be formed at these surface metal atoms with low coordination numbers. Rodríguez-Reinoso and his co-workers, however, showed that only the hydrogenolysis of n-butane was structure sensitive over a carbon supported Pt catalyst, the isomerisation of n-butane being structure insensitive (101). This suggests that isomerisation reactions can take place at sites

comprising of higher coordination numbers.

Assuming then that the sites required for C-C bond rupture are located on a certain part of the metal crystallite (edge, corner or kink), the following mechanism for hydrogenolysis can be envisaged,

- (1) indiscriminate adsorption of a gaseous molecule on a face site of the metal to form a weakly adsorbed molecule.
- (2) superficial migration from the adsorption site,  $S_a$ , to a reactive site,  $S_r$ , located on some specific region of the metal particle.
- (3) formation on the reactive site of a highly dehydrogenated species.
- (4) cracking of this strongly adsorbed species.
- (5) rehydrogenation, superficial migration and desorption to yield the reaction products.

One would expect that the rate determining step would be one of the two reactions (3) and (4) which occur on the reactive sites  $S_r$ . The mechanism proposed above can explain the various situations which may arise concerning the dependence of specific rates and

selectivity on the size of metal particles.

Firstly supposing that on one crystallite that the total number,  $N_R$ , of reactive sites,  $S_R$ , is much larger than the number,  $N_a^*$ , of weakly adsorbed hydrocarbon molecules, i.e. only a small fraction of the surface is covered by chemisorbed alkanes. Then only some of the available reactive sites are occupied, the number of which,  $N_R^*$ , should be proportional to the number,  $N_a^*$ , of weakly adsorbed molecules. Since  $N_a^*$  itself is proportional to the number of superficial metal atoms,  $N_S$ , the number of reacted molecules is proportional to  $N_S$ . One therefore expects the turnover number to be independent of the size of the metal crystallite. On the other hand the distribution of the various reactive sites,  $N_{R1}$ ,  $N_{R2}$ , (with  $\sum_i N_{Ri} = N_R$ ) associated with various reaction pathways, generally depends on the size of the metal crystallite. This explains the situation where the selectivity widely varies with metal dispersion while the specific rate remains constant.

A second possibility is that the number,  $N_R$ , of reactive sites of any type is much smaller than the number,  $N_a^*$ , of weakly adsorbed hydrocarbons. All the reactive sites are then occupied ( $N_a^* = N_a$ ), consequently the number of reacted molecules is no longer proportioned to the number of weakly adsorbed

hydrocarbons,  $\text{Na}^+$ , and to the number of superficial metal atoms. In this case not only the selectivity, but also the specific rate depend upon the metal particle size. This situation occurs especially when the change in particle size has been obtained by sintering a supported metal catalyst (84, 97). The effect of sintering is to smooth the catalyst surface, reducing considerably the numbers of those irregularities (steps, kinks etc.) with which the reactive sites may be associated.

A third possibility is that for some reason the rate of superficial migration becomes much smaller than the rate of weak adsorption or desorption. In this case only the molecules adsorbed in the vicinity of a reactive site may be strongly adsorbed and react. The reaction is again proportional to the number of reaction sites, not the number of surface atoms so that the reaction is again structure sensitive for rate.

Several crystallographic models have been proposed to date providing reasonable explanations of particle size effects in metal catalysis. According to the first and most simple model, different reactivities are associated with surface atoms of different coordination numbers. Following the polyhedral theory developed by Poltorak (102), face atoms and edge atoms in metal crystallites act as specific active centres.

The relative numbers of edge and face atoms vary widely when the size of the metal particle varies between 1 and 5 nm, below 1nm the crystallites have only edge atoms or atoms of even lower coordination number. Beyond 5nm more than 90% of the surface atoms are regular face atoms. One therefore expects the largest changes in selectivity or reaction mechanisms to appear in the 1-5nm range.

According to the second model groups or ensembles of atoms with a specific geometrical arrangement are required for some catalytic reactions. Such sites arise when incomplete layers are added over [111] and [110] faces of fcc crystals. Of particular interest are the  $B_5$  sites, including edge and face atoms in [110] or [311] configuration on the fcc cubo-octahedron. The ratio between the maximum number of  $B_5$  sites to the number of edge and corner atoms remains practically constant for particles larger than 2nm and then decreases rapidly to zero for the smallest particles (103).

Burton (104) related the occurrence of some catalytic particle size effects to the existence of non-lattice symmetries ( $D_{5H}$  or icosahedral) observed in the case of very small metal aggregates.

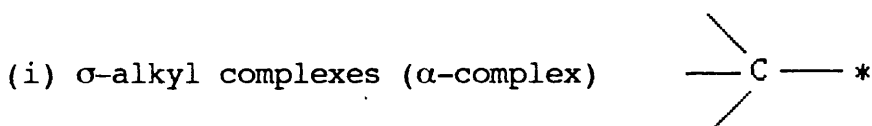
Using the Lennard Jones and Morse potentials Hoare and Pal (105) suggested that polytetrahedra with

an equivalent radius of 0.5 to 1nm (40-60 atoms) would consist of a central core of twenty to thirty atoms on which the surface atoms would show a distinctly liquid phase mobility. For clusters of more than seventy atoms, beyond a size of roughly 2nm, the more stable aggregates would be expected to recover a regular fcc lattice symmetry and normal catalytic behaviour.

These crystallographic models all place emphasis on geometrical and structural considerations. There are however significant changes to the electronic properties of metal clusters smaller than 1.5nm (106). Calculations show that the local density of states and also the asphericity of the charge density around a surface metal atom vary with particle size and are different for fcc and icosahedral clusters (107).

## 1.9 CHEMISORPTION COMPLEXES OF HYDROCARBONS

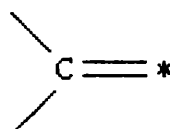
As discussed earlier, the kinetics of hydrogenolysis reactions suggest that strongly adsorbed hydrocarbon intermediates with a high degree of metal-organic bond multiplicity are formed during the reaction (section 1.4). The hydrocarbon-metal complexes that are involved are defined as follows;



These have a single bond from the attached carbon

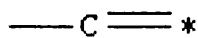
to the metal surface.

(ii) metal carbene complexes ( $\alpha\alpha$ -complex)



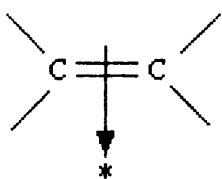
These have two bonds between the attached carbon and the metal surface. The adsorption site \* consisting of one or two metal atoms.

(iii) metal carbyne complex ( $\alpha\alpha\alpha$ -complex)

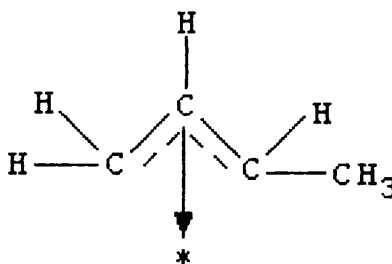


Here the carbon atom is attached to the metal surface by three bonds. The adsorption site \* usually consisting of three metal atoms.

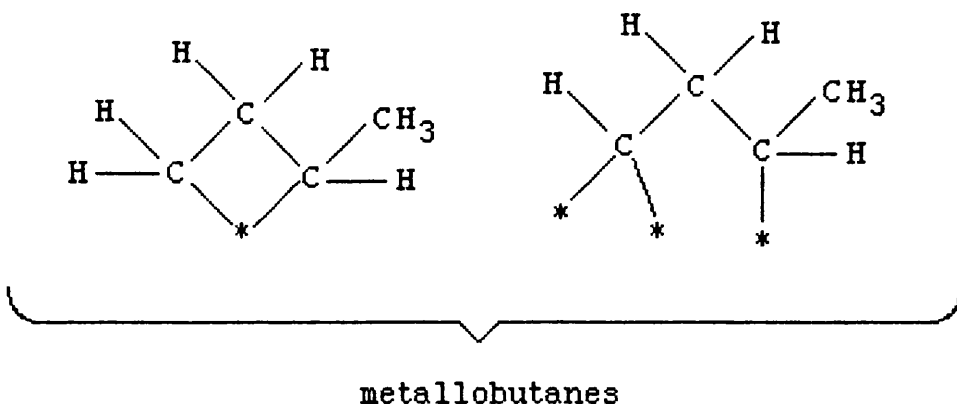
For bond shift isomerisation reactions  $\pi$ -adsorbed, metallobutanes and allylic complexes are often involved in the proposed reaction mechanisms (section 1.7). e.g.



$\pi$  - complex

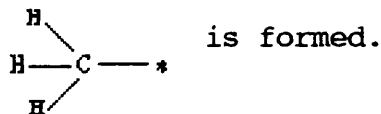


allylic complex



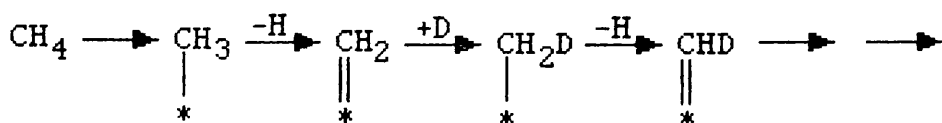
Various techniques such as a deuterium exchange, low energy electron diffraction (LEED), high resolution electron energy loss spectroscopy (HREELS), Fourier transform infrared (FTIR) and  $^{13}\text{C}$  and deuterium NMR have all provided evidence for these types of complexes.

$\text{D}_1$  products formed during exchange reactions of methane with deuterium (108,26) can be considered as evidence for the  $\sigma$ -alkyl complex, that is, a C-H bond is dissociated and a complex



This complex then accepts a D atom and desorbs.

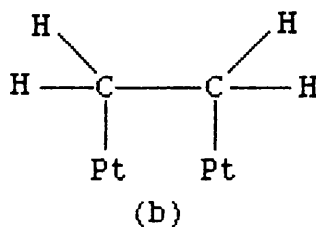
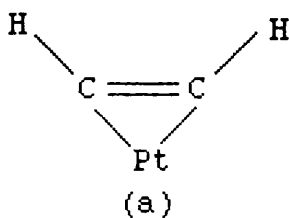
The multiple exchange of deuterium with methane particularly on Rh and Ni catalysts led to the following mechanism being suggested by Kemball (108).



Other evidence for the  $\alpha$ -complex comes from high resolution mass spectrometry of deuterioethanes (109) made by exchange with  $D_2$  on Ni or Pt. The major part of the  $d_2$  products on Ni have both deuterium atoms on the same carbon atom, at higher temperatures, suggesting an asymmetric exchange via a carbene like complex. Ni was found to show a greater tendency to form these complexes than Pt (109) as expected from earlier results (53).

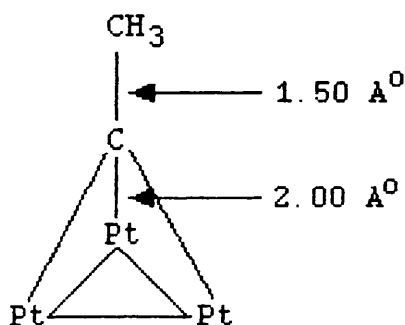
Neither of these experiments rule out the involvement of a carbyne,  $\alpha\alpha\alpha$ -complex  $—C\equiv*$ , although Frennet and Lienard (110,31) suggested, from experimentally measured degrees of dissociation of the C-H bonds, that the degree of dissociation was not higher than  $\begin{array}{l} \diagup \\ C= \\ \diagdown \end{array}*$  at moderate temperatures ( $<200^\circ C$ ).

LEED and HREELS studies by Somorjai et al. (111, 112) have shown that ethene and ethyne chemisorb associatively below 300K on Pt [111] surfaces forming (2x2) structures in which the C-C bond is orientated approximately parallel to the surface. e.g.



The ethyne structure (a) is bound to one platinum atom almost at an "on top" site with a Pt-C distance of  $2.5\text{\AA}$  and a C-C bond length of  $1.20\text{\AA}$ . The adsorbed ethene is shown to have a near  $sp^3$ -hybridisation suggesting a di- $\sigma$  bonding model (b) with a normal C-C single bond length of  $1.5\text{\AA}$ .

These species are both metastable and on heating to 310K in hydrogen they both form a more stable ethylidyne complex  $-\text{C}\equiv\text{C}^*$ , with the C-C internuclear axis directed perpendicular to the platinum surface (112).



ethylidyne

The  $\alpha$ -carbon atom is bonded equivalently to three Pt atoms with a Pt-C bond length of  $2.0\text{\AA}$  and a normal single C-C bond length of  $1.5\text{\AA}$ .

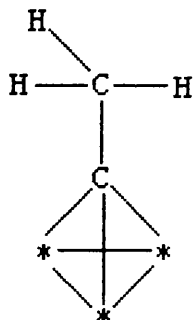
Similar metastable and stable species have been formed on Rh [111] surfaces, the conversion to the more stable ethylidyne species occurring at lower temperatures over rhodium ( $\sim 270\text{K}$ ) compared with platinum

(~310K) (113, 114).

This can be correlated with the periodic positions of the metals since, in general, the bonding of small molecules to transition metal surfaces becomes stronger as one moves from right to left across the periodic table (49).

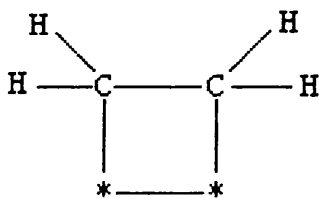
While these unsaturated molecules remain intact and form well ordered structures over Pt[111] at 300K they produce poorly ordered structures over Ni[111] surfaces (115). This poor ordering characteristic reflects a lack of mobility and stronger substrate bonding over Ni. Thermal desorption studies (115,116) also show that molecules bind much less reversibly on Ni [111] when compared with Pt[111].

Using the metal-surface selection rule (MSSR), FTIR studies on Pt/SiO<sub>2</sub> catalysts (117,118) have produced evidence for the following structures for ethene and propene chemisorption at room temperature.



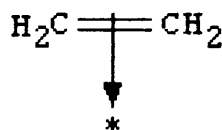
(I)

ethynylidyne



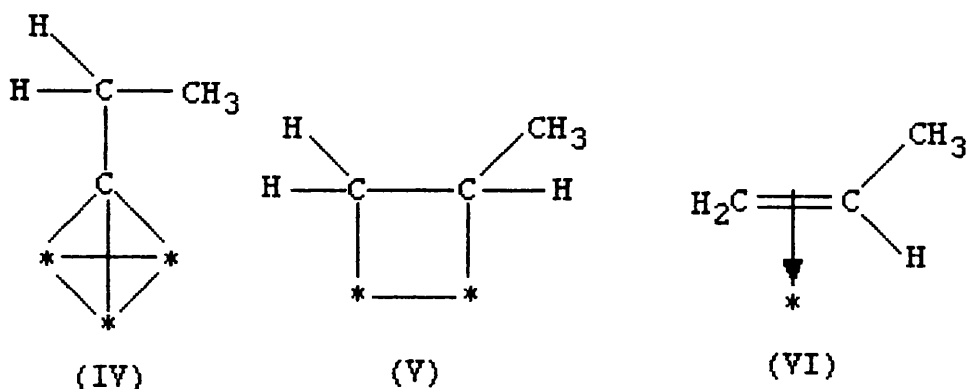
(II)

di- $\sigma$  species



(III)

$\pi$ -bonded species



propylidyne

di-σ species

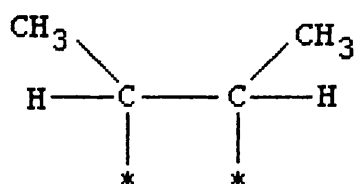
π-bonded species

De La Cruz and Sheppard (117) have shown from internal spectroscopic evidence that, on ethene chemisorption, species (I) and (II) exist in approximately equal numbers. The relative amount of the π-species (III) is not known. Similarly Shahid and Sheppard (118) have shown that the chemisorption of propene produces significant amounts of the propylidyne species (IV) and the di-σ species (V) together with a smaller unqualified amount of the π-adsorbed species (VI). Heating the adsorbed propene above 300K in vacuum leads to the breakdown of the initially formed species to give ethylidyne. The chemisorption of propane produced mainly the propylidyne species (IV).

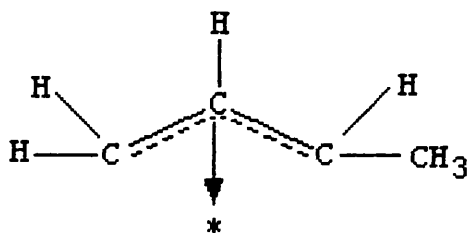
The chemisorption of but-1-ene on a Ni/SiO<sub>2</sub> catalyst at room temperature has been studied by Campione and Ekerdt also by FTIR (119). From their results they suggested the following strongly and weakly

adsorbed species.

(i) weakly adsorbed

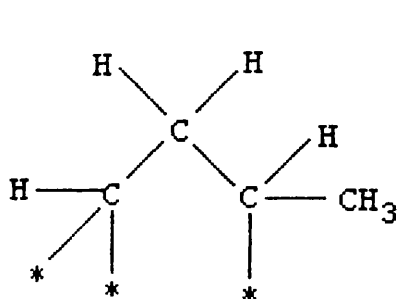


2,3 adsorbed species

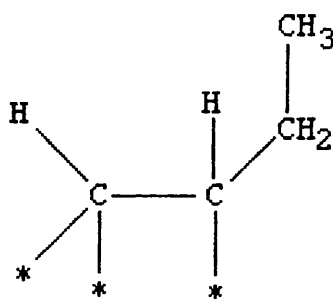


$\pi$ -allyl species

(ii) strongly adsorbed metallobutanes

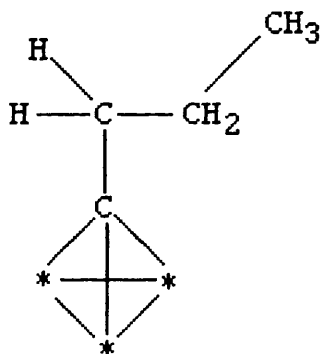


1,1,3 species



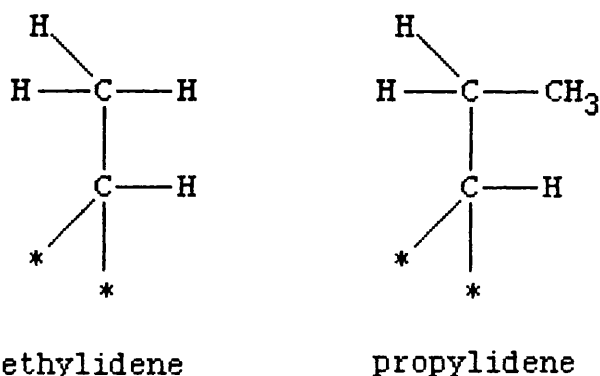
1,1,2 species

On heating these strongly adsorbed species to 350K in hydrogen the butylidyne species was also detected. e.g.



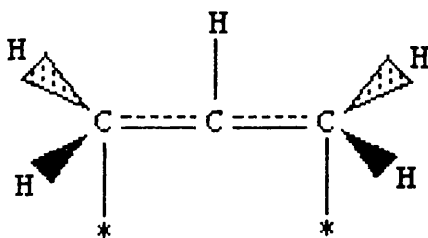
butylidyne

Carbon-13 and deuterium NMR studies for ethene and propene adsorbed on a Pt/Al<sub>2</sub>O<sub>3</sub> catalyst at room temperature have shown that the ethylidene and propylidene structures are formed (120).



These may be formed in preference to the carbyne structures, in this case, due to the excess of hydrogen available from the alumina support.

The adsorption of propene also showed strong evidence for the allyl species. e.g.



There is, therefore, some good evidence for the existence at room temperature of all the species that have been proposed as intermediates in hydrogenolysis

and bond-shift isomerisation reactions e.g.  $\sigma$ -alkyl, carbene, carbyne, metallobutanes,  $\pi$ -adsorbed and allylic complexes. At higher temperatures, especially in the presence of  $H_2$ , however, there is a strong preference for forming the alkylidyne and other strongly bound dehydrogenated species (119,121).

#### 1.10 SUPPORT MATERIALS

The early concept of a support or carrier was of an inert substance that provided a means of spreading out an expensive catalyst ingredient, such as platinum, for its most effective use, or a means of improving the mechanical strength of an inherently weak catalyst. However, the carrier may actually contribute catalytic activity, depending on the reaction conditions and it may react to some extent with other catalyst ingredients during the manufacturing process. It can also help stabilise the catalytically active structure (21). In this study four support materials have been used, two traditional supports silica and alumina and two less conventional supports molybdenum trioxide and tungsten trioxide.

Conventional support materials can be classified into

(a) inert supports, like silica, supplying high surface areas for dispersion of the active component

(b) catalytically active supports, like aluminas, silica-aluminas and zeolites (molybdenum trioxide, tungsten trioxide)

(c) supports influencing active components by strong interaction e.g. partially reducible oxides

( $\text{TiO}_2$ ,  $\text{Nb}_2\text{O}_5$ ,  $\text{V}_2\text{O}_5$ )

(d) structural supports which are of increased importance for exhaust gas purification (monoliths)

(122).

The selection of a carrier is based on it having certain desirable characteristics, which may be listed,

(1) economic

(a) to reduce cost by extending an expensive catalyst

(2) mechanical

(a) to give mechanical strength

(b) to optimise bulk density

(c) to provide a heat sink or heat source

(d) to dilute an overactive phase

(3) geometric

(a) to increase the surface area (high surface area is usually but not always desirable)

- (b) to optimise the porosity of a catalyst  
(high area implies fine pores, but relatively small pores, such as <2nm may become plugged in catalyst preparation especially if high loadings are sought)
- (c) to optimise crystal and particle size
- (d) to allow the catalyst particles to adopt the most favourable configurations

(4) Chemical

- (a) to be inert to undesired reactions
- (b) to be stable under reaction and regeneration conditions
- (c) to react with the catalyst either to improve specific activity or to minimise sintering

(5) Deactivation

- (a) to stabilise the catalyst against sintering
- (b) to minimise poisoning (123)

Obviously no support can fulfil and optimise all these requirements. The most common supports used are alumina, silica, chromia, tungstia and activated carbon.

A necessary requirement for any carrier is resistance to sintering under reaction conditions. The

temperature at which lattices begin to be appreciably mobile is sometimes termed the Tammann temperature; and that at which surface atoms become significantly mobile, the Hüttig temperature. For simple compounds without phase changes on heating and of low vapour pressure, the Tammann temperature is very approximately  $0.5T_m$  and the Hüttig temperature about  $0.3T_m$ , where  $T_m$  is the melting point in absolute units. Consequently suitable carriers must usually have fairly high melting points as a minimum requirement. The transition metals iron, cobalt and nickel have melting points of about 1800K and become mobile at temperatures above roughly 250–300°C. The platinum group metals melt at higher temperatures but are usually supported for economy (122).

### 1.11 ALUMINA

Stoichiometrically there is only one oxide of aluminium, namely, alumina ( $Al_2O_3$ ). This simplicity, however, is compensated by the occurrence of various polymorphs, hydrated species and so on, the formation of which depends upon the conditions of preparation. There are two forms of anhydrous  $Al_2O_3$  namely  $\alpha-Al_2O_3$  and  $\gamma-Al_2O_3$ . Other trivalent metals (Ga, Fe) form oxides that crystallise in the same two structures. In  $\alpha-Al_2O_3$  the oxide ions form a hexagonal close packed array and the aluminium ions are distributed symmetrically among

the octahedral interstices. The  $\gamma\text{-Al}_2\text{O}_3$  structure is sometimes regarded as a "defect" spinel structure, that is, as having the structure of a spinel with a deficit of cations (124).

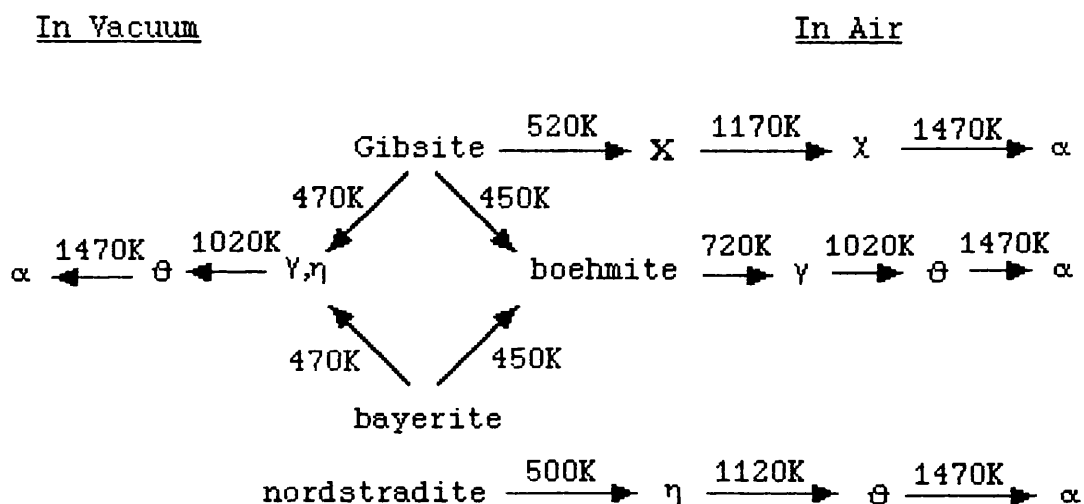
Alpha- $\text{Al}_2\text{O}_3$  is stable at high temperatures and is also indefinitely metastable at low temperatures. It occurs in nature as corundum and may be prepared by heating  $\gamma\text{-Al}_2\text{O}_3$  or any hydrous oxide above  $1000^\circ\text{C}$ . Gamma- $\text{Al}_2\text{O}_3$  is obtained by dehydration of hydrous oxides at low temperatures ( $\sim 450^\circ\text{C}$ ).

Alpha- $\text{Al}_2\text{O}_3$  is very hard and resistant to hydration and attack by acids whereas  $\gamma\text{-Al}_2\text{O}_3$  readily takes up water and dissolves in acids. The  $\text{Al}_2\text{O}_3$  that forms on the surface of the metal has still another structure, namely, a defect rock salt structure; there is an arrangement of Al and O ions in the rock salt with every third Al ion missing (124).

Aluminas represent the most important commercial support materials and their preparation and properties have been extensively researched and dealt with in numerous publications (125, 126). Aluminas of high surface areas ( $100\text{-}600\text{ m}^2/\text{g}$ ) are generally prepared by thermal decomposition of well crystallised hydroxides or precipitation of colloidal gels. The latter process is

often favoured since it yields aluminas of controlled surface areas and porosities depending on the choice of gelation conditions (127).

Upon dehydration of the precipitate a variety of crystalline modifications form depending on the starting hydroxides or oxyhydroxides and the dehydration conditions (air or vacuum and temperature). Lippens (125) summarised the sequence as follows.



All of these structures are based on more or less close packed oxygen lattices with aluminium ions in the octahedral or tetrahedral interstices and have been classified by Kirschner (128) according to the arrangement of close packed oxygen layers into three series.

- (i) α-series with hexagonal close packed stacking

- (ABAB) represented by  $\alpha\text{-Al}_2\text{O}_3$  (corundum)
- (ii)  $\beta$ -series with alternating close packed stacking  
(ABAC-ABAC)
- (iii)  $\gamma$ -series with cubic close packed stacking (ABC-ABC)

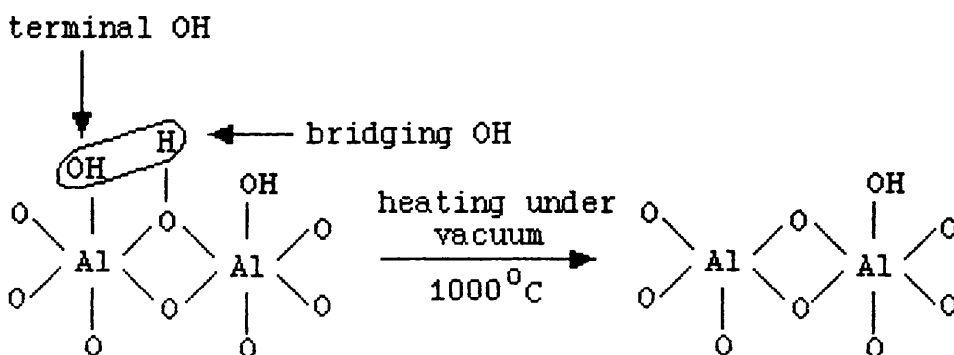
The most commonly used supports are the low temperature representatives of the  $\gamma$ -series,  $\gamma$ - and  $\eta$ -alumina.  $\gamma\text{-Al}_2\text{O}_3$  is of great interest since it has a high area and is relatively stable over the temperature range of interest for most catalytic reactions.  $\eta\text{-Al}_2\text{O}_3$  has been of interest in the past because it is inherently more acidic than  $\gamma$ -, so it becomes a useful support in catalytic reforming.

At present, however, acidity in catalytic reforming is controlled more precisely by addition of minute amounts of chloride and water over a  $\gamma\text{-Al}_2\text{O}_3$  based catalyst, and presently there are few uses of  $\eta\text{-Al}_2\text{O}_3$  as such.

Both aluminas possess defect spinel structures which are slightly tetragonally distorted. A spinel structure has the general formula  $\text{A}^{\text{II}}\text{B}_2^{\text{III}}\text{O}_4$  and the unit cell consists of 32 oxygen atoms in a close packed array. In the normal spinel the metal "A" atoms will occupy 1/8 of the tetrahedral sites and the metal "B" 1/2 of the octahedral sites. For  $\gamma$ - and  $\eta\text{-Al}_2\text{O}_3$  the

unit cell is built of 32 close packed oxygen atoms and the  $21\frac{1}{3}$  aluminium atoms are distributed over the 24 cation positions, leaving  $2\frac{2}{3}$  sites vacant.  $\gamma\text{-Al}_2\text{O}_3$  is a more ordered structure compared to  $\eta\text{-Al}_2\text{O}_3$  where stacking faults are very common. This is reflected in the values for the average Al-O bond lengths calculated from radial electron distributions, of 1.818-1.820Å for  $\gamma\text{-Al}_2\text{O}_3$  and 1.825-1.838Å for  $\eta\text{-Al}_2\text{O}_3$  (129). The cation distribution is slightly different for both modifications with a somewhat higher fraction of  $\text{Al}^{3+}$  ions present in tetrahedral positions in the case of  $\gamma\text{-Al}_2\text{O}_3$ .

The surface of aluminas terminate as OH groups. Infrared absorption reveals the existence of at least five types of OH groups, the properties of which depend on their immediate environment (21). These OH groups are potential Brönsted acid sites. The calcination process can also produce coordinately unsaturated Al atoms on the surface which can behave as Lewis acid sites. e.g.



Stronger acidity may be produced by deliberately incorporating halogens such as chloride or fluoride in the structure to catalyse reactions of various hydrocarbons as in catalytic reforming. The halide may be introduced inadvertently if a metal halogen compound such as  $\text{PdCl}_2$  or  $\text{H}_2\text{PtCl}_6$  is used in the catalyst preparation.

In practice aluminas are available in a wide range of surface areas ( $100\text{--}600 \text{ m}^2/\text{g}$ ) and pore sizes and are characterised by excellent thermal stability. Heating above  $850\text{K}$ , however, results in the closure of micropores and a reduction in surface area (130).

#### 1.12 SILICA

Pure silica,  $\text{SiO}_2$ , occurs in only two forms quartz and cristobalite. The silicon is always tetrahedrally bound to four oxygen atoms, but the bonds have considerable ionic character. In cristobalite the Si atoms are placed as are the C atoms in diamond with the O atoms midway between each pair. In quartz there are helices so that enantiomorphic crystals occur, and these may be easily recognised and separated mechanically (124).

From the natural silicas only kieselguhr is of

commercial importance. Kieselguhr is a naturally occurring finely divided silica consisting of the skeletal remains of diatoms. Depending on the deposit, it typically contains small amounts of alumina and iron as part of the skeletal structure. It is inexpensive, but for use in catalysts it must usually be purified by acid treatment. The surface area is usually in the range of 20-40  $\text{m}^2/\text{g}$  and a rather broad range of particle size exists, mostly in the order of 100nm or more (21).

Synthetic silicas are generally preferred in commercial applications since porosity and surface area can be controlled by the preparation conditions, for example, pH of precipitation, ageing of precipitate, speed of precipitation and calcination conditions. Commercial grade silicas are generally classified according to their preparation into:

(1) silica gels, which consist of three dimensional networks of contiguous particles of colloidal silica. They are prepared either by polymerisation of silicic acid or aggregation of colloidal silica. If the polymerisation is carried out at low pH values, high surface area hydrogels with lower pore volume are obtained. If, however, the precipitation is carried out at higher pH values, hydrogels of lower surface area and larger pore volume are formed (131). Upon dehydration

of the hydrogel "xerogel" forms, often accompanied by structural change. To minimise pore shrinkage and loss of surface area the water is often replaced with a liquid of lower surface tension before the drying process, or alternatively the water is removed at a temperature above its critical point, the so formed material is known under the name, "Aerogel".

Commercial material usually has a high surface area, as high as about  $700 \text{ m}^2/\text{g}$ . The average pore diameter is correspondingly very low, typically in the range 2.5 to 4 nm. These pores are significantly larger than those in zeolites and are substantially greater than the sizes of most reactant molecules of interest. Normally no macropores are present, in contrast with many aluminas that have macropores as well as high area. Consequently diffusion problems may be more severe with many silica gels than with available aluminas (21).

Silica gel is generally more difficult to form than alumina. It is not as mechanically rugged but is generally more inert. Commercial products typically contain small amounts of impurities such as sodium, calcium, iron and alumina in the concentration range of hundreds of parts per million (21).

## (2) colloidal silica

A variety of colloidal silicas are available

containing up to 40% wt.%  $\text{SiO}_2$  in the form of spherical non-porous particles. The colloid is stabilised by ammonium or sodium ions. It may be gelled by increasing temperature or by altering pH and since it is a good binder, it is useful in formulating catalysts.

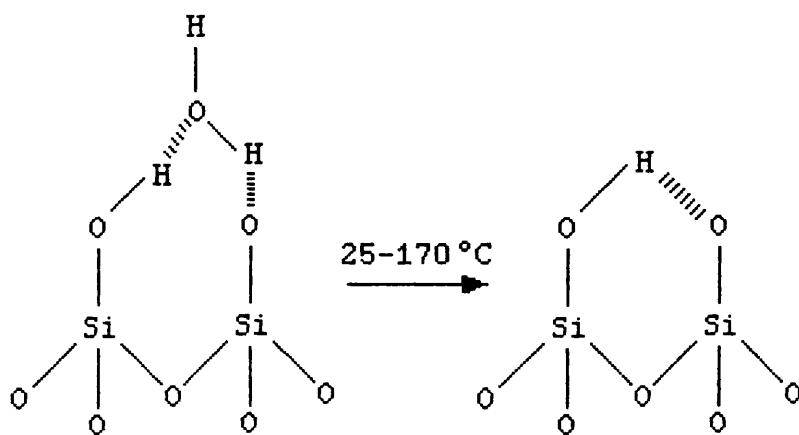
(3) fumed (pyrogenic) silica

A finely divided, non-porous and highly pure silica powder (Cabosil, Aerosil) is manufactured from high purity  $\text{SiCl}_4$ , which is hydrolysed in an oxygen - hydrogen flame. HCl formed is adsorbed on the silica surface, but can be removed by subsequent high temperature calcination. Particle sizes are about 40-50nm and surface areas about 200-400  $\text{m}^2/\text{g}$  (21).

High surface area silicas, prepared as gels or via the pyrogenic route, are x-ray amorphous and reasonably stable up to temperatures of 800K, however, significant surface area losses due to collapse of the internal pore structure are observed on heating above such temperatures.

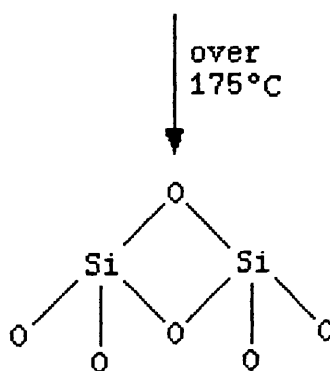
Silica is relatively unreactive towards  $\text{Cl}_2$ ,  $\text{H}_2$ , acids and most metals at ordinary or slightly elevated temperatures, but it is attacked by fluorine, gaseous HF, alkaline hydroxides and fused carbonyls (122).

The surface of silica is characterised by silanol groups (-SiOH). Since the silicon atoms on the surface of amorphous silica, are by definition, not in a regular geometrical arrangement; it is obvious that the hydroxyl groups attached to these silicon atoms will not be exactly equidistant from each other. They are therefore not all equivalent in their behaviour in adsorption or in chemical reactions. Several types of surface hydroxyls are shown below.

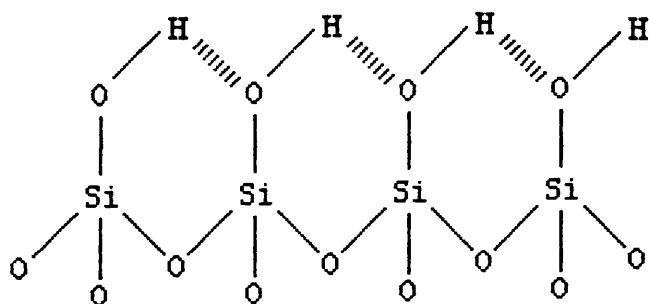


(a) vicinal hydrated

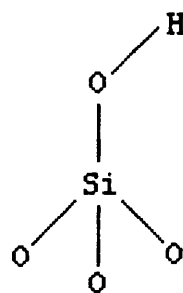
(b) vicinal anhydrous



(c) siloxane dehydrated



(d) hydroxylated surface



(e) isolated hydroxyl

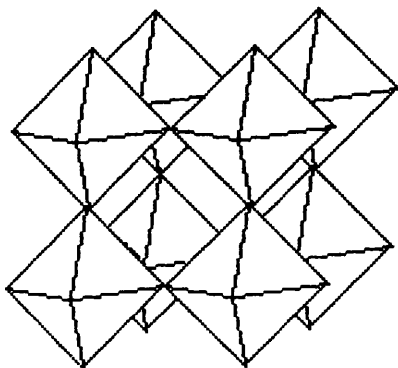
It is generally accepted that on the smooth, heat-stabilised amorphous silica that is fully hydroxylated there are 4-5 SiOH groups  $\text{nm}^{-2}$  which remain when the sample is dried at 120-150 °C (132).

The combination of useful properties of aluminas make them generally the first choice for carriers. However, active aluminas can dissolve or become soft and mushy under acidic conditions - conditions under which silica is stable. The relative inertness of silica may also be a significant factor. If adsorption of products or reactants on alumina is deleterious then the non-adsorptive character of silica may be an improvement (21).

### 1.13 MOLYBDENUM TRIOXIDE AND TUNGSTEN TRIOXIDE

We shall discuss the trioxides of Mo and W together but it should be noted that there is only a

general structural similarity between these two compounds. Although they are both based on the distorted rhenium trioxide structure, shown below, they are not isostructural.

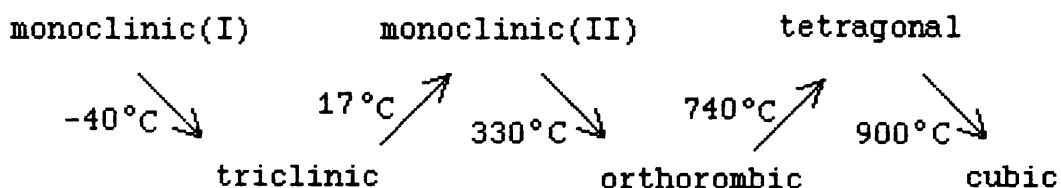


Structure of  $\text{ReO}_3$

Both  $\text{MoO}_3$  and  $\text{WO}_3$  are built of octahedral groups.  $\text{MoO}_3$  has a unique layer structure. Each octahedral  $\text{MoO}_6$  group shares two adjacent edges with similar groups and in a direction perpendicular to the plane the octahedra are linked through vertices. Three O atoms are therefore common to three octahedra, two are shared between two octahedra and the sixth is unshared. The octahedral coordination in  $\text{MoO}_3$  is highly distorted and this characteristic distortion of  $\text{Mo}^{\text{VI}}\text{O}_6$  groups is found with other compounds (e.g. heteropolyacids) (133).

$\text{WO}_3$  provides an extraordinarily complex example of polymorphism, for no fewer than eight phase transitions have been observed up to  $900^\circ\text{C}$ . All polymorphs apparently represent distortions of the cubic

ReO<sub>3</sub> structure.



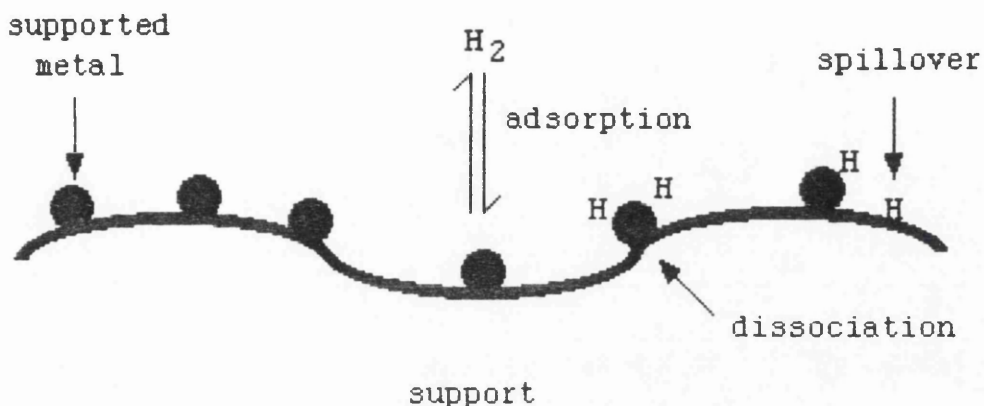
The metal atom is displaced from the centre of the O<sub>6</sub> octahedron resulting in bond lengths ranging from 1.7-2.0Å. A characteristic feature of these structures is the alternation of longer and shorter bonds along the axial directions (133).

Molybdenum trioxide is a white solid at room temperature but becomes yellow when hot and melts at 795°C to a deep yellow liquid. Tungsten trioxide is a yellow lemon solid with a melting point of 1200°C. They are not attacked by acids but dissolve in bases to form molybdate and tungstate solutions (124).

#### 1.14 HYDROGEN SPILLOVER

Described as, "an apparent metal-support interaction", by Sermon and Bond (134) the phenomenon of hydrogen spillover involves the dissociative adsorption of molecular hydrogen on metal sites. The atomic hydrogen so-formed migrates to another phase of the catalyst which contains hydrogen acceptor sites but which could not adsorb hydrogen directly under identical conditions. A schematic diagram of hydrogen spillover

is shown.



The phenomenon of spillover was first noticed in the 1950's (135) when it was observed by Kuriacose that the decomposition of  $\text{GeH}_4$  on a Ge film was increased by contact with a Pt wire used to measure the conductivity. Taylor proposed that the wire provided a "porthole" for the recombination of H to  $\text{H}_2$  (136).

The first direct experimental evidence for spillover was presented by Khoobiar in 1964, who documented that the formation of tungsten bronzes ( $\text{H}_x\text{WO}_3$ ) was possible at room temperatures for a mechanical mixture of  $\text{WO}_3$  with Pt/ $\text{Al}_2\text{O}_3$  (137). Sinfelt and Lucchesi postulated that reaction intermediates (presumably H) had migrated from Pt/ $\text{SiO}_2$  on to  $\text{Al}_2\text{O}_3$  during ethene hydrogenation (138).

Sermon and Bond (139) defined two types of

spillover; primary spillover, which occurs in systems where the initiating and accepting phases are in contact and secondary spillover which occurs when the phases are not in direct contact. Primary spillover is faster and more extensive than secondary spillover.

It is generally accepted that spillover depends on at least two prerequisites: a source of a spillage species (a group VIII metal, for example) and an acceptor (an oxide or active carbon, for instances). The phenomenon of hydrogen spillover is believed to take place via surface rather than gas phase transport of hydrogen species (140).

Spillover may result in a spectrum of changes in the non-metallic phase on to which it occurs. In the weakest sense, the spillover species (e.g.  $H_{3P}$  for spillover hydrogen) is transported across the surface of this phase as a two dimensional gas. It may exchange with similar surface species (e.g.  $OH + D_{3P} \longrightarrow OD + H_{3P}$ ). The spillover species may react with the surface (e.g.  $H_{3P} + M-O-M \longrightarrow M-O-H + M'$ ) which can result in the creation of surface defects and/or active sites. Further the bulk of the solid may be transformed into a different structure (as in the transformation of oxides to hydrogen bronzes). In each of these cases, the second phase is no longer inert. It is now serving to promote the inherent activity of the first phase. The

second phase is participating directly in the transport, exchange and reaction with the spillover species. In some cases it is able to become catalytically active on its own and thereby to participate directly in subsequent catalysis (141).

Most of the earlier work on hydrogen spillover was concerned with enhanced  $H_2$  adsorption (142,143) (expressed as H/Mt ratios, where H stands for the H atomic species adsorbed per total number of metallic atoms, Mt) usually at atmospheric pressure and temperatures of around  $200^\circ C$ . Values of H/Pt as high as 64 and 68 for Pt/ $Al_2O_3$  and Pt/ $SiO_2$  catalysts, respectively, have been quoted by Altham and Webb (144), while H/Pt ratios between 3 and 277 have been calculated by Sermon and Bond (139) for reverse spillover involving the two platinised bronzes  $H_xWO_3$  and  $H_xMoO_3$ .

The kinetics of the chemisorption of spillover hydrogen species have been fully detailed from a mathematical and physical point of view for carbon as well as for alumina by Robell et al. (145), and Kramer and Andre (146) respectively. Both groups concluded that surface diffusion was the rate-determining step in the overall process of hydrogen spillover. Stepping-stone molecules such as water, alcohols or even grease, may be adsorbed on the support close to the edge of the metal

particles to facilitate transport of H atoms across the phase boundary. Carbon present on the surface of the catalyst can also act as a bridge between the metal and the support, facilitating hydrogen spillover (141).

Spillover hydrogen can undergo a reverse migration process whereby the atomic hydrogen migrates back to the metal particles where it can either combine to form molecular hydrogen or react with another hydrogen acceptor such as  $O_2$ , pentene, ethene etc..

In the majority of cases if spillover hydrogen is to react it must first undergo reverse spillover from the support to the metal. Sermon and Bond (147) titrated hydrogen adsorbed on silica supported platinum using pent-1-ene. They found that the pent-1-ene first reacted with the hydrogen chemisorbed on the platinum to form n-pentane. Only after all the platinum-bound hydrogen had reacted did the hydrogen on the silica migrate back to the platinum where it reacted with 1-pentene to form n-pentane and the pent-2-enes.

It has been shown that the metal content above 0.8% does not influence the spillover process. When the metal loadings are less than 0.00008% no spillover occurs even as primary spillover. For Pt, spillover starts to become significant for loadings of 0.03% (139). The rate of hydrogen spillover was also found to

depend more on the nature of the initiating phase (148). An example of this is the spillover of hydrogen to carbon which only takes place at temperatures above 350°C (145) compared to room temperature for Pt to  $\text{WO}_3$  or  $\text{MoO}_3$ .

Boudart et al. (149) demonstrated the requirement for the presence of water or some other proton acceptor during the spillover process. Levy and Boudart (150) studied a variety of co-catalysts with varying proton affinities and concluded that a solvated proton was formed on the surface of the metal. More recently, Ambs and Mitchell (151) studied the effects of water on the spillover of hydrogen on platinum-alumina. They concluded that when water was present in the catalyst, it reacted with the alumina to form surface hydroxyls which acted as bridges enabling H-atoms to migrate further (secondary spillover) than if no water had been present. Reverse or back-spillover (primary as well as secondary) is hindered by  $\text{H}_2\text{O}$  (139).

Hydrogen spillover on to irreducible oxides such as  $\text{Al}_2\text{O}_3$  and  $\text{SiO}_2$  does not seem to precipitate reduction even at temperatures of 500°C. The exchange of deuterium with surface OH groups can be used to measure the extent of hydrogen spillover on these supports (152) which does not appear to be greater than 1% of the surface and is therefore far less than the number of

surface hydroxyls (153). When hydrogen spills over on to reducible oxides such as  $\text{MoO}_3$  and  $\text{WO}_3$ , hydrogen metal bronzes can be formed at or just above ambient temperature (147). A fuller description of the formation, structure and reactivity of hydrogen bronzes is given in section 1.15.

Spillover of hydrogen on to partially reducible oxides such as  $\text{TiO}_2$  can lead to the formation of  $\text{Ti}^{3+}$  and  $\text{OH}^-$  ions for  $\text{Rh/TiO}_2$  or  $\text{Pt/TiO}_2$ . Partial reduction of the support followed by its migration to the metal particles can give rise to metal-support interactions which alter the chemisorption and catalytic properties of the catalyst (154).

Teichner et al. (155) found that hydrogen was adsorbed on alumina in the presence of a  $\text{Ni/Al}_2\text{O}_3$  catalyst. After the catalyst was removed, ethene in a hydrogen-ethene mixture was converted into ethane. The amount of ethane formed was found to be much higher than the amount of hydrogen initially adsorbed on the alumina. The authors, concluded, therefore, that the reaction was catalytic and that the reaction used hydrogen from the gas phase instead of a simple addition of the hydrogen pre-adsorbed on the alumina to the ethene. The authors found that spillover hydrogen could be removed by evacuation at room temperature, implying that spillover H or D was weakly bound to the surface.

Lenz and Conner (156) found that silica could be activated using hydrogen spillover without direct contact between the silica and the supported metal. Hydrogenation and exchange activity was induced which was found to be independent of the metal. The induced catalytic activity was an activated process, which required high temperatures and long contact times. The hydrogenation mechanism was found to be similar to that on metal oxides and, as such, the molecular identity of the reacting hydrogen was retained.

The presence of spillover hydrogen on  $\text{Al}_2\text{O}_3$  and  $\text{SiO}_2$  can have an important role in determining the catalytic activity in reactions involving hydrogen and hydrocarbons. For instance,  $\gamma\text{-Al}_2\text{O}_3$  and  $\text{SiO}_2$  both show an induction period in the hydrogenation of a first dose of ethene at  $180^\circ\text{C}$  which has been attributed to the presence of spiltover hydrogen (157, 158).

Altham and Webb (144) investigated the behaviour of  $^{14}\text{C}$ -ethene,  $^{14}\text{C}$ -propene and tritium on platinum supported on alumina and silica. They found evidence which indicated that the hydrogen migration between the metal and the support was of significance. The rate of hydrogen exchange between the gas phase and the tritiated catalyst was found to be fast relative to the rate of reaction of the adsorbed hydrocarbon with

hydrogen.

### 1.15 HYDROGEN METAL BRONZES

The term bronze was originally used by Wohler in 1825 (159) to describe  $\text{Na}_x\text{WO}_3$ , but is now used to describe a variety of crystalline phases of transition metal oxides.

Hydrogen metal bronzes,  $\text{H}_x\text{MO}_3$  can be formed from metal oxides with an incomplete d shell and for which the nd electron energy is higher than the (n+1)p electron energy (160). Example of oxides which form hydrogen metal bronzes are molybdenum (VI) oxide,  $\text{MoO}_3$ , tungsten (VI) oxide,  $\text{WO}_3$  and vanadium (V) oxide,  $\text{V}_2\text{O}_5$ .

The addition of small quantities of metal catalysts, such as Pt or Pd has been shown to be dramatically lower the temperature of reduction of oxides such as  $\text{MoO}_3$ ,  $\text{WO}_3$  and  $\text{V}_2\text{O}_5$  (161). For example, for Pd/ $\text{MoO}_3$  the reduction temperature of  $\text{MoO}_3$  is lowered by 400°C by formation of atomic hydrogen on the palladium which then spills over on to the  $\text{MoO}_3$  resulting in its reduction. The atomic hydrogen produced by spillover can diffuse inside the host lattice, with or without the help of a co-catalyst and lead to the formation of hydrogen metal bronzes.

The hydrogen metal bronzes formed in this way

are insertion compounds and exhibit metallic conductivity (133). In hydrogen tungsten bronzes,  $H_xWO_3$ ,  $x$  lies in the range  $0 < x < 0.6$ , whereas for the analogous hydrogen molybdenum bronzes  $H_xMoO_3$ ,  $0 < x < 2$  (142). The bronzes formed by hydrogen spillover are  $H_{0.4}WO_3$  and  $H_{1.6}MoO_3$  (163). The bronzes are formed topotactically, characterised by the fact that they are formed without any major structural change to the layer lattice. Dickens et al. (164) found the X-ray powder patterns of the  $H_xMoO_3$  bronze closely resembled that of  $MoO_3$  from which they concluded that the hydrogen had been readily inserted into the parent oxide with little crystallographic rearrangement.

By carrying out elastic and inelastic neutron studies of hydrogen metal bronzes Dickens et al. (164) were able to conclude that hydrogen was present as -OH groups in  $H_{0.4}WO_3$  and  $H_{0.34}MoO_3$ . However, for bronzes with a higher hydrogen content, they found evidence that hydrogen was present in the form of  $-OH_2$  groups. This was confirmed by solid state NMR carried out on  $H_{0.36}MoO_3$  and  $H_{1.71}MoO_3$  (165). On the basis of these results, Slade et al. (165) suggested that  $H_{0.36}MoO_3$  and  $H_{0.4}WO_3$  should be formulated as oxide hydroxides  $MO_{3-x}(OH)_x$ . The molybdenum and tungsten oxide bronzes are believed to have analogous structures at these similar hydrogen contents.

Ritter et al. (166) carried out NMR studies on hydrogen molybdenum bronzes prepared electrochemically. They found that for  $x < 0.85$  in  $H_x MoO_3$  almost all the hydrogen was intralayer, lying along the zig-zag line connecting vertex sharing oxygen atoms of the  $MoO_6$  octahedra. For higher values of  $x$ , the hydrogen starts to occupy interlayer positions coordinated with terminal oxygen groups at atoms in the Van der Waals gap. For  $H_{1.66} MoO_3$  about half of the protons reside in the interlayer positions (166).

Structural modifications of  $MoO_3$ , can take place during the formation of  $H_{1.6} MoO_3$  from spillover hydrogen. When the hydrogen atoms enter the  $MoO_3$  lattice, there is a tendency for the oxide to cleave in planes parallel to its  $c$  crystallographic axis (167). This results in a increase in surface area, but it also decreases the contact between the metal particles, for example platinum, and the oxide layers. There is also a tendency for rather large clusters of metal particles to form. The surface area can increase from around  $1 \text{ m}^2/\text{g}$  for  $MoO_3$  by a factor of two or three (160).

$H_x WO_3$  can be decomposed under vacuum or by thermal treatment. Crystalline hydrogen tungsten bronzes are stable in vacuo to temperatures greater than 400K (167). However, they are unstable in air with

respect to oxidation. Over the temperature range 470-670K, decomposition of  $H_xWO_3$  takes place with the formation of both  $H_2$  and  $H_2O$  as gaseous products, indicating that decomposition and disproportionation occur simultaneously at elevated temperatures (168).

Hydrogen molybdenum bronzes undergo dehydrogenation and dehydration under vacuum at temperatures higher than  $120^\circ C$ , and in flowing  $H_2$  at temperatures higher than  $100^\circ C$  (168). Water molecules are formed from inserted hydrogen atoms and lattice oxygen atoms. The removal of lattice oxygen atoms in the form of water is accompanied by structural modification. As a result, the external layers of the oxide become partially amorphous. Depletion of hydrogen affects the outer layers first.

The hydrogen metal bronzes  $H_xMO_3$  ( $M = Mo$  or  $W$ ) formed by hydrogen spillover may become catalytically active. Sermon and Bond (147) found that the chemical stability and reactivity of hydrogen molybdenum bronze,  $H_{1.6}MoO_3$ , and hydrogen tungsten bronze,  $H_{0.5}WO_3$ , was different. They found that it was more difficult to remove hydrogen from  $Pt/H_{1.6}MoO_3$  than from  $Pt/H_{0.5}WO_3$  by reverse spillover using oxygen or other hydrogen acceptors.

It is believed that for spillover hydrogen to

react, it must first undergo the reverse spillover from the support back to the metal. Removal of hydrogen from the hydrogen metal bronzes must occur via reverse spillover since  $H_xWO_3$  alone is stable in air at ambient temperatures (143), whereas the introduction of air into a mixture of Pt/ $Al_2O_3$  and  $WO_3$  at ambient temperatures leads to reoxidation of the bronze (168). It is generally believed that spillover hydrogen on the support is rather unreactive (169).

The rate of hydrogenation of hydrogen acceptors such as ethene or oxygen gives a measure of the rate of reverse spillover. The rate depends on the concentration of spillover hydrogen, its stability on the support and the degree of contact between the metal and the hydrogen acceptor phase (152). The rate of reverse spillover is lower than the rate of spillover (166).

$H_{1.6}MoO_3$  containing Pt reacts with ethene at  $160^\circ C$  to form ethane. The reaction rate depends on the platinum content, and can be increased by the presence of gaseous hydrogen. The platinum particles are regarded as "gates" by which the H-atoms leave the host oxide by a reverse spillover process.

The platinum particles are also believed to be the catalytic sites (166,167) which are in contact with

the bronze, which thereby acts as a hydrogen reservoir (167). For the hydrogenation of ethene to ethane, about 30% of the initial hydrogen content can be removed whereas about 90% of the initial hydrogen content can be removed by treatment with oxygen (167).

Benali et al. (170) found that hydrogenation of ethene on  $H_{1.6}MoO_3$  took place in the absence of the Pt/ $Al_2O_3$  required to produce the bronze. Reaction commenced at ca. 80°C and resulted in the transformation of  $H_{1.6}MoO_3$ . From this, the authors concluded that palladium or platinum particles did not need to be present to act as gates through which the H-atoms could leave the host lattice to hydrogenate ethene. If gaseous hydrogen is present,  $H_{1.6}MoO_3$  can catalyse the hydrogenation of ethene without structural modifications (170).

Fripiat et al. (166) found that for the hydrogenation of ethene over  $H_xMoO_3$ , the reaction rate increased with increasing hydrogen pressure indicating that the gaseous hydrogen was consumed before the spillover hydrogen.

## CHAPTER 2

### OBJECTIVES OF THE PRESENT STUDY

As hydrogenolysis is a "structure sensitive" reaction (section 1.8) the surface environment of the catalyst has a great influence on the activity and selectivity of the reaction. Although the reaction has been greatly studied many aspects of its mechanism are still uncertain, such as the reasons for the activity and selectivity differences between metals and the relation between the inverse dependence of hydrogen pressure on the reaction rate and the identity of the surface reaction intermediates.

Simple alkanes can be used as "archetype" molecules for studying hydrogenolysis reactions as they allow comparisons between possible 1,2, 1,3 and 1,4 adsorptions of hydrocarbons on the metal function of the catalyst.

While the hydrogenolysis reaction is primarily related to the metal function of the catalyst, the simple bond shift isomerisations of n-butane and iso-butane can follow either a bifunctional mechanism involving acid support sites or a metal-only rearrangement.

The main objective of the work described in this thesis is to examine the hydrogenolysis and isomerisation reactions of ethane, propane, iso-butane and n-butane over a range of well characterised supported (alumina, silica, molybdenum trioxide and tungsten trioxide) platinum and nickel catalysts and to relate the activities, selectivities and kinetic parameters of the reactions to the metal, support and the physical characteristics of the catalysts.

To achieve this objective the following aspects of the reaction were studied;

(i) the relation between the hydrogenolysis activation energies and the carbon chain lengths of the hydrocarbon feedstocks.

(ii) the relation between the selectivity during hydrogenolysis and the metal function of the catalyst.

(iii) the relation between the selectivity for isomerisation over hydrogenolysis and the catalyst metal and support.

(iv) the hydrogen pressure effect on the rate of hydrogenolysis of saturated and unsaturated hydrocarbons.

## CHAPTER THREE

## CHAPTER 3

### EXPERIMENTAL

#### 3.1 INTRODUCTION

A range of platinum and nickel catalysts with varying supports were prepared and extensively characterised by the Glasgow, Hull, ICI group (171). The catalysts were prepared using impregnation, co-crystallisation and metal-vapour deposition methods using silica, alumina, tungstia and molybdena supports.

The characterisations carried out by the group included elemental analyses, surface area measurements, thermogravimetric analyses (TGA), temperature programmed reduction (TPR), electronic spectroscopy and high resolution transmission electron microscopy (HRTEM). A summary of some of these results is given in the results chapter (Section 5.1).

This work concentrates on the hydrogenolysis reactions of simple alkanes (ethane, propane, iso-butane and n-butane) and other hydrocarbons (ethene, propene) over the series of impregnated catalysts. The activity, selectivity and kinetic parameters of the reactions were

examined with respect to the metal, support and physical characterisation of the catalysts.

Carbon monoxide chemisorption and HRTEM experiments were also carried out to complete the characterisation of the nickel catalyst samples.

## 3.2 CATALYST PREPARATION

### 3.2.1 Materials

Hexachloroplatinic acid,  $H_2PtCl_6$  (Johnson Matthey Chemicals Ltd.) and nickel(II) hexahydrate  $Ni(NO_3)_2(H_2O)_6$  (ICI C&P Ltd.) were used to prepare the catalysts used in this study. The supports used were silica (M5 Cab-o-sil), alumina (Degussa Aluminium Oxid C), molybdenum(VI) oxide (BDH Analar grade 99.5%) and tungsten(VI) oxide (BDH Analar grade 99.5%).

### 3.2.2 Preparation

Each of the catalysts used in this study were prepared by the Glasgow, Hull, ICI group (171). The platinum catalysts were prepared by dissolving hexachloroplatinic acid in 600ml of deionised water in a round bottomed flask. The required support was then added and mixed until the suspension began to gel, at which point further deionised water (ca. 500ml) was

added to promote mobility. This process was repeated until all the support had been introduced, the total volume of water required being 2.5l. The flask was then attached to a Buchi rotary evaporator and the water slowly removed at 353K under a partial pressure of dry nitrogen for 48 hours, producing a free flowing powder.

A similar impregnation procedure was adopted for the preparation of the nickel catalysts using nickel(II) nitrate hexahydrate as a precursor (171).

Seven catalysts were prepared by this impregnation method,

Pt/Al <sub>2</sub> O <sub>3</sub>	Ni/Al <sub>2</sub> O <sub>3</sub>
Pt/SiO <sub>2</sub>	Ni/SiO <sub>2</sub>
Pt/MoO <sub>3</sub>	Ni/MoO <sub>3</sub>
	Ni/WO <sub>3</sub>

Before use the finely divided catalyst powders were pressed into discs, crushed and sieved between 180 and 500µm meshes. This avoided internal diffusion limitations and blockage of the reactor tubes (172).

### 3.3 CATALYST CHARACTERISATION

#### 3.3.1 Gas chemisorption apparatus

Carbon monoxide chemisorption experiments were carried out on the nickel catalysts using the pulse-flow gas chemisorption apparatus shown schematically in Fig.1. The apparatus consisted of a vacuum section, a flow line and a sample loop.

In the vacuum section, the vacuum was maintained at pressures  $\leq 10^{-4}$  torr by means of a mercury diffusion pump backed by a rotary oil pump. The vacuum was measured using a Pirani Gauge (Speedivac Pirani Type Vacuum Gauge, Edwards High Vacuum Ltd.). A pressure transducer was used to measure the pressure of carbon monoxide (C.P. Grade 99.5% B.O.C.) admitted to the vacuum section manifold.

The sample loop consisted of three spring loaded glass taps. By following the procedure shown in Fig.2 a known pressure of CO gas could be injected into the carrier gas flow of H<sub>2</sub>.

The reactor section is shown in Fig.3. The catalyst sample (typically 0.1500g) was supported on a silica sinter. The reactor temperature was measured with a Cr/Al thermocouple inserted level with the catalyst sample and attached to a Comark electronic thermometer. The reactor section was heated by a Watlow furnace controlled by a Variac variable transformer.

The CO pulses were detected by a thermal conductivity detector (TCD), with a reference side attached to the initial gas stream and a sample side attached to the reactor effluent stream.

Fig. 1 Gas Adsorption Apparatus  
(Schematic Diagram)

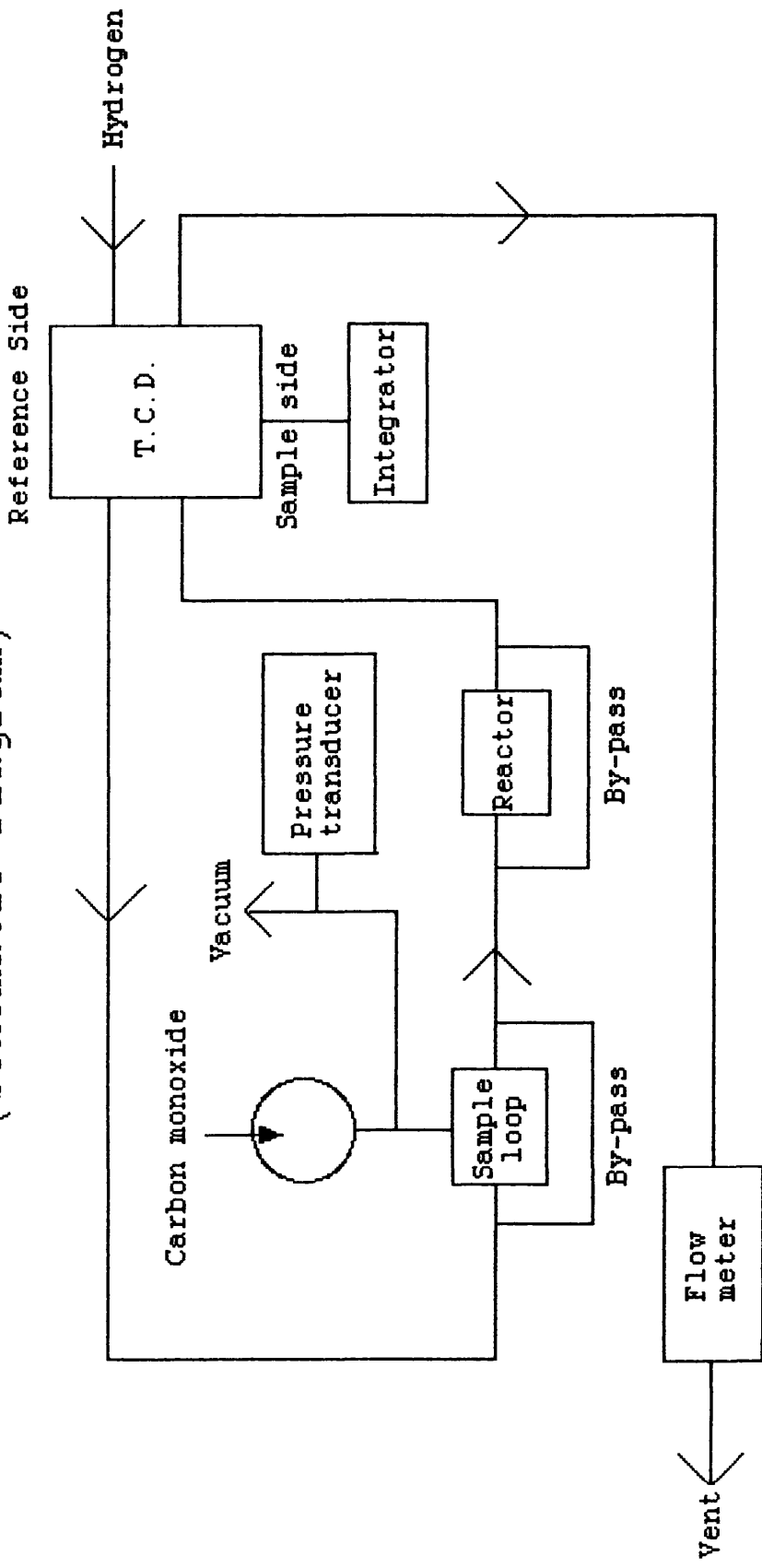
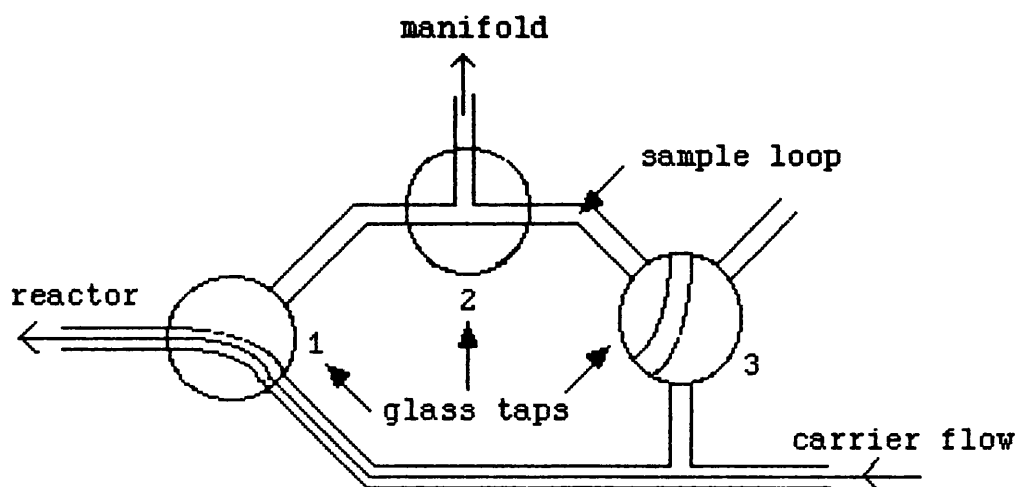
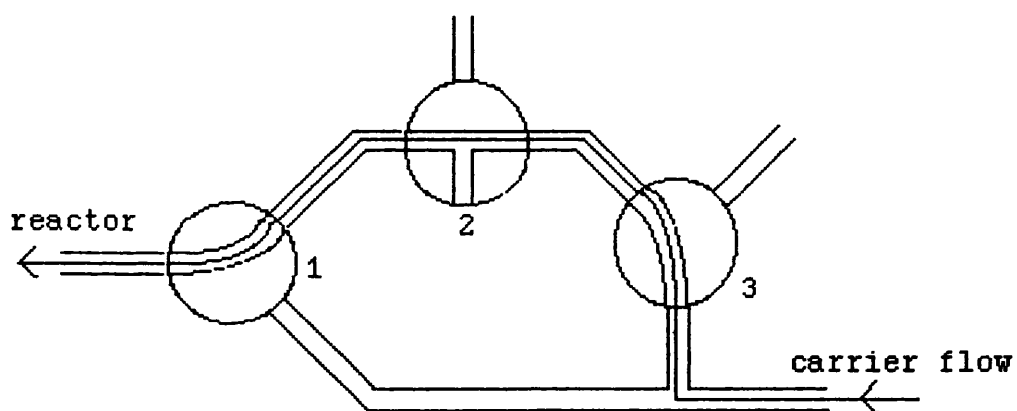


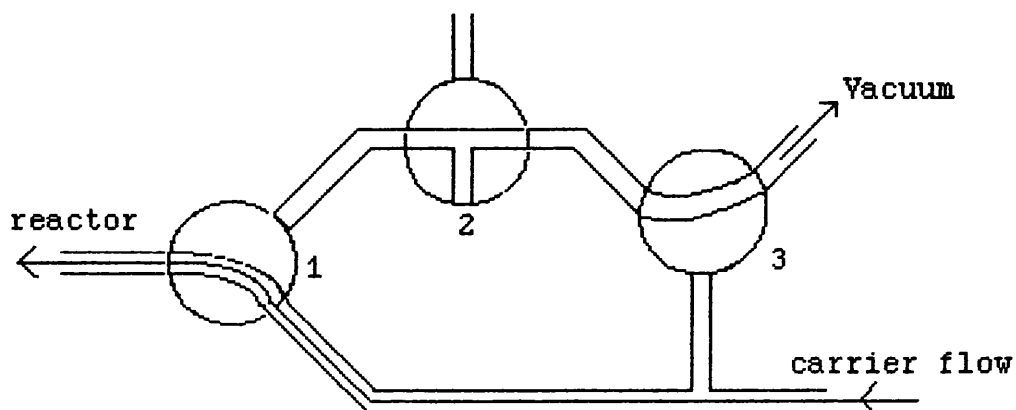
Fig.2 CO Sample Loop



A. loading sample

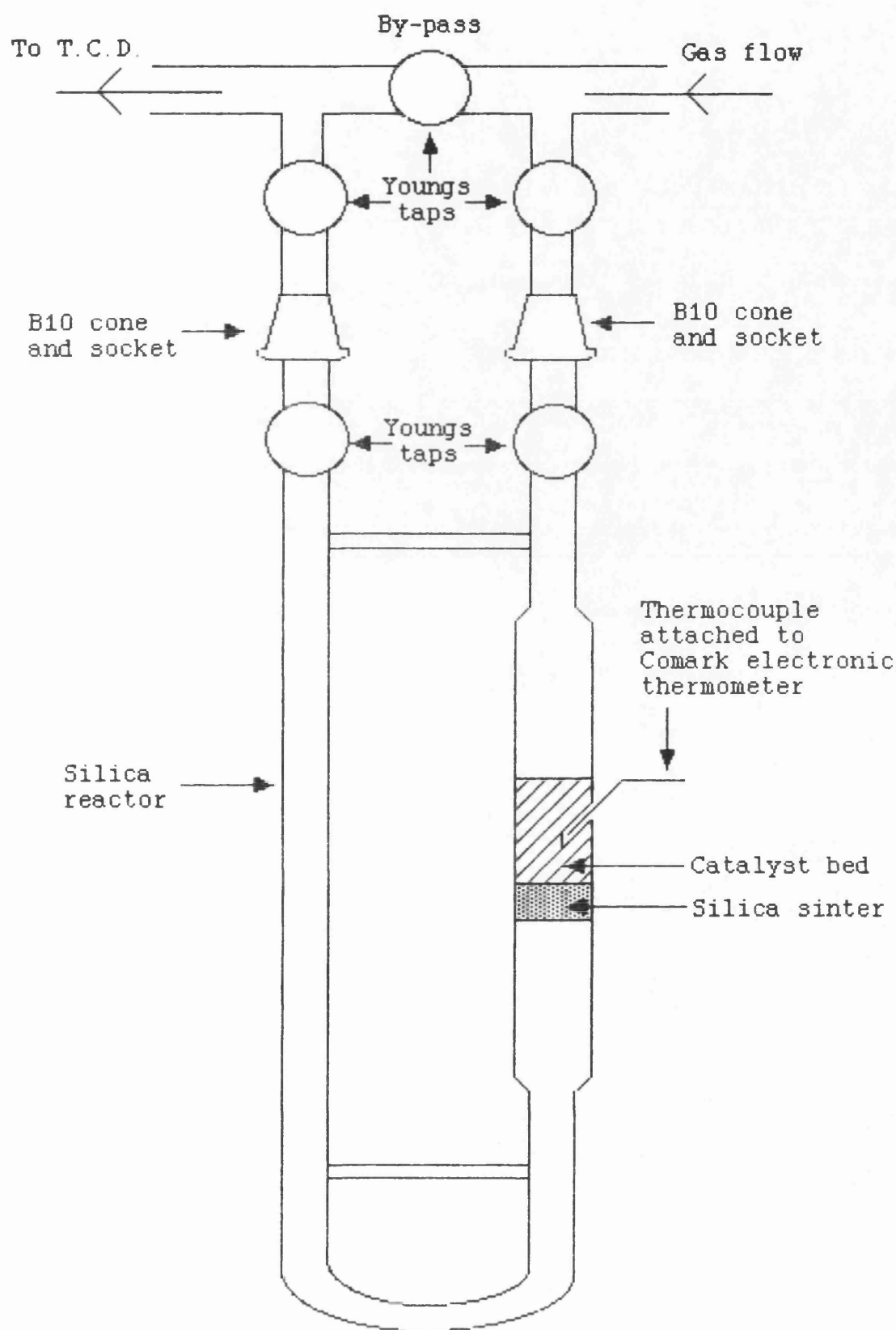


B. injecting sample



C. evacuating sample loop

Fig.3 Reactor Section



### 3.3.2 Standard reduction

A standard reduction procedure was used to activate the catalyst samples for both the carbon monoxide chemisorption experiments and the hydrogenolysis reactions in the microreactor system (section 3.5). This was as follows,

(i) the catalyst sample was heated to 420°C at a heating rate of 10° per minute in a flow of hydrogen of 40 ml min<sup>-1</sup>.

(ii) the sample was held at 420°C for three hours in the flow of hydrogen to complete the reduction.

### 3.3.3 Carbon monoxide chemisorption procedure

After a standard reduction (section 3.3.2) the catalyst sample (typically 0.1500g) was cooled to 0°C in a flow of hydrogen of 60 ml min<sup>-1</sup>. With the reactor on bypass three fixed pulses of carbon monoxide (typically 5 torr) were injected into the hydrogen carrier stream and passed through the thermal conductivity detector (TCD) to produce a background trace. Fixed pulses of carbon monoxide were then injected over the reduced catalyst sample in the flow of hydrogen. The TCD

detected the carbon monoxide that was not chemisorbed by the catalyst sample. The initial carbon monoxide pulses were almost entirely adsorbed or produced the smallest peaks. Subsequent pulses produced increasingly large peaks. Pulsing was continued until three sequential peaks of the same height were obtained, indicating that the catalyst was completely saturated at the metal surface sites with a monolayer of chemisorbed species.

#### 3.3.4 Transmission electron microscopy

High resolution transmission electron microscopy (HRTEM) was carried out on the platinum (171) and nickel catalysts using a Jeol 200C instrument. Particle size distributions for the platinum catalysts as determined by measurement of these electron micrographs are shown in the results section (section 5.1.6). The nickel electron micrographs are discussed in section 5.2.2.

### 3.4 MICROREACTOR SYSTEM

#### 3.4.1 Gas supply

The gas supply for the microreactor system was purified in the following manner. The He (Grade A, British Oxygen Company, hereafter referred to as B.O.C.) was passed through a molecular sieve (Prolab 4A) to remove traces of water, a Pd/WO<sub>3</sub> trap to remove oxygen and a 15 micron molecular sieve. The Pd/WO<sub>3</sub> was prepared by impregnating a Pd/Cl<sub>2</sub> solution onto WO<sub>3</sub> and was activated by a flow of H<sub>2</sub> at room temperature. The H<sub>2</sub> (B.O.C.) was passed through a Pd/WO<sub>3</sub> trap and a 15 micron molecular sieve. The ethane, propane, isobutane, n-butane (all B.O.C. pure grade N.2.0), propene (99% BDH Laboratory gas service) and ethene (B.O.C. Research Grade) were similarly purified with a Pd/WO<sub>3</sub> trap and a 15 micron molecular sieve.

#### 3.4.2 Microreactor

The microreactor system is shown schematically in Fig.4. It was constructed from 1/8" stainless steel tubing and was designed to produce a controlled flow of helium, hydrogen and a hydrocarbon over a small charge of catalyst.

After purification (section 3.4.1) the gases were passed through forward pressure handling. The He and hydrocarbon supplies were regulated by Hale-Hamilton pressure regulators (Type L15 MK1 He/CO 15-150 psi), the H<sub>2</sub> supply by a Brooks pressure regulator (8607 0-10 bar). These forward pressures were shown on Budenburg pressure gauges (0-300 psi).

The gas flow rates were controlled by separate mass flow controllers. The He by a Brooks controller (5850e N<sub>2</sub> 0-100sccm), the H<sub>2</sub> by a Unit controller (UFC 1020 CO 0-50sccm) and the hydrocarbon also by a Unit controller (UFC 1020 N<sub>2</sub> 0-100sccm). A Unit Control (URS-100-5) was used as a multiple readout and power supply for all these controllers.

After mixing the gases entered the reactor section shown in Fig.5. The reactor tube was constructed from a 1/4" glass lined steel tube with the catalyst sample (typically 0.1500g) supported on a glass wool plug. The reactor temperature was measured with a Cr/Al thermocouple inserted level with the catalyst sample and attached to a Comark electronic thermometer. This reactor section was heated by a Watlow furnace controlled by a Variac variable transformer.

A gas sample valve (Fig.6) was used to send

fixed volumes of the reactor effluent stream to a Perkin Elmer Gas Chromatograph 8500. By turning the sample valve from position A to position B, a fixed volume of the effluent stream was sent through a column to a flame ionisation detector (FID).

A bubble flow meter was used to measure the effluent flow rate before going to exhaust.

Fig. 4 Micro-reactor system  
(schematic diagram)

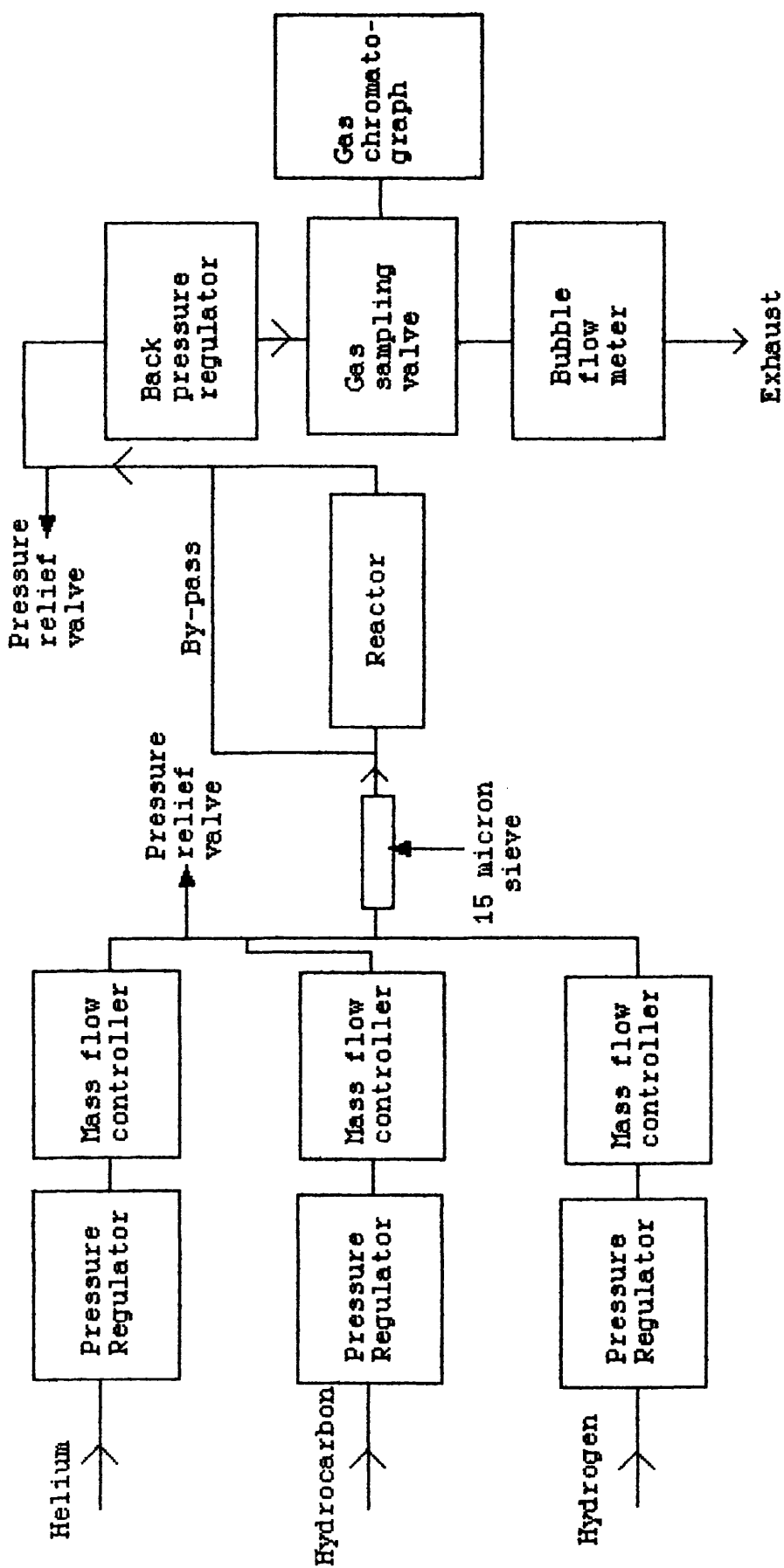


Fig.5 Reactor section

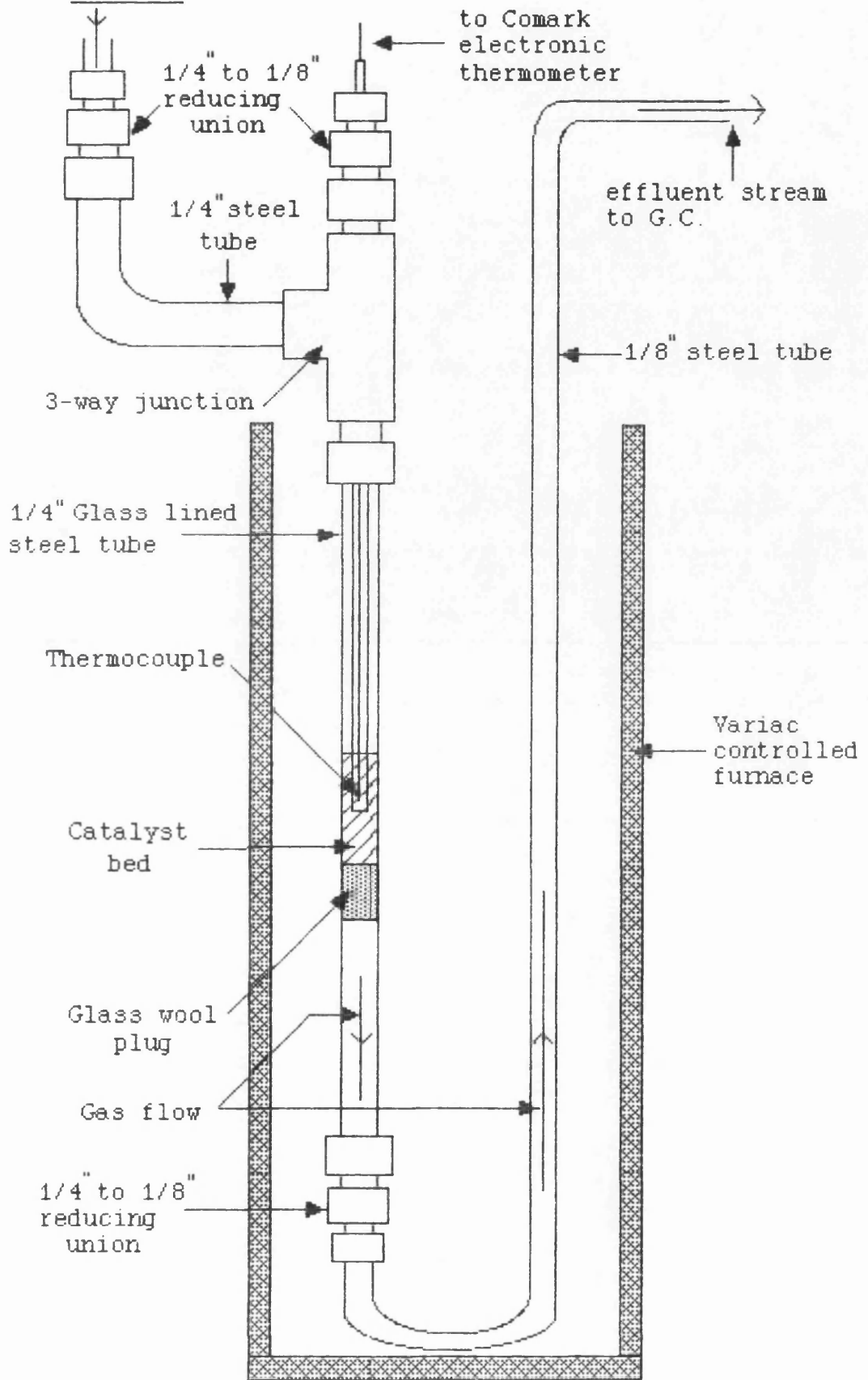
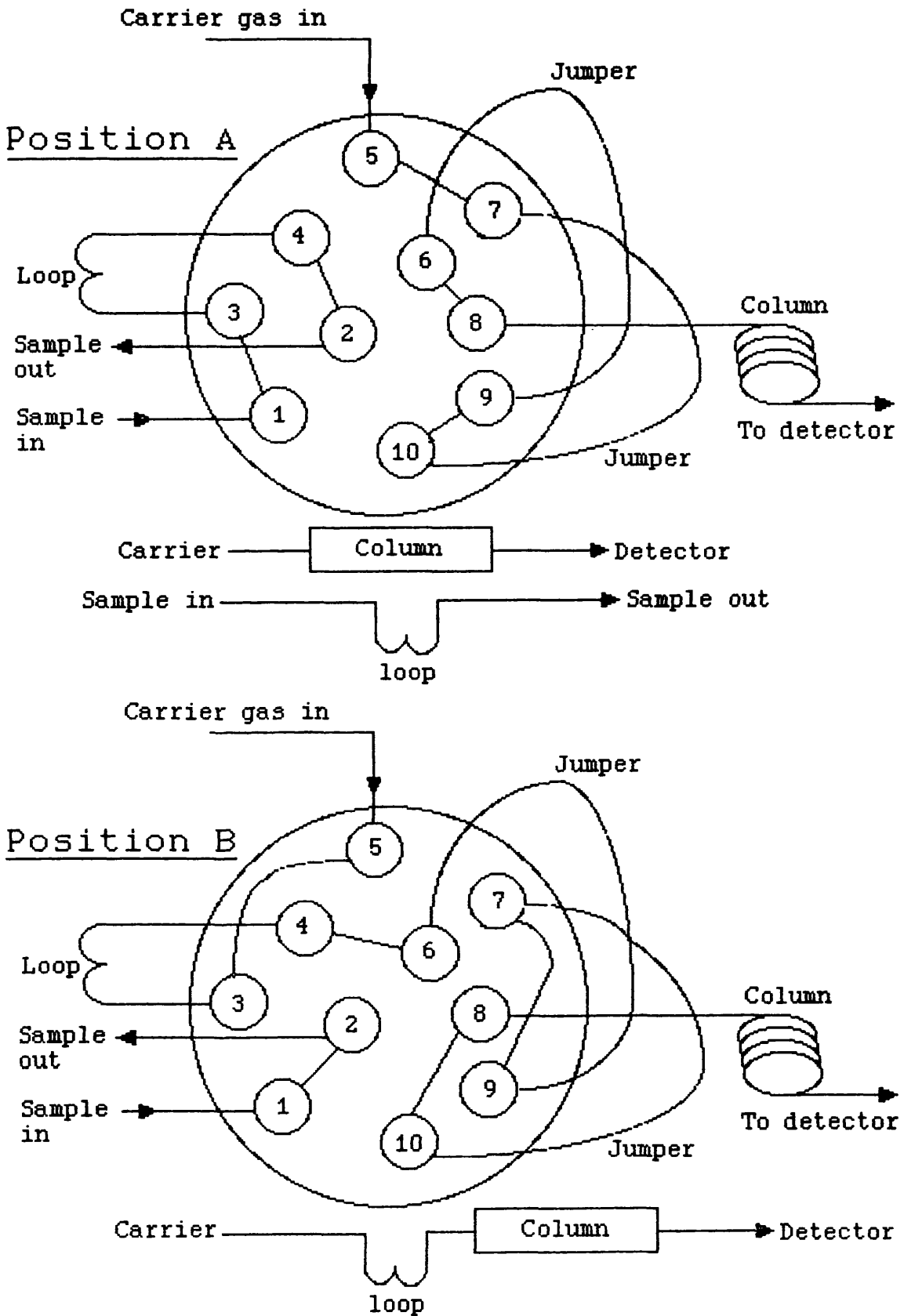


Fig. 6 Gas Sample Valve



### 3.4.3 Mass flow control

Mass flow controllers were used in the microreactor system (section 3.4.2) to produce the desired flows of hydrogen, helium and hydrocarbon.

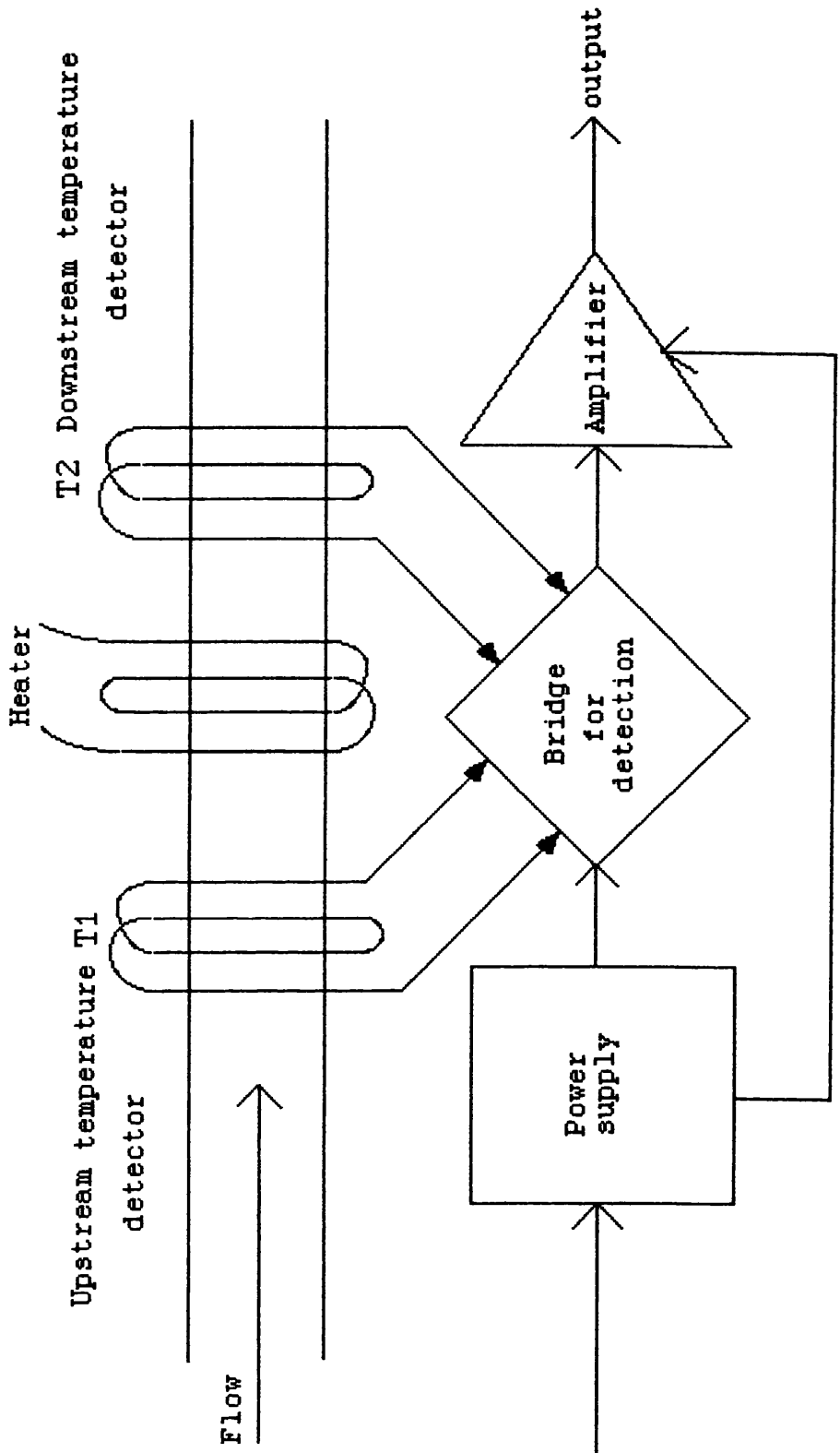
Mass flow control differs from volumetric flow control in that it measures the number of molecules in the process gas rather than the volume of the gas. This produces a more consistent measurement of gas flow as the mass of the gas is not affected, as volume, by such environmental factors as temperature and pressure.

Mass flow controllers consist of three basic units, a flow sensor, a control valve and an electronic control system. The flow sensor works by a thermodynamic process. Heat is directed to the midpoint of a flow carrying sensor tube (Fig.7). Resistance temperature elements ( $T_1$  and  $T_2$ ) are placed at equidistant points upstream and downstream of the heat input. With flow the gas stream carries an increasing amount of heat towards the downstream element,  $T_2$ , from the upstream element,  $T_1$ . A temperature difference, proportional to the amount of gas flow is interpreted by a bridge circuit and an amplifier provides the output to the controller readout. The power supply to each controller can be adjusted between 0 and 100% to produce

a range of flows.

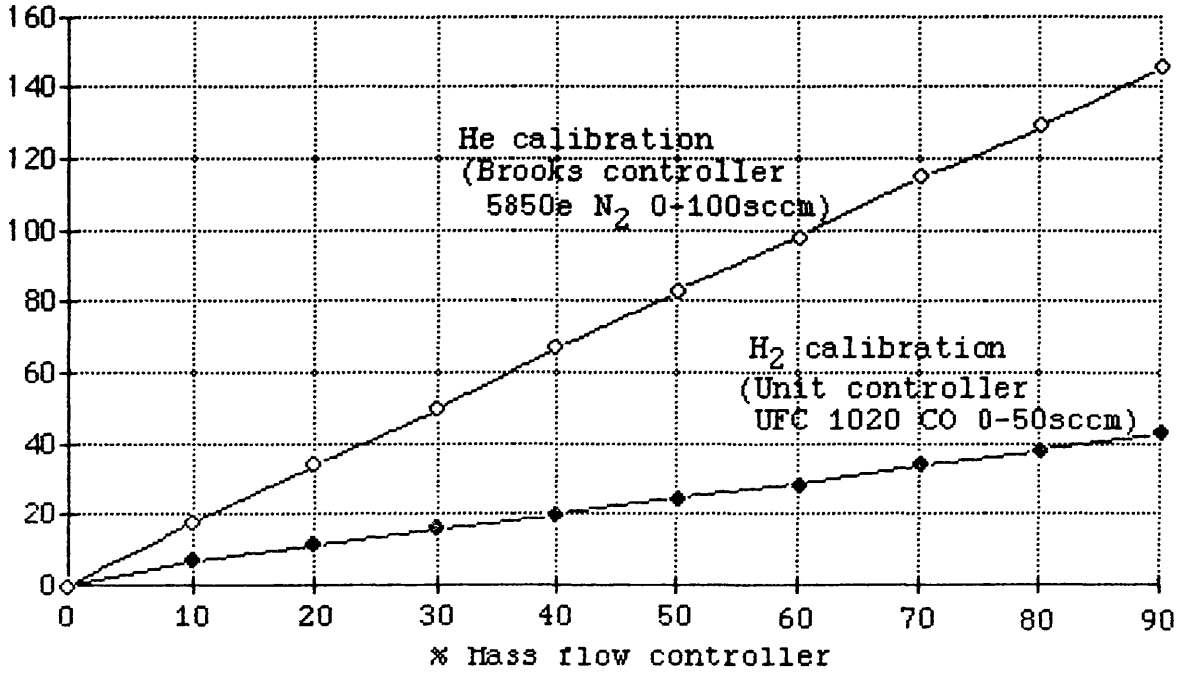
A bubble flow meter attached to the reactor effluent stream was used to calibrate these flows for each reactant gas (graphs 1 and 2).

Fig. 7 Mass flow controller - Flow sensor



Flow Rate  
(mlmin<sup>-1</sup>)

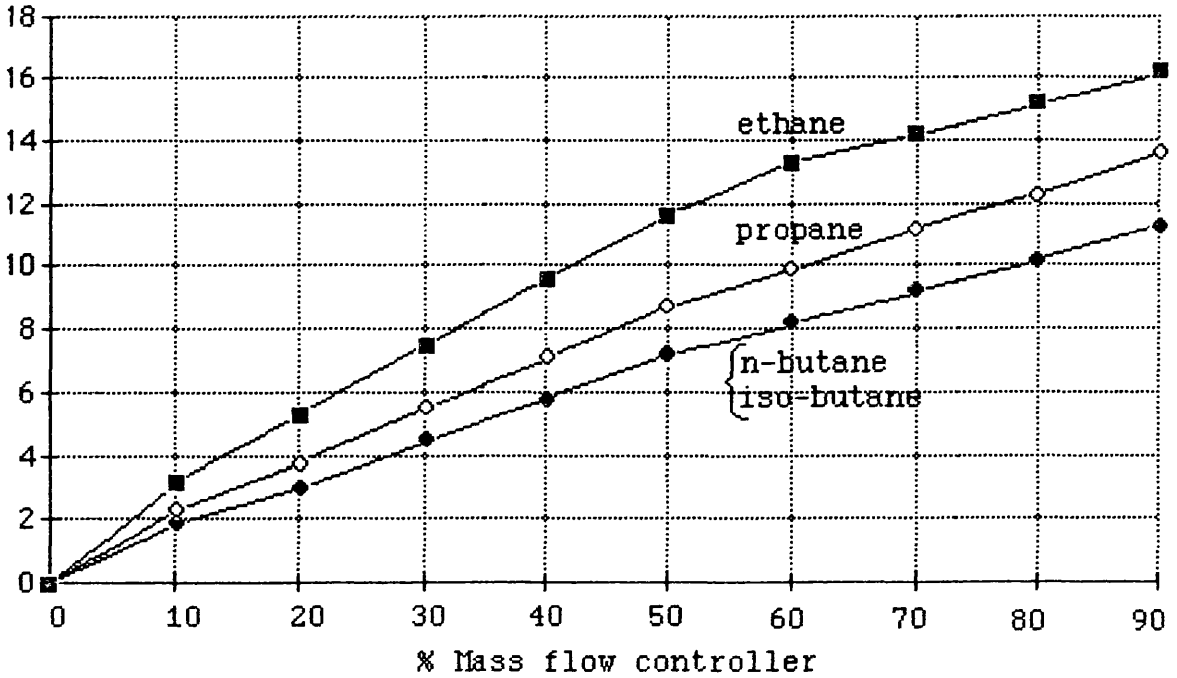
Graph 1 - He and H<sub>2</sub> calibration



Flow rate  
(mlmin<sup>-1</sup>)

Graph 2 - Hydrocarbon calibration

(Unit controller UFC 1020 N<sub>2</sub> 0-100sccm)



#### 3.4.4 Reactor tube

In a reactor tube with a small diameter, as used in the microreactor system, the mixing of the gas phase proceeds through the radial diffusion of the gas molecules from the centre of the tube, or catalyst bed, to the walls of the vessel, and vice-versa. The rate of this radial mixing is governed by the following expression,

$$t = \frac{(dT)^2}{8Dr} \quad (173)$$

where  $t$  = time taken for a molecule to move from the centre of the tube to the wall (independent of flow rate for laminar flow)

$dT$  = tube diameter

$Dr$  = radial diffusivity

Therefore as the reaction vessel diameter becomes smaller the rate of radial mixing increases.

Provided that the catalyst bed is of sufficient length to allow at least one complete radial mixing stage (theoretical plate) to occur (i.e. bed length > reaction chamber diameter), the concentration of gas phase reactant molecules, and the residence time of the individual molecules, within the catalyst bed, is likely to be uniform.

In tubular reaction vessels of small diameter, heat transfers by convection, in which the gas phase molecules themselves transport the heat, and it is, therefore, as rapid as mass transfer. Hence, even in the presence of exothermic and endothermic reactions, the temperature gradient across the diameter of the catalyst bed is likely to be negligible when the catalyst vessel is of small diameter.

Given that the average density of the catalysts was  $0.5 \text{ gcm}^{-3}$ , a typical sample of 0.15g would have a catalyst bed length of 2.4cm compared to the reactor diameter of 0.4cm, ensuring that the observed product distributions were not influenced by mass and heat transfer limitations.

#### 3.4.5 Diffusion limitation

Diffusion limitation of a reaction can be recognised by

- (i) The rate being proportional to the catalysts weight raised to a power less than unity, which in the limit may be zero.
- (ii) The rate being increased by improving the

movement of the gas or liquid with respect to the catalyst (62).

Tables 1 and 2, below, for the hydrogenolysis of n-butane over Pt/Al<sub>2</sub>O<sub>3</sub> with respect to catalyst loading and hydrocarbon flow rate demonstrate that the reaction is not diffusion limited according to (i) and (ii) above.

As the apparent activation energy is high (130 kJ mol<sup>-1</sup>) for this and the other hydrogenolysis reactions (section 5.3) it can be assumed that the reactions are not diffusion limited.

Table 1 - hydrogenolysis of n-butane over Pt/Al<sub>2</sub>O<sub>3</sub> at 743K

Wt(g) catalyst	Fractional conversion	Reaction rate (mlmin <sup>-1</sup> g <sub>cat</sub> <sup>-1</sup> )
0.0258	0.011	2.77
0.0482	0.021	2.83
0.1032	0.042	2.65
0.1530	0.064	2.72
0.2103	0.084	2.60
0.2507	0.096	2.50

Table 2 - hydrogenolysis of n-butane over Pt/Al<sub>2</sub>O<sub>3</sub>  
at 713K

Flow rate n-C <sub>4</sub> H <sub>10</sub> (ml min <sup>-1</sup> )	Fractional conversion	Reaction rate (ml min <sup>-1</sup> g <sub>cat</sub> <sup>-1</sup> )
4.5	0.040	1.16
5.2	0.034	1.14
6.5	0.028	1.16
7.7	0.024	1.18
8.1	0.022	1.14
8.7	0.020	1.12

### 3.4.6 Microreactor experimental procedures

Two experimental procedures were used on the microreactor system, one to calculate apparent activation energies (section 3.4.6.1), the other to find the order of the reaction with respect to the pressure of hydrogen (section 3.4.6.2).

Following the work of F. Rodríguez-Reinoso et al. (101) the activation energies were calculated by repeating the hydrogenolysis reactions at 10° intervals over the same catalyst sample, reactivating and cleaning the catalyst surface between reactions in a flow of hydrogen (174).

The order of the reaction with respect to the pressure of hydrogen was calculated, similar to the work of R.B. Anderson and P.K. Tsjeng (175) by using the back pressure regulator to build up a pressure of hydrogen in the reactor before each reaction.

#### 3.4.6.1 Activation energies

After a standard reduction (section 3.3.2) the reactor was taken to the initial reaction temperature (typically 400°C) in a flow of H<sub>2</sub>. At this temperature

the He and hydrocarbon flows were turned on to produce the required He, H<sub>2</sub> and hydrocarbon mixture (typically He and H<sub>2</sub> 20ml min<sup>-1</sup>, hydrocarbon 4ml min<sup>-1</sup>). The gas mixture was allowed to flow over the catalyst for fifteen minutes to allow the system to reach equilibrium. The reactor effluent stream was then sampled by gas chromatography (section 3.4.6). After sampling, the He and hydrocarbon flows were turned off and the reaction temperature raised by 10° to the next reaction temperature in a flow of hydrogen. After fifteen minutes the He and hydrocarbon flows were turned on again and the reaction was repeated at this temperature. This process was continued, repeating the reaction at 10° intervals over a range of 60 to 100°C.

#### 3.4.6.2 Hydrogen pressure rate coefficient

After a standard reduction (section 3.3.2) the reactor was taken to a temperature of 430°C in a flow of hydrogen of 60ml min<sup>-1</sup>. At this temperature the forward and back pressure regulators were used to build up an initial pressure of hydrogen in the reactor section (~ 10 lb. in<sup>-2</sup>). The hydrocarbon stream (typically 3ml min<sup>-1</sup>) was then turned on and allowed to flow over the catalyst for fifteen minutes to allow the system to reach equilibrium. The reactor effluent stream was then sampled by gas chromatography (section 3.6). After

sampling the hydrocarbon flow was switched off and the hydrogen pressure increased by 5 lb. in<sup>-2</sup>. After fifteen minutes the hydrocarbon flow was turned on again and the reaction repeated at this hydrogen pressure. This process was continued until the hydrogen pressure reached 50 lb. in<sup>-2</sup>.

#### 3.4.7 Microreactor analytical system

Gas chromatography was used to analyse the hydrogenolysis reaction products. As previously mentioned, a 10 port sample valve was used to send a fixed volume of the reactor effluent stream to a Perkin Elmer Chromatograph 8500.

Using a carrier stream of He, the effluent sample was separated with a Poropak QS (50-80 mesh) packed column and its constituents detected with a flame ionisation detector (FID).

The alkane products were eluted from the column in the order

methane < ethane < propane < iso-butane < n-butane

Hydrocarbons of the same chain length were eluted from the column in the order

alkanes < alkenes < alkynes

As each product was detected its retention time and integrated peak area was recorded.

To calibrate the G.C. each product gas was fed directly into the gas sampling valve via a pressure regulator. At a constant pressure of 15 lb. in<sup>-2</sup> ten samples of each gas were taken. A range of sample loop sizes was used to verify the linear response of the detector (graph 3).

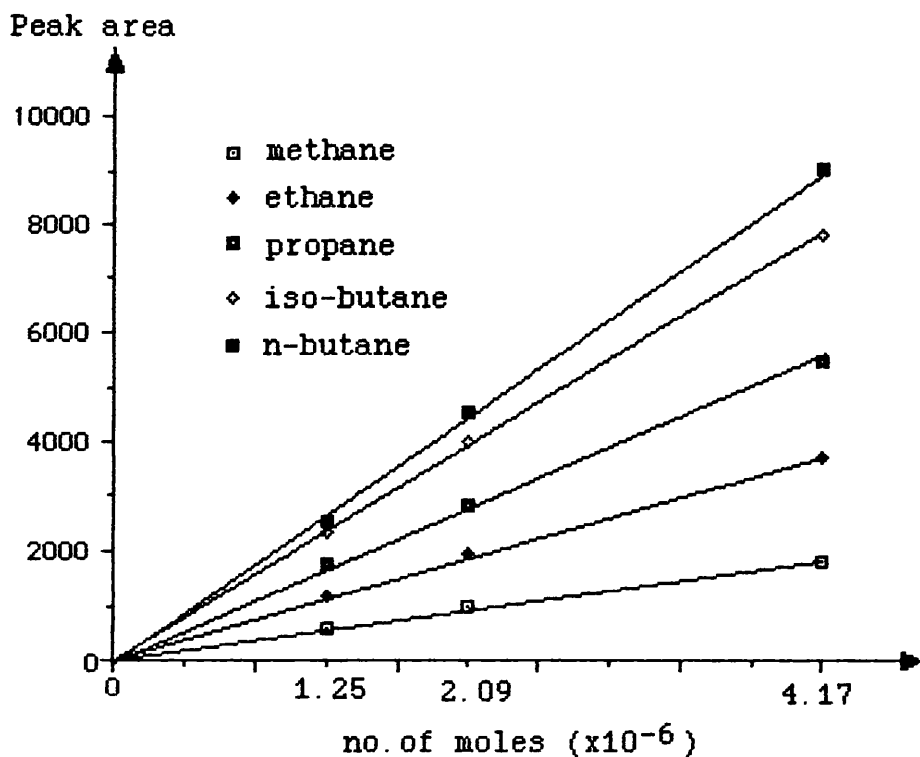
From these results a response factor was calculated for each gas (table 3) to relate its peak area to a number of moles such that,

no. of moles of gas = response factor x peak area

Table 3 - Gas chromatograph response factors

Gas	Retention time (mins)	Response Factor ( $\frac{\text{mol}}{\text{area units}} \times 10^{-9}$ )
methane	5.17	2.29
ethane	6.01	1.13
ethene	6.19	1.04
propane	7.04	0.764
propene	8.49	0.709
iso-butane	9.20	0.566
n-butane	11.39	0.463

Graph 3 - Calibration of gas chromatogram



## CHAPTER FOUR

## CHAPTER 4

### TREATMENT OF RESULTS

#### 4.1 CARBON MONOXIDE CHEMISORPTION EXPERIMENTS

##### 4.1.1 Molecules of CO chemisorbed on catalyst

Carbon monoxide chemisorption experiments were carried out in the pulse flow system described in section 3.3.1. As described, a known pressure of carbon monoxide was entered into the vacuum line manifold and pulsed over the reduced catalyst sample. A thermal conductivity detector (TCD) was used to detect any unadsorbed carbon monoxide in the effluent stream from the reactor.

From the size of the sample loop ( $V = 4.18\text{ml}$ ) and the pressure of carbon monoxide used, the number of moles of carbon monoxide gas injected into the hydrogen carrier stream per pulse could be calculated from the gas equation,

$$n = \frac{PV}{RT}$$

where  $n$  = number of moles of carbon monoxide

$P$  = pressure of carbon monoxide

R = gas constant

T = absolute temperature

By multiplying the number of moles of carbon monoxide by the Avogadro number, the number of carbon monoxide molecules injected per pulse was calculated.

Carbon monoxide was pulsed over the catalyst until three sequential peaks of the same height were obtained by the TCD, indicating that the catalyst was completely saturated. From the TCD peak areas of the carbon monoxide pulses prior to saturation the total number of carbon monoxide molecules chemisorbed on the catalyst was calculated from the equation,

$$\begin{array}{l} \text{molecules of CO} \\ \text{chemisorbed} \\ \text{on catalyst} \end{array} = \sum_{i=1}^{i=n} \begin{array}{l} \text{molecules of} \\ \text{CO per pulse} \end{array} \times \left( 1 - \frac{\text{peak area } i}{\text{peak area } n} \right)$$

n = number of pulses required to reach saturation

#### 4.1.2 Dispersion (d)

Assuming, that on a platinum catalyst, the predominant chemisorbed carbon monoxide species is linearly bound (171), the number of carbon monoxide molecules chemisorbed is equal to the number of available surface platinum atoms. On the nickel catalysts a bridged species is predominately formed

(176) and the number of surface nickel atoms is equal to twice the number of carbon monoxide molecules chemisorbed.

The dispersion,  $d$ , of a catalyst is then defined as

$$d = \frac{\text{number of surface metal atoms}}{\text{total number of metal atoms}} \times 100\%$$

#### 4.1.3 Mean surface average diameter (<d>)

The mean surface average diameter,  $\langle d \rangle$ , is related to the dispersion by the equation,

$$(i) \quad d = \frac{f \times A \times 100}{\rho \times S_R \times N} \times \frac{S}{V} \quad (177)$$

where

$d$  = dispersion (%)

$f$  = fraction of the surface area effectively exposed

$A$  = Atomic Wt. of the active atoms

$N$  = Avogadro's number

$\rho$  = the specific mass (density) of the active phase

$S_R$  = average surface area occupied by one atom at the surface. An average value derived from the crystallographic planes [100], [110] and [111] of a single metal crystal, assuming that the areas of each plane are equal.

$V$  = total volume of the active phase

$S$  = total surface area of the active phase

Given that the volume of a sphere is  $V = \frac{4}{3}\pi r^3$  and that the surface area is  $S = 4\pi r^2$ , then assuming identical spheres of diameter  $\langle d \rangle$ , it can be shown that

$$(ii) \quad \frac{S}{V} = \frac{6}{\langle d \rangle}$$

where  $\langle d \rangle$  = mean surface average diameter

Assuming that  $f=1$ , rearranging equations (i) and (ii) gives,

$$(iii) \quad \langle d \rangle = \frac{A \times 6 \times 100}{\rho \times S_A \times N \times d}$$

From the following data table for platinum and nickel,

metal	A(amu)	$\rho$ (g/nm <sup>3</sup> )	$S_A$ (nm <sup>3</sup> )
platinum	195.08	$21.5 \times 10^{-21}$	0.0861
nickel	58.69	$8.90 \times 10^{-21}$	0.0651

equation (iii) simplifies to

$$(iv) \quad \langle d \rangle = \frac{101}{d} \text{ (nm) for nickel and}$$

$$(v) \quad \langle d \rangle = \frac{105}{d} \text{ (nm) for platinum.}$$

These equations assume that particles of less than 1nm are 100% dispersed.

#### 4.1.4 Metal surface area (MSA)

Another useful parameter derived from chemisorption measurements is the metal surface area (MSA) per gram of the catalyst, which can be calculated from the equation ,

$$\text{MSA} = M_s \times S_A \quad (\text{m}^2 \text{g}_{\text{cat}}^{-1})$$

where

$M_s$  = number of surface metal atoms per gram of catalyst

$S_A$  = surface area of one metal atom

This MSA can be converted into a surface area per gram of metal present,  $S$ , by taking into account the loading of the catalyst.

$$S = \frac{100}{l} \times \text{MSA} \quad (\text{m}^2 \text{g}_{\text{metal}}^{-1})$$

where  $l$  = metal loading (%)

In a similar way to equation (iv) and (v) in section 4.1.3,  $S$  can be related to the mean surface average diameter,  $\langle d \rangle$ , by the equations

$$\langle d \rangle = \frac{674}{S} \text{ (nm)} \quad \text{for nickel and}$$

$$\langle d \rangle = \frac{279}{5} \text{ (nm) for platinum.}$$

#### 4.2 TRANSMISSION ELECTRON MICROSCOPY

From the measurement from electron micrographs of a large number of metal particles (>200) a frequency distribution of metal particle sizes can be produced for supported catalyst samples. Spherical particles can be measured directly from the electron micrographs, particularly at the edge of the support where the contrast is greater. Irregular or elliptical particles can be estimated from the mean of the largest and smallest dimensions of the particle (178). The measured particles are then sorted into classes. Each class,  $i$ , is represented by a class mark,  $d_i$ , and comprises of a number,  $n_i$ , of particles whose sizes lie between the class boundaries of the  $i$ th class.

To allow comparison with the chemisorption data it can be shown that

$$\langle d \rangle = \frac{\sum (n_i d_i^3)}{\sum (n_i d_i^2)} \quad (179)$$

where  $\langle d \rangle$  = mean surface average diameter

### 4.3 HYDROGENOLYSIS REACTIONS

The hydrogenolysis reactions were carried out in the microreactor system described in section 3.4. As previously mentioned, gas chromatography was used to analyse the reaction products. As each product was eluted from the column and detected by a FID its peak area was multiplied by a response factor to convert it to a number of moles (section 3.6).

#### 4.3.1 Number of moles ( $C_i$ )

The number of moles of each reaction product is denoted as  $C_i$  where  $i$  is the products carbon number.

i.e.

$C_1$  = moles of methane

$C_2$  = moles of ethane

$C_3$  = moles of propane

For the butanes, n-butane and iso-butane are denoted as,

iso- $C_4$  = moles of iso-butane

n- $C_4$  = moles of n-butane

#### 4.3.2 Moles converted (A)

The number of moles of reactant hydrocarbon

which have undergone hydrogenolysis is denoted as A.

When ethane is the reactant gas,

$$A = \frac{C_1}{2}$$

as 2 moles of methane are produced from the hydrogenolysis of 1 mole of ethane.

With propane as the reactant gas,

$$A = \frac{C_1 + 2C_2}{3}$$

as 3 moles of methane or  $1\frac{1}{2}$  moles of ethane can be produced from the hydrogenolysis of 1 mole of propane.

Similarly for n-butane and iso-butane,

$$A = \frac{C_1 + 2C_2 + 3C_3}{4}$$

as 4 moles of methane, 2 moles of ethane or  $1\frac{1}{3}$  moles of propane can be produced from the hydrogenolysis of 1 mole of butane.

#### 4.3.3 Fractional conversion ( $X_{\text{HYD}}$ )

The fractional conversion,  $X_{\text{HYD}}$ , calculates the fraction of the initial gas stream which has undergone hydrogenolysis.

$$X_{\text{HYD}} = \frac{\text{moles of reactant gas which have undergone hydrogenolysis}}{\text{moles of reactant gas initially}}$$

This can be shown to be equal to

$$X_{\text{HYD}} = \frac{A}{A + \text{moles of reactant gas unreacted}}$$

where A = moles of reactant gas converted

For ethane and propane, the fractional conversion can be calculated from the equations below,

$$\text{For ethane } X_{\text{HYD}} = \frac{A}{A + C_2}$$

$$\text{For propane } X_{\text{HYD}} = \frac{A}{A + C_3}$$

For n-butane and iso-butane, as isomerisation can also take place, the fractional conversions are calculated from the equation,

$$X_{\text{HYD}} = \frac{A}{A + \text{iso-C}_4 + \text{n-C}_4}$$

The fractional conversion to the isomerised product,  $X_{\text{ISO}}$ , can be calculated from the equations

$$\text{For n-butane } X_{\text{ISO}} = \frac{\text{iso-C}_4}{A + \text{iso-C}_4 + \text{n-C}_4}$$

$$\text{For iso-butane } X_{\text{ISO}} = \frac{\text{n-C}_4}{A + \text{iso-C}_4 + \text{n-C}_4}$$

In both these cases the isomerised product appears as a numerator of the fraction.

#### 4.3.4 Selectivity ( $S_i$ )

For propane and the butanes, where there is a choice of hydrogenolysis products, the selectivity to each product is denoted by  $S_i$ , where  $S_i = \frac{C_i}{A}$ . i.e.

$$S_1 = \frac{C_1}{A} = \frac{\text{moles of methane produced}}{\text{moles converted}}$$

$$S_2 = \frac{C_2}{A} = \frac{\text{moles of ethane produced}}{\text{moles converted}}$$

For propane hydrogenolysis it can be shown that

$$S_1 = 3 - 2S_2$$

and for the hydrogenolysis of butanes,

$$S_1 = 4 - 3S_3 - 2S_2$$

The selectivity for isomerisation over hydrogenolysis for the butanes can be calculated from the following equations.

For n-butane  $\frac{\text{iso-C}_4}{A} = \frac{\text{moles of iso-butane formed}}{\text{moles of n-butane undergoing hydrogenolysis}}$

For iso-butane  $\frac{\text{n-C}_4}{A} = \frac{\text{moles of n-butane formed}}{\text{moles of iso-butane undergoing hydrogenolysis}}$

#### 4.3.5 Reaction rate and turnover

The overall hydrogenolysis reaction rate can be calculated from the equation,

$$\text{reaction rate} = \frac{\text{flow rate of hydrocarbon (ml min}^{-1}) \times \text{fractional conversion (X}_{\text{HYD}} \text{ or X}_{\text{ISO}})}{\text{Wt. (g) of catalyst}}$$

(ml min<sup>-1</sup> g<sub>CAT</sub><sup>-1</sup>)

Where the catalyst loading and dispersion figures are known, this can be converted into a turnover figure with units of molecules s<sup>-1</sup> surface metal atom<sup>-1</sup>.

#### 4.3.6 Activation energies

According to the Arrhenius equation the reaction rate can be increased by increasing the temperature.

i.e.

$$\text{reaction rate} = A e^{-\frac{E_a}{RT}}$$

where  $E_a$  = activation energy for the reaction

$T$  = absolute temperature (K)

$R$  = gas constant

$A$  = pre-exponential factor

Taking natural logs of each side of this equation gives

$$\ln \text{ rate} = \ln A - \frac{E_a}{RT}$$

Therefore plotting the natural log of the rate (or turnover) against the inverse of the absolute temperature gives a straight line of gradient =  $-\frac{E_a}{R}$ . By using this method apparent activation energies for hydrogenolysis reactions over each of the catalysts were calculated.

#### 4.3.7 Rate law

The simplest rate law for the hydrogenolysis reaction takes the form,

$$\text{rate} = A P_{C_xH_y}^n P_{H_2}^m$$

where  $A$  = a constant

$P_{C_xH_y}$  = partial pressure of hydrocarbon  $C_xH_y$

$P_{H_2}$  = partial pressure of hydrogen

$n$  = order of the reaction with respect to  $C_xH_y$

$m$  = order of the reaction with respect to hydrogen

Taking logs of each side of this equation gives,

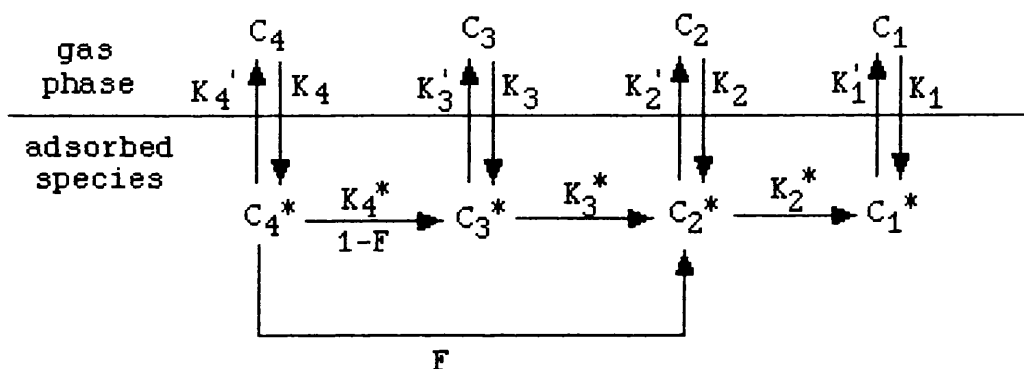
$$\log \text{ rate} = \log A + n \log P_{C_xH_y} + m \log P_{H_2}$$

Following the procedure in section 3.5.2 where the total pressure of the reactor is raised and a high

hydrogen to hydrocarbon mixture is used it can be assumed that the  $\ln P_{C_xH_y}$  term makes a small contribution to the overall rate. Plotting log rate against the log of the reactor pressure gives a straight line of gradient  $m$ .

#### 4.3.8 Kempling-Anderson reaction network

Kempling and Anderson (180) developed a simple but comprehensive reaction network for describing the hydrogenolysis of alkanes. They envisaged the hydrogenolysis reaction as a successive reaction of adsorbed intermediates ( $C_j^*$ ) containing  $j$  carbon atoms ( $j = 1-4$ ). e.g. for n-butane



Where  $C_j$  represents a linear alkane containing  $j$  carbon atoms in the gas phase and  $C_j^*$  its adsorbed form.  $F$  is defined as the probability of breaking the central bond in n-butane.

The constants  $T_j$  ( $j = 2, 3$ ) as defined by

$$T_j = \frac{K_j'}{K_j' + K_j^*} \quad (i)$$

are particularly useful parameters as they can be taken as a measure of the intrinsic reactivity of the adsorbed species, high values indicating that hydrogenative desorption is favoured over further C-C bond splitting.

Steady state analysis (180) leads to the following expressions involving  $T_2$ ,  $T_3$  and  $F$  for  $S_2$  and  $S_3$  (the selectivity for ethane and propane) at low conversions (<ca.20%).

$$S_2 = (1 + F - S_3)T_2 \quad (ii)$$

$$S_3 = (1-F)T_3 \quad (iii)$$

From the hydrogenolysis of n-butane alone there is this not enough information to derive the three constants  $T_2$ ,  $T_3$  and  $F$ . It is possible to estimate  $T_2$ , however, from the hydrogenolysis of propane under the same experimental conditions where,

$$S_2 = T_2 \quad (iv)$$

Alternatively, as all the C-C bonds in isobutane are equivalent and there is no splitting factor  $F$ , equations (ii) and (iii) above can be simplified to

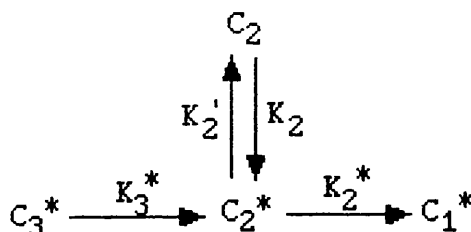
$$S_2 = (1 - S_3)T_2 \quad (v)$$

$$S_3 = T_3 \quad (\text{vi})$$

again allowing  $T_2$  and  $T_3$  to be estimated.

There is therefore a choice between using information derived from either propane hydrogenolysis or iso-butane hydrogenolysis to estimate  $T_2$  and  $T_3$ . This choice depends on deciding which molecule would behave most similarly to n-butane as part of a Kempling-Anderson reaction network.

In the hydrogenolysis of propane, ethane can only be produced from the single hydrogenolysis of the  $C_3^*$  intermediate.



Therefore the selectivity for ethane,  $S_2$ , is a good guide to the reactivity,  $T_2$ , of the adsorbed species  $C_2^*$ .

Similarly as propane is only produced from the single hydrogenolysis of iso-butane,  $S_3$ , the selectivity for propane is a good guide to the reactivity  $T_3$  of the adsorbed  $C_3^*$  species.

$T_2$  is therefore best derived from the hydrogenolysis of propane (where  $S_2 = T_2$ ) and  $T_3$  is best derived from the hydrogenolysis of iso-butane (where  $S_3 = T_3$ ).

Rearranging equation (ii) and (iii) above gives the following equation for  $F$ , the splitting factor for n-butane,

$$F = \frac{1}{2} \left( S_3 + \frac{S_2}{T_2} - \frac{S_3}{T_3} \right)$$

where

$T_2 = S_2$  from propane hydrogenolysis

$T_3 = S_3$  from iso-butane hydrogenolysis

$S_2$  = selectivity for ethane from n-butane hydrogenolysis

$S_3$  = selectivity for propane from n-butane hydrogenolysis

## CHAPTER FIVE

## CHAPTER 5

### RESULTS

#### 5.1 SUMMARY OF RESULTS FROM GLASGOW-HULL-ICI GROUP (171)

##### 5.1.1 Characterisation of support materials

The support materials were fully characterised in respect of (i) their surface area and pore volume (ii) their full analysis by ICP-MS. The measured surface areas and impurity levels are summarised in Table 1 below. The surface areas were, within experimental error, unchanged during impregnation, reduction and reoxidation.

Table 1 - Properties of support materials

Support	Surface Area $\text{m}^2 \text{g}^{-1}$	Impurities ppm
$\text{SiO}_2$	203	Cl(537), Cu(20) Na(20)
$\text{Al}_2\text{O}_3$ (Degussa Aluminium Oxid C)	102	Cl(2780), Fe(110) Zn(90), Ni(45) other elements below 35
$\text{MoO}_3$ (BDH Analar, 99.5%)	2.1	Cl(0), Pb(1000max), Fe(500max), Cu(500max)

All samples have zero pore volume.

### 5.1.2 Microanalytical data

Elemental analyses were carried out by inductively coupled-mass spectrometry (ICP-MS). In addition chloride levels were determined by chemical analysis coupled with x-ray fluorescence (XRF).

Table 2 - Elemental analyses

Catalyst	Metal content (wt.%)	% Chloride	
		A	B
Pt/Al <sub>2</sub> O <sub>3</sub>	0.89	1.28	1.01
Pt/SiO <sub>2</sub>	0.75	0.64	<0.02
Pt/MoO <sub>3</sub>	0.48	a	<0.02
Ni/Al <sub>2</sub> O <sub>3</sub>	0.95		
Ni/SiO <sub>2</sub>	0.97		
Ni/MoO <sub>3</sub>	0.54		
Ni/WO <sub>3</sub>	0.50		

A = pre-reduction

B = post-reduction and storage in air

a - detected but quantification impossible because of interference with Mo

Figures quoted to an accuracy of  $\pm 0.02$

### 5.1.3 Temperature programmed reduction (TPR)

The temperature programmed reduction studies were performed using a pulse-flow reactor system, heating to 573K in flowing 5%  $H_2/N_2$ .

Table 3 - Temperature programmed reduction

Catalyst	Temperature (K) of reduction maxima	H : Metal ratio
Pt/ $Al_2O_3$	500	23
Pt/ $SiO_2$	400-410	28
Pt/ $MoO_3$	405	323
-----		
Ni/ $Al_2O_3$	573	14
Ni/ $SiO_2$	578	19
Ni/ $MoO_3$	560	12
Ni/ $WO_3$	563	12

### 5.1.4 Hydrogen bronze formation

Values of x in  $H_xMoO_3$ , the hydrogen bronze formed by the Pt/ $MoO_3$  catalyst were determined from TPR,

thermogravimetric analysis (TGA) and x-ray photoelectron spectroscopy (XPS) as follows,

Table 4 - Values of x in  $H_xMoO_3$

	<u>TGA</u>	<u>TPR</u>	<u>XPS</u>
Value of x	0.9	1.2	0.8

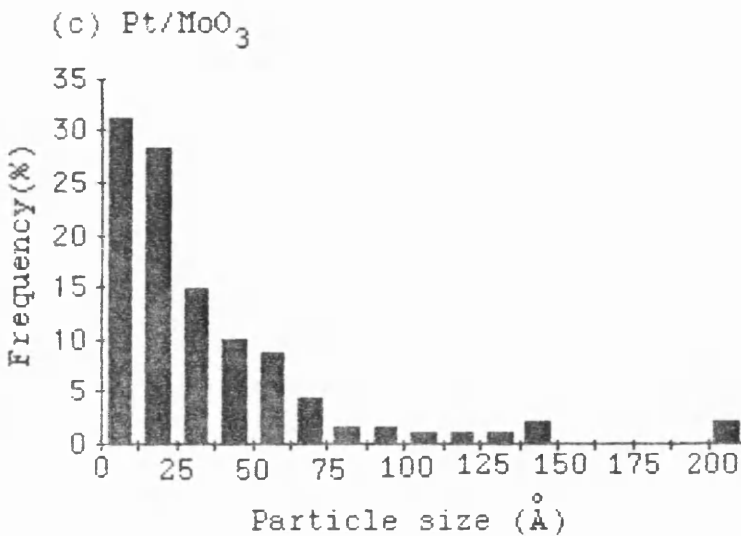
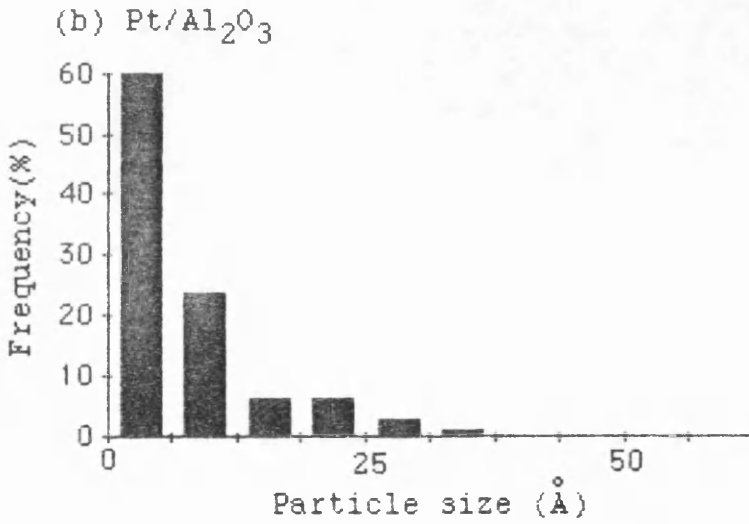
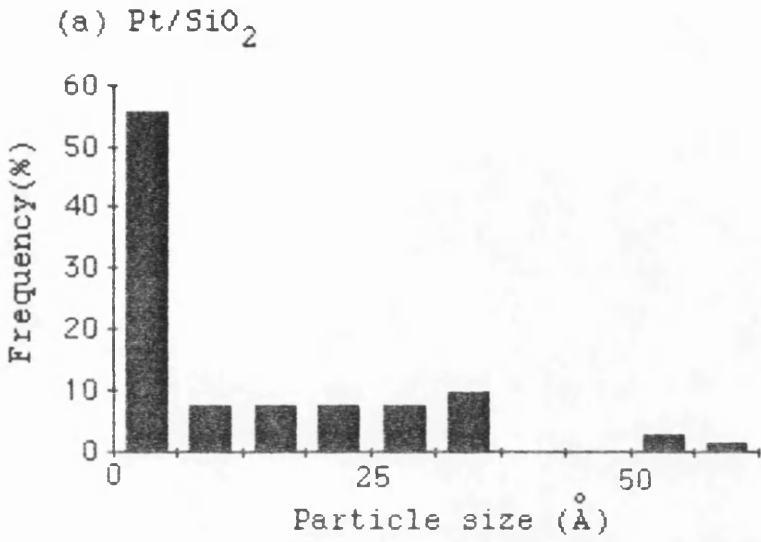
### 5.1.5 Gas chemisorption studies

Carbon monoxide and dioxygen chemisorption studies were carried out on the platinum samples, in a dynamic mode using a pulse-flow reactor. The results were as follows,

Table 5 - Gas chemisorption results

Catalyst	Temp(K)	adsorbate	Amount adsorbed (molecules $g^{-1}$ )	Dispersion (%)
Pt/ $Al_2O_3$	273	CO	$1.979 \times 10^{19}$	72
Pt/ $SiO_2$	273	$O_2$	$5.73 \times 10^{18}$	50
Pt/ $MoO_3$	273	CO	$5.16 \times 10^{18}$	35

5.1.6 Pt catalysts - Particle size distributions



## 5.2 CHARACTERISATION OF NICKEL CATALYSTS

### 5.2.1 Carbon monoxide chemisorption

Carbon monoxide chemisorption is the most common technique used for the measurement of catalyst dispersion as it provides a simple and direct way of measuring the number of surface metal atoms.

Using the gas adsorption apparatus described in section 3.3.1 and following the procedure given in section 3.3.3 the series of nickel catalysts was characterised by carbon monoxide chemisorption. From the number of carbon monoxide molecules chemisorbed the dispersion, mean surface average diameters ( $\langle d \rangle$ ) and the metal surface areas were calculated for each of the catalysts (section 4.1), assuming that each chemisorbed carbon monoxide molecule was bonded to two surface nickel atoms.

Table 6 - Carbon monoxide chemisorption on Ni catalysts

Catalyst	Temp (K)	CO adsorbed (molecules $g_{cat}^{-1}$ )	Dispersion (%)	$\langle d \rangle$ (nm)	Surface metal area ( $m^2 g_{metal}^{-1}$ )
Ni/SiO <sub>2</sub>	273	1.83x10 <sup>19</sup>	38	2.66	254
		1.49x10 <sup>19</sup>			
		2.29x10 <sup>19</sup>			
Ni/Al <sub>2</sub> O <sub>3</sub>	273	4.41x10 <sup>18</sup>	10	10.1	66.7
		5.16x10 <sup>18</sup>			
		5.40x10 <sup>18</sup>			
Ni/MoO <sub>3</sub>	273	1.30x10 <sup>19</sup>	47	2.14	315
		1.31x10 <sup>19</sup>			
Ni/WO <sub>3</sub>	273	8.23x10 <sup>18</sup>	26	3.88	174
		6.40x10 <sup>18</sup>			
		5.39x10 <sup>18</sup>			

### 5.2.2 Transmission microscopy

The polydispersed population of metal particles on a supported catalyst can be characterised from the measurement of a fairly large number of particles chosen at random from an electron micrograph.

From the electron micrographs of the platinum catalysts the following mean surface average diameters,  $\langle d \rangle_{\text{TEM}}$ , were calculated.  $\langle d \rangle_{\text{CHEM}}$  values derived from the gas chemisorption studies are included for comparison.

Table 7 - mean surface average diameters

Catalyst	$\langle d \rangle_{\text{TEM}}$ (nm)	$\langle d \rangle_{\text{CHEM}}$ (nm)
Pt/Al <sub>2</sub> O <sub>3</sub>	2.03	1.46
Pt/SiO <sub>2</sub>	3.87	2.10
Pt/MoO <sub>3</sub>	12.50	3.10

Although some evidence for the presence of nickel was obtained from the micrographs of the nickel catalysts, the definition was not sufficient to allow the calculation of metal particle size distributions.

### 5.3 HYDROGENOLYSIS REACTIONS

#### 5.3.1 Ethane hydrogenolysis

After a standard reduction (section 3.3.2) the hydrogenolysis of ethane was carried out in the microreactor system (section 3.4) over each of the supported catalysts, following the experimental procedure given in section 3.5.1, varying the reaction temperature to calculate activation energies.

All the reactions were carried out with a He flow rate of  $17.8 \text{ ml min}^{-1}$ , a  $\text{H}_2$  flow of  $22.0 \text{ ml min}^{-1}$  and a flow of ethane of  $10.5 \text{ ml min}^{-1}$ . The gas forward pressures were held at  $30 \text{ lb. in}^{-2}$ .

The fractional conversions and turnover figures are given in Tables 8 and 9 for the platinum and nickel catalysts respectively. The reproducibility of the fractional conversions was within 3%. The tables are accompanied by Arrhenius graphs of  $\ln(\text{turnover})$  against  $1/T$  (Graphs 1 and 2).

Table 8 - Hydrogenolysis of ethane over Pt catalysts

Temp (K)	Pt/Al <sub>2</sub> O <sub>3</sub>		Pt/SiO <sub>2</sub>		Pt/MoO <sub>3</sub>	
	Fractional conversion	Turnover (molecules s <sup>-1</sup> surfacePt atom <sup>-1</sup> )	Fractional conversion	Turnover (molecules s <sup>-1</sup> surfacePt atom <sup>-1</sup> )	Fractional conversion	Turnover (molecules s <sup>-1</sup> surfacePt atom <sup>-1</sup> )
683	2.8x10 <sup>-3</sup>	4.4x10 <sup>-3</sup>	2.3x10 <sup>-3</sup>	6.1x10 <sup>-3</sup>	1.2x10 <sup>-3</sup>	7.1x10 <sup>-3</sup>
693	4.0x10 <sup>-3</sup>	6.3x10 <sup>-3</sup>	3.6x10 <sup>-3</sup>	9.7x10 <sup>-3</sup>	2.0x10 <sup>-3</sup>	0.012
703	6.5x10 <sup>-3</sup>	0.010	6.0x10 <sup>-3</sup>	0.016	3.7x10 <sup>-3</sup>	0.022
713	0.011	0.017	9.6x10 <sup>-3</sup>	0.026	7.7x10 <sup>-3</sup>	0.046
723	0.020	0.031	0.015	0.042	0.014	0.085
733	0.032	0.050	0.026	0.070	0.026	0.16
743	0.051	0.079	0.039	0.10	0.037	0.22
753	0.083	0.13	0.053	0.14	0.056	0.33
763	0.125	0.19	0.058	0.16	0.062	0.36

Table 9 (a) - Hydrogenolysis of ethane over Ni catalysts

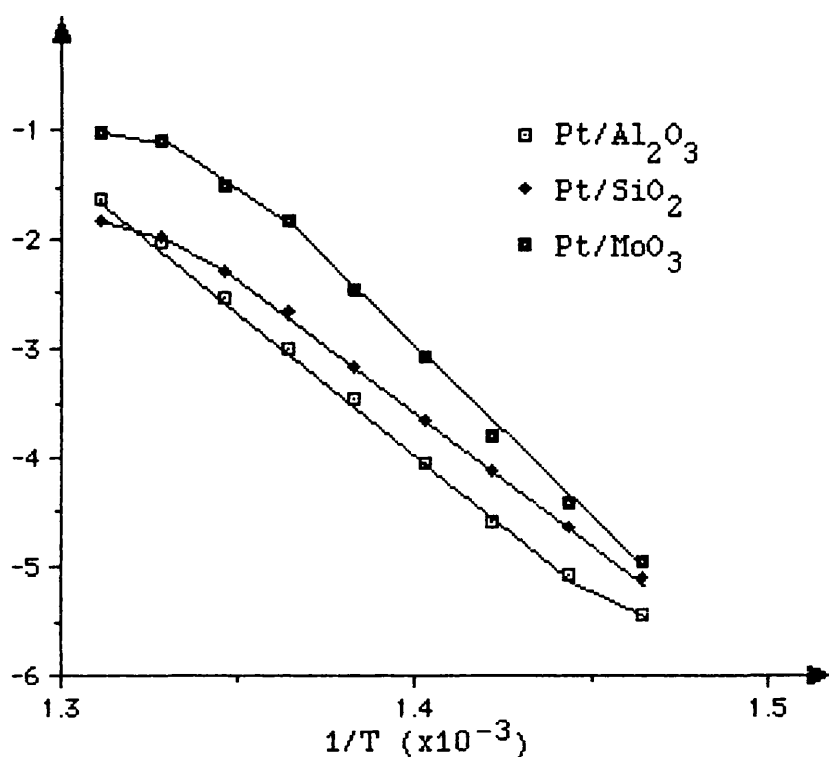
Temp (K)	Ni/Al <sub>2</sub> O <sub>3</sub>		Ni/MoO <sub>3</sub>		Ni/WO <sub>3</sub>	
	Fractional conversion	Turnover (molecules s <sup>-1</sup> surface Ni atom <sup>-1</sup> )	Fractional conversion	Turnover (molecules s <sup>-1</sup> surface Ni atom <sup>-1</sup> )	Fractional conversion	Turnover (molecules s <sup>-1</sup> surface Ni atom <sup>-1</sup> )
638	9.6x10 <sup>-3</sup>	0.029	-	-	-	-
643	0.014	0.043	0.010	0.011	1.3x10 <sup>-3</sup>	2.9x10 <sup>-3</sup>
653	0.021	0.063	0.017	0.019	2.8x10 <sup>-3</sup>	6.4x10 <sup>-3</sup>
663	0.032	0.099	0.038	0.041	3.8x10 <sup>-3</sup>	8.7x10 <sup>-3</sup>
673	0.063	0.19	0.069	0.074	6.8x10 <sup>-3</sup>	0.015
683	0.11	0.32	0.11	0.11	0.010	0.023
693	0.16	0.48	0.15	0.16	0.014	0.032
703	0.30	0.91	0.24	0.25	0.018	0.040
713	0.42	1.28	0.31	0.34	0.022	0.050
723	0.64	1.96	0.34	0.38	0.023	0.050

Table 9(b) - Hydrogenolysis of ethane over Ni catalysts

Ni/SiO <sub>2</sub>	
Temp (K)	Turnover (molecules s <sup>-1</sup> surface Ni atom <sup>-1</sup> )
523	1.1x10 <sup>-3</sup>
533	1.9x10 <sup>-3</sup>
543	7.8x10 <sup>-3</sup>
553	0.012
563	0.030
573	0.078
583	0.21
593	0.80

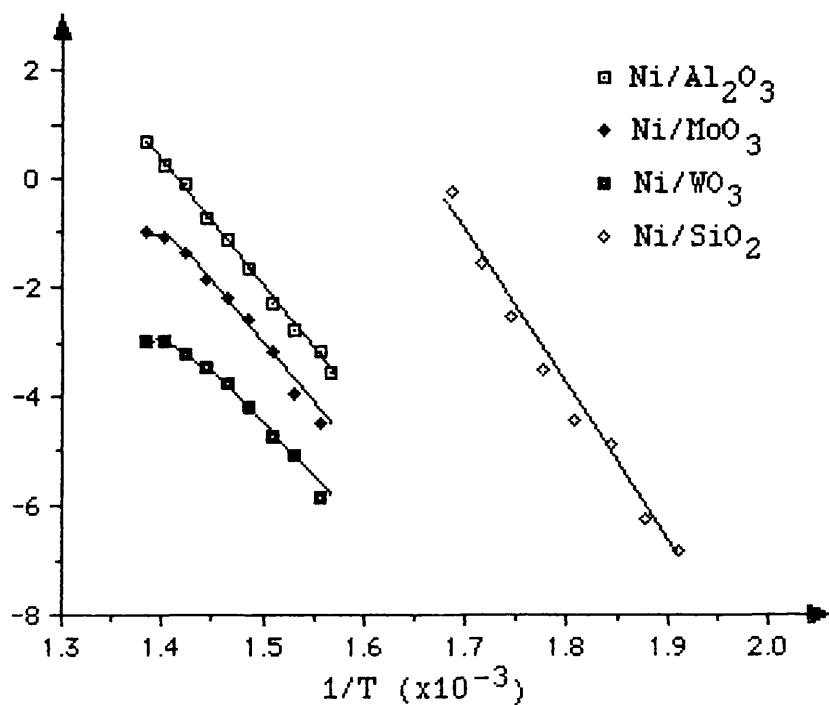
Graph 1 - Ethane hydrogenolysis over Pt catalysts

Ln Turnover



Graph 2 - Ethane hydrogenolysis over Ni catalysts

Ln Turnover



### 5.3.1.2 Activation energies for the hydrogenolysis of ethane

The apparent activation energies for the hydrogenolysis of ethane were calculated from the Arrhenius plots of  $\ln(\text{turnover})$  against  $1/T$  (see section 4.3.6). Where the plots deviated from linearity at high temperatures the gradient of the linear region was used to calculate the activation energy. This deviation from linearity is a common feature of hydrogenolysis reactions (47).

Table 10 gives the activation energies calculated from the least squares best fit line through the points and  $\ln A$  the intercept of this line.

Table 10 - Activation energies for ethane hydrogenolysis

Catalyst	Temp (K)	Ea (kJmol <sup>-1</sup> )	ln A
Pt/Al <sub>2</sub> O <sub>3</sub>	683-763	219	32.9
Pt/SiO <sub>2</sub>	683-763	203	24.4
Pt/MoO <sub>3</sub>	683-763	253	42.0
Ni/Al <sub>2</sub> O <sub>3</sub>	638-723	185	34.5
Ni/SiO <sub>2</sub>	523-593	237	47.4
Ni/MoO <sub>3</sub>	643-723	199	36.9
Ni/WO <sub>3</sub>	643-723	175	30.5

Units of A - molecules s<sup>-1</sup> surface metal atom<sup>-1</sup>

### 5.3.2 Propane hydrogenolysis

The hydrogenolysis of propane was carried out over the series of supported catalysts following the experimental procedure given in section 3.5.1, varying the temperature to calculate apparent activation energies. The reactions over the platinum catalysts were carried out with a He flow of  $17.8 \text{ ml min}^{-1}$ , a  $\text{H}_2$  flow of  $22.0 \text{ ml min}^{-1}$  and a flow of propane of  $8.0 \text{ ml min}^{-1}$ . The reactions over the nickel catalysts were carried out in the same He and  $\text{H}_2$  flows but a flow rate of propane of  $4.0 \text{ ml min}^{-1}$ . All gas forward pressures were held at  $30 \text{ lb. in}^{-2}$ .

The results of these reactions giving fractional conversions, turnovers and selectivities for methane ( $S_1$ ) are given in Tables 11 and 12 for the platinum and nickel catalysts respectively.

Each Table is accompanied by an Arrhenius graph of  $\ln(\text{turnover})$  against  $1/T$  and a graph of  $S_1$  against temperature.

Table 11 - Hydrogenolysis of propane over Pt catalysts

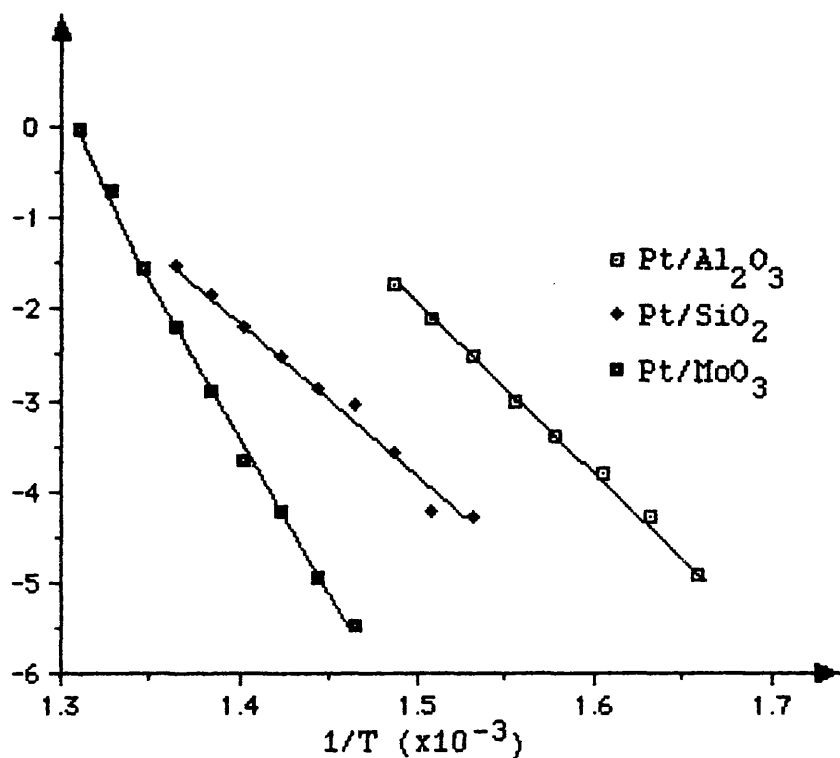
Pt/Al <sub>2</sub> O <sub>3</sub>					Pt/SiO <sub>2</sub>					Pt/MoO <sub>3</sub>				
Temp (K)	X <sub>HYD</sub>	Turnover	S <sub>1</sub>		Temp (K)	X <sub>HYD</sub>	Turnover	S <sub>1</sub>		Temp (K)	X <sub>HYD</sub>	Turnover	S <sub>1</sub>	
603	6.3x10 <sup>-3</sup>	7.4x10 <sup>-3</sup>	0.88		653	7.1x10 <sup>-3</sup>	0.014	1.04		683	7.9x10 <sup>-4</sup>	4.2x10 <sup>-3</sup>	0.96	
613	0.012	0.014	0.98		663	7.5x10 <sup>-3</sup>	0.015	1.04		693	1.4x10 <sup>-3</sup>	7.2x10 <sup>-3</sup>	0.93	
623	0.019	0.022	0.99		673	0.014	0.028	1.06		703	3.2x10 <sup>-3</sup>	0.015	1.03	
633	0.029	0.034	1.00		683	0.024	0.048	1.08		713	5.6x10 <sup>-3</sup>	0.026	1.11	
643	0.042	0.049	1.02		693	0.028	0.056	1.08		723	0.012	0.055	1.22	
653	0.068	0.080	1.05		703	0.040	0.080	1.09		733	0.027	0.11	1.21	
663	0.099	0.012	1.06		713	0.057	0.11	1.09		743	0.048	0.21	1.24	
673	0.15	0.018	1.06		723	0.082	0.16	1.08		753	0.068	0.50	1.25	
					733	0.11	0.22	1.05		763	0.085	0.97	1.27	

X<sub>HYD</sub> - Fractional hydrogenolysis conversion

Turnover - molecules s<sup>-1</sup> surface Pt atom<sup>-1</sup>

Graph 3 - Propane hydrogenolysis over Pt catalysts

Ln Turnover



Graph 4 - Propane hydrogenolysis over Pt catalysts  
Selectivity for methane ( $S_1$ )

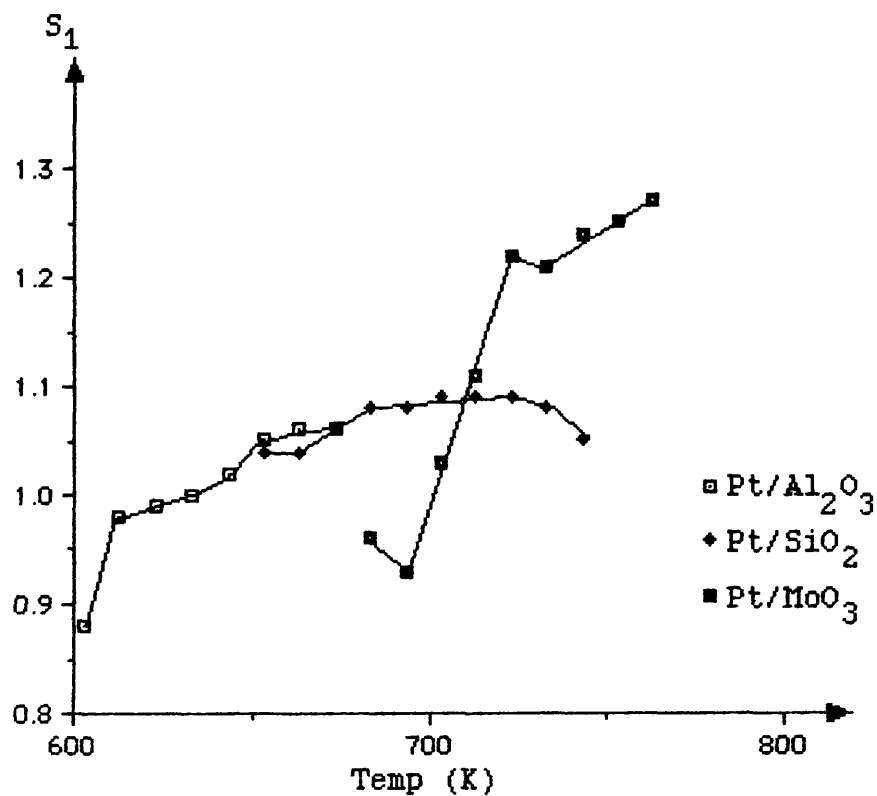


Table 12(a) - Hydrogenolysis of propane over Ni catalysts

Ni/Al <sub>2</sub> O <sub>3</sub>					Ni/SiO <sub>2</sub>						
Temp (K)	X <sub>HYD</sub>	Turnover	S <sub>1</sub>	Temp (K)	X <sub>HYD</sub>	Turnover	S <sub>1</sub>	Temp (K)	X <sub>HYD</sub>	Turnover	S <sub>1</sub>
683	8.8x10 <sup>-3</sup>	0.011	2.33	563	1.9x10 <sup>-3</sup>	6.0x10 <sup>-4</sup>	0.74	693	3.7x10 <sup>-3</sup>	1.2x10 <sup>-3</sup>	0.86
693	0.015	0.018	2.52	573	3.7x10 <sup>-3</sup>	1.2x10 <sup>-3</sup>	0.86	703	0.022	0.027	2.56
703	0.022	0.027	2.56	583	0.010	3.2x10 <sup>-3</sup>	0.95	713	0.034	0.041	2.66
713	0.034	0.041	2.66	593	0.023	7.2x10 <sup>-3</sup>	1.07	723	0.045	0.054	2.71
723	0.045	0.054	2.71	603	0.052	0.016	1.17	733	0.070	0.087	2.85
733	0.070	0.087	2.85	613	0.13	0.040	1.29				

X<sub>HYD</sub> - Fractional hydrogenolysis conversion

Turnover - molecules s<sup>-1</sup> surface Ni atom<sup>-1</sup>

Table 12(b) - Hydrogenolysis of propane over Ni catalysts

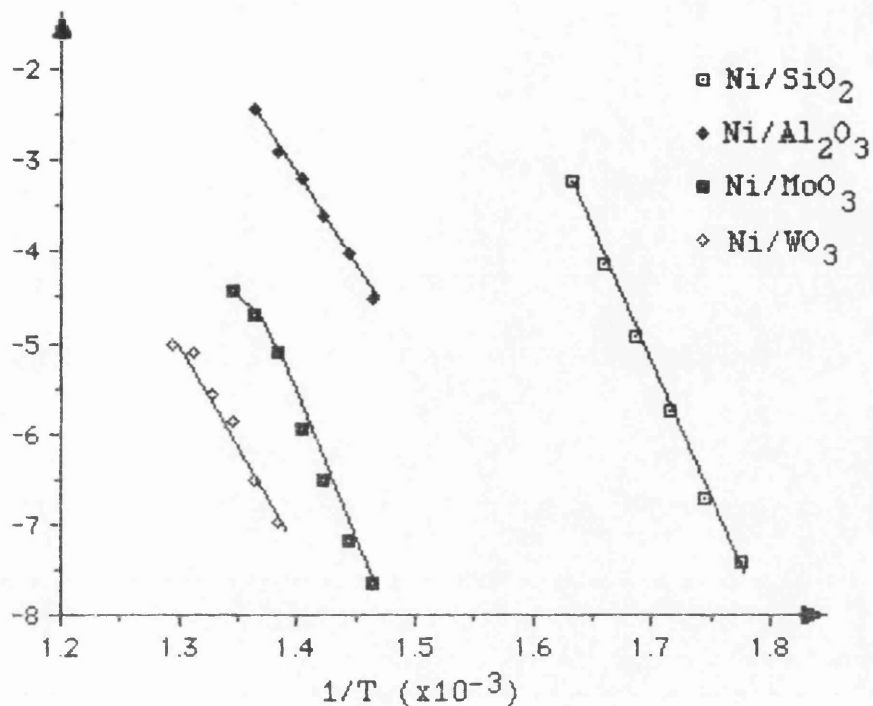
Ni/MoO <sub>3</sub>				Ni/WO <sub>3</sub>			
Temp (K)	X <sub>HYD</sub>	Turnover	S <sub>1</sub>	Temp (K)	X <sub>HYD</sub>	Turnover	S <sub>1</sub>
683	1.1x10 <sup>-3</sup>	4.8x10 <sup>-4</sup>	1.09	723	3.2x10 <sup>-3</sup>	9.3x10 <sup>-3</sup>	1.66
693	1.7x10 <sup>-3</sup>	7.5x10 <sup>-4</sup>	1.29	733	4.9x10 <sup>-3</sup>	1.5x10 <sup>-3</sup>	1.86
703	3.5x10 <sup>-3</sup>	1.5x10 <sup>-3</sup>	1.43	743	9.5x10 <sup>-3</sup>	2.8x10 <sup>-3</sup>	2.27
713	5.9x10 <sup>-3</sup>	2.6x10 <sup>-3</sup>	1.46	753	0.013	3.8x10 <sup>-3</sup>	2.28
723	0.014	6.0x10 <sup>-3</sup>	1.55	763	0.021	6.0x10 <sup>-3</sup>	2.29
733	0.021	9.2x10 <sup>-3</sup>	1.64	773	0.023	6.6x10 <sup>-3</sup>	2.31
743	0.028	0.012	1.73				

X<sub>HYD</sub> - Fractional hydrogenolysis conversion

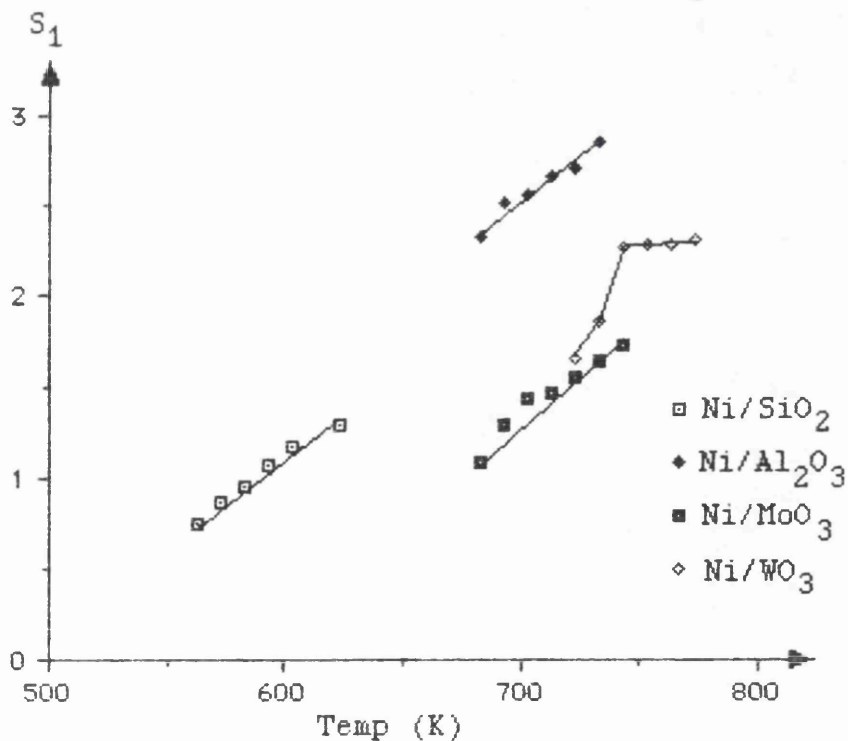
Turnover - molecules s<sup>-1</sup> surface Ni atom<sup>-1</sup>

Graph 5 - Propane hydrogenolysis over Ni catalysts

Ln Turnover



Graph 6 - Propane hydrogenolysis over Ni catalysts  
Selectivity for methane (S<sub>1</sub>)



### 5.3.2.2 Activation energies for hydrogenolysis of propane

The apparent activation energies, in Table 13 below, were calculated from the Arrhenius plots of  $\ln(\text{turnover})$  against  $1/T$  in a similar way to the hydrogenolysis of ethane (section 5.3.1.2).

Table 13 - Activation energies for propane hydrogenolysis

Catalyst	Temp (K)	Ea (kJmol <sup>-1</sup> )	ln A
Pt/Al <sub>2</sub> O <sub>3</sub>	603-673	147	24.4
Pt/SiO <sub>2</sub>	653-733	157	27.6
Pt/MoO <sub>3</sub>	683-763	310	51.2
Ni/Al <sub>2</sub> O <sub>3</sub>	683-733	171	28.7
Ni/SiO <sub>2</sub>	563-613	243	48.7
Ni/MoO <sub>3</sub>	683-743	257	41.5
Ni/WO <sub>3</sub>	723-773	218	33.8

Units of A - molecules s<sup>-1</sup> surface metal atom<sup>-1</sup>

### 5.3.3 n-butane hydrogenolysis

The hydrogenolysis of n-butane was carried out over the series of supported catalysts, varying the temperature to calculate activation energies. All the reactions were carried out with a He flow rate of 17.8 ml min<sup>-1</sup>, a H<sub>2</sub> flow rate of 22.0 ml min<sup>-1</sup> and a flow of n-butane of 6.5 ml min<sup>-1</sup>. The forward gas pressures were held at 15 lb. in<sup>-2</sup>.

For each catalyst there is a table of results containing fractional conversions and turnover figures for hydrogenolysis and isomerisation, selectivities for methane (S<sub>1</sub>), ethane (S<sub>2</sub>) and propane (S<sub>3</sub>) and selectivity for isomerisation over hydrogenolysis (i-C<sub>4</sub>/A). Each table is accompanied by a graph of ln(turnover) against 1/T and a graph of selectivity against temperature.

Table 14 - Hydrogenolysis of n-butane over Pt/Al<sub>2</sub>O<sub>3</sub>

Temp (K)	S <sub>1</sub>	S <sub>2</sub>	S <sub>3</sub>	$\frac{iC_4}{A}$	X <sub>HYD</sub>	X <sub>ISO</sub>	Turnover (hydrog)	Turnover (isom)
693	0.74	0.56	0.72	0.08	0.017	1.4x10 <sup>-3</sup>	0.017	1.2x10 <sup>-3</sup>
703	0.87	0.54	0.69	0.07	0.023	1.5x10 <sup>-3</sup>	0.022	1.5x10 <sup>-3</sup>
713	0.91	0.54	0.68	0.07	0.030	2.2x10 <sup>-3</sup>	0.029	2.1x10 <sup>-3</sup>
723	0.93	0.47	0.72	0.08	0.043	3.5x10 <sup>-3</sup>	0.041	3.4x10 <sup>-3</sup>
733	0.88	0.50	0.71	0.08	0.070	5.3x10 <sup>-3</sup>	0.067	5.2x10 <sup>-3</sup>
743	0.87	0.45	0.74	0.08	0.081	6.7x10 <sup>-3</sup>	0.078	6.3x10 <sup>-3</sup>
753	0.87	0.47	0.72	0.09	0.10	9.3x10 <sup>-3</sup>	0.095	8.8x10 <sup>-3</sup>

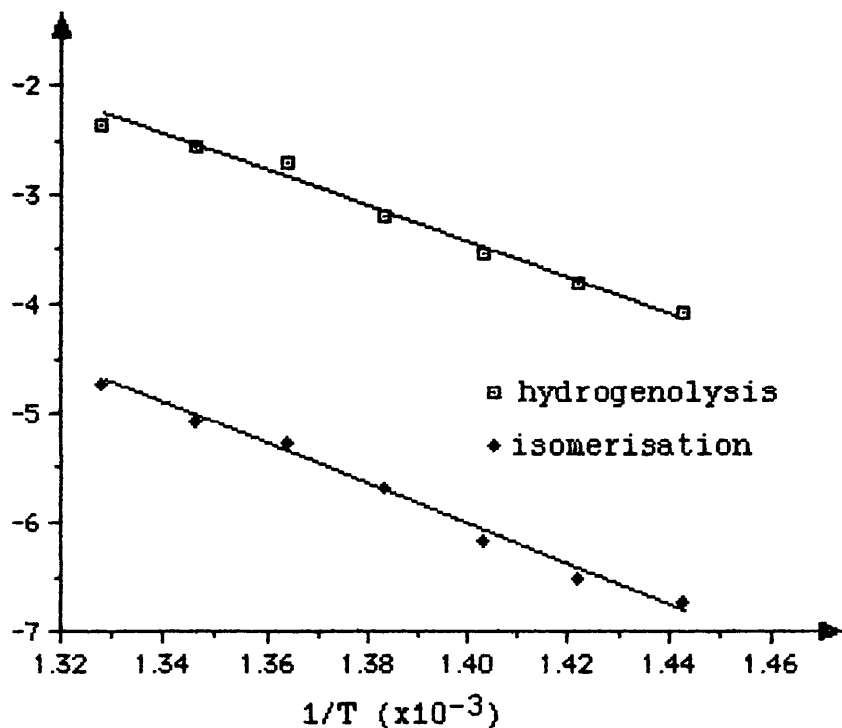
X<sub>HYD</sub> - Fractional hydrogenolysis conversion

X<sub>ISO</sub> - Fractional isomerisation conversion

Turnover - molecules s<sup>-1</sup> surface Pt atom<sup>-1</sup>

Graph 7 - Hydrogenolysis of n-butane over Pt/Al<sub>2</sub>O<sub>3</sub>

Ln Turnover



Graph 8 - Selectivity for n-butane hydrogenolysis over Pt/Al<sub>2</sub>O<sub>3</sub>

Selectivity

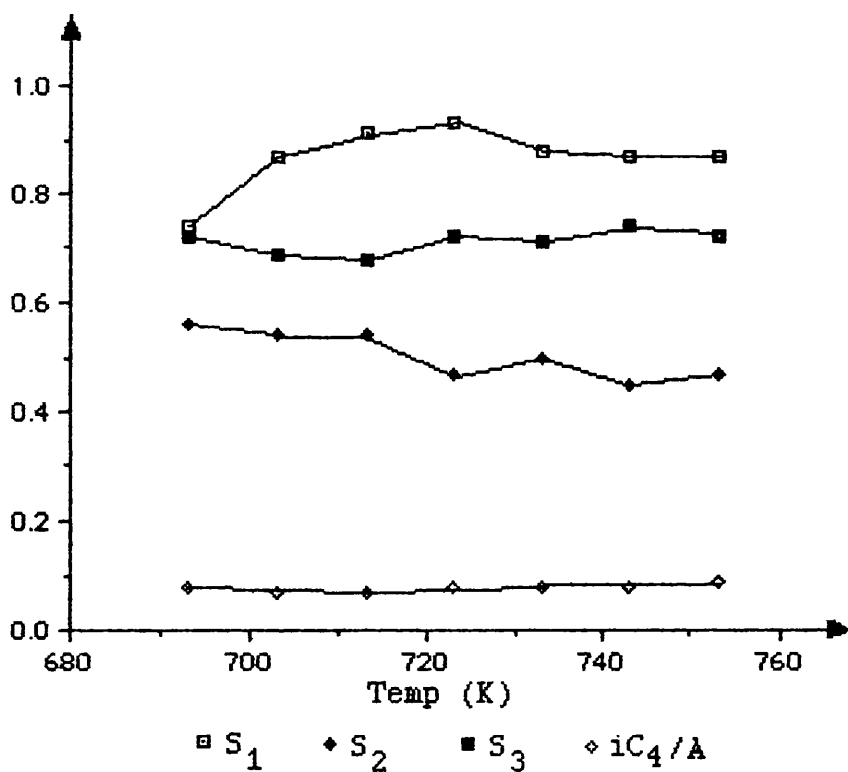


Table 15 - Hydrogenolysis of n-butane over Pt/SiO<sub>2</sub>

Temp (K)	S <sub>1</sub>	S <sub>2</sub>	S <sub>3</sub>	$\frac{iC_4}{A}$	X <sub>HYD</sub>	X <sub>ISO</sub>	Turnover (hydrog)	Turnover (isom)
593	0.45	0.52	0.83	0.66	7.1x10 <sup>-3</sup>	4.6x10 <sup>-3</sup>	5.7x10 <sup>-3</sup>	3.7x10 <sup>-3</sup>
603	0.55	0.61	0.74	0.73	7.6x10 <sup>-3</sup>	5.6x10 <sup>-3</sup>	6.1x10 <sup>-3</sup>	4.5x10 <sup>-3</sup>
613	0.71	0.65	0.67	0.75	0.010	7.8x10 <sup>-3</sup>	8.3x10 <sup>-3</sup>	6.2x10 <sup>-3</sup>
623	0.74	0.67	0.64	0.80	0.014	0.011	0.011	8.9x10 <sup>-3</sup>
633	0.73	0.70	0.62	0.82	0.019	0.016	0.015	0.013
643	0.79	0.70	0.60	0.80	0.024	0.019	0.019	0.016
653	0.81	0.71	0.59	0.78	0.033	0.026	0.027	0.021
663	0.92	0.84	0.57	0.70	0.042	0.030	0.034	0.024
673	0.87	0.70	0.57	0.66	0.051	0.033	0.041	0.027

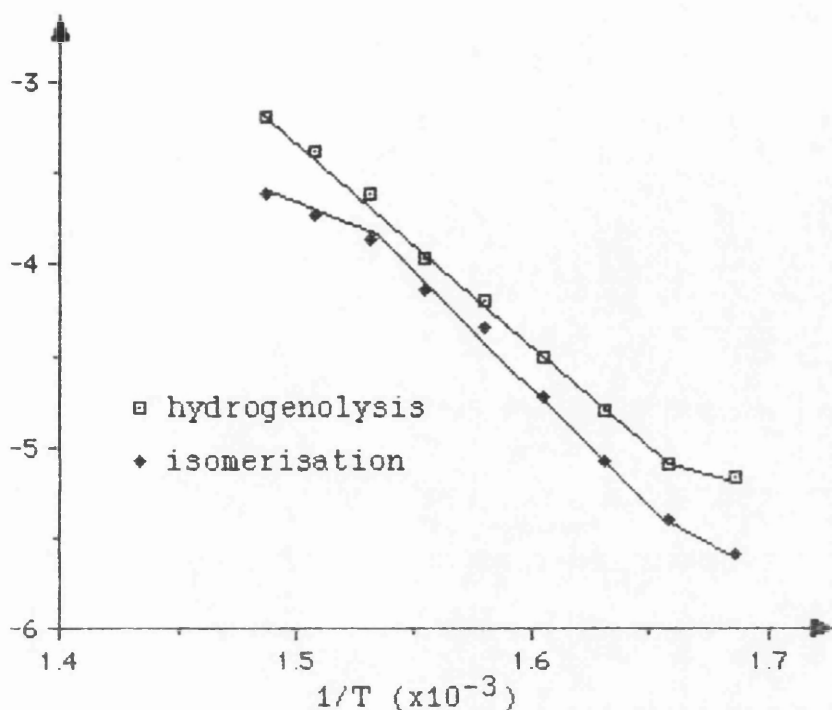
X<sub>HYD</sub> - Fractional hydrogenolysis conversion

X<sub>ISO</sub> - Fractional isomerisation conversion

Turnover - molecules s<sup>-1</sup> surface Pt atom<sup>-1</sup>

Graph 9 - Hydrogenolysis of n-butane over Pt/SiO<sub>2</sub>

Ln Turnover



Graph 10 - Selectivity n-butane hydrogenolysis over Pt/SiO<sub>2</sub>

Selectivity

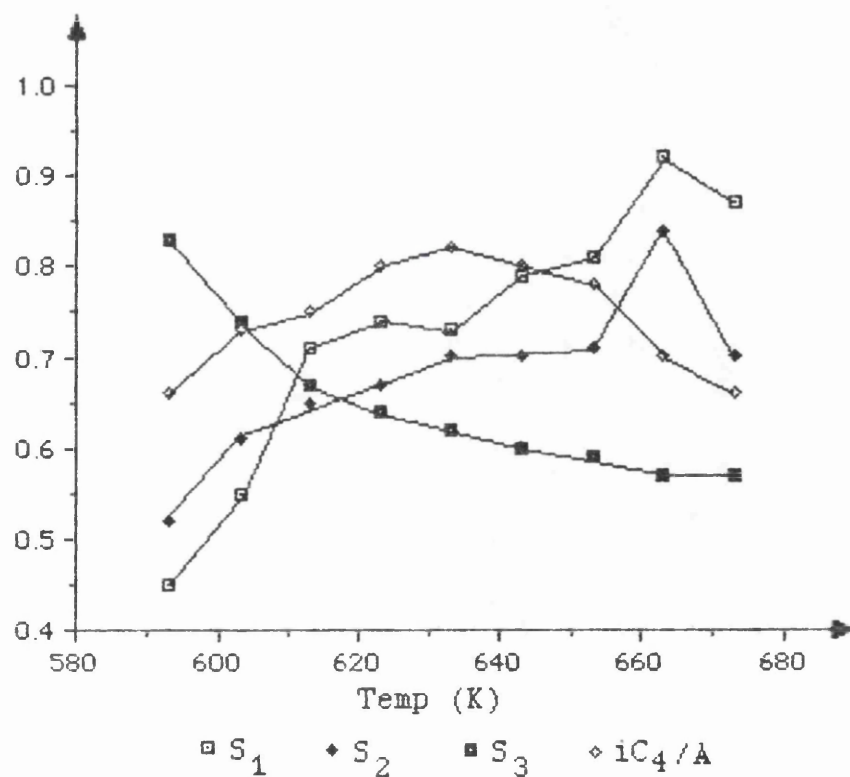


Table 16 - Hydrogenolysis of n-butane over Pt/MoO<sub>3</sub>

Temp (K)	S <sub>1</sub>	S <sub>2</sub>	S <sub>3</sub>	$\frac{iC_4}{A}$	X <sub>HYD</sub>	X <sub>ISO</sub>	Turnover (hydrog)	Turnover (isom)
693	0.76	0.91	0.47	1.01	8.4x10 <sup>-3</sup>	8.5x10 <sup>-3</sup>	0.016	0.016
703	0.96	0.89	0.42	1.26	8.8x10 <sup>-3</sup>	0.011	0.017	0.021
713	1.11	0.79	0.44	1.81	0.011	0.020	0.022	0.039
723	1.02	0.88	0.40	2.84	0.013	0.038	0.025	0.073
733	1.13	0.77	0.44	5.01	0.015	0.075	0.028	0.14
743	1.36	0.50	0.55	7.55	0.017	0.13	0.033	0.25
753	1.27	0.38	0.65	6.12	0.020	0.13	0.039	0.25

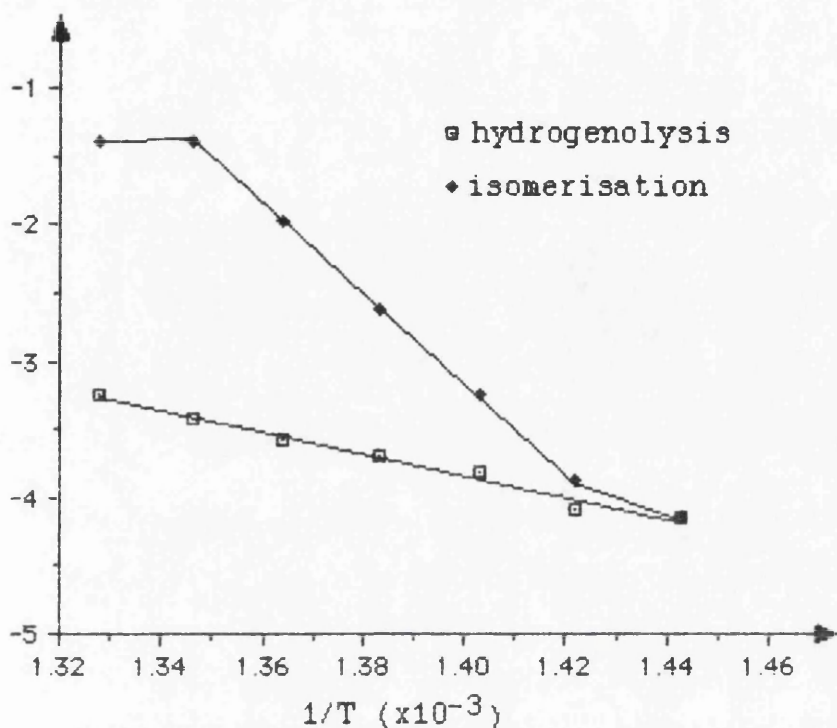
X<sub>HYD</sub> - Fractional hydrogenolysis conversion

X<sub>ISO</sub> - Fractional isomerisation conversion

Turnover - molecules s<sup>-1</sup> surface Pt atom<sup>-1</sup>

Graph 11 - Hydrogenolysis of n-butane over Pt/MoO<sub>3</sub>

Ln Turnover



Graph 12 - Selectivity n-butane hydrogenolysis over Pt/MoO<sub>3</sub>

Selectivity

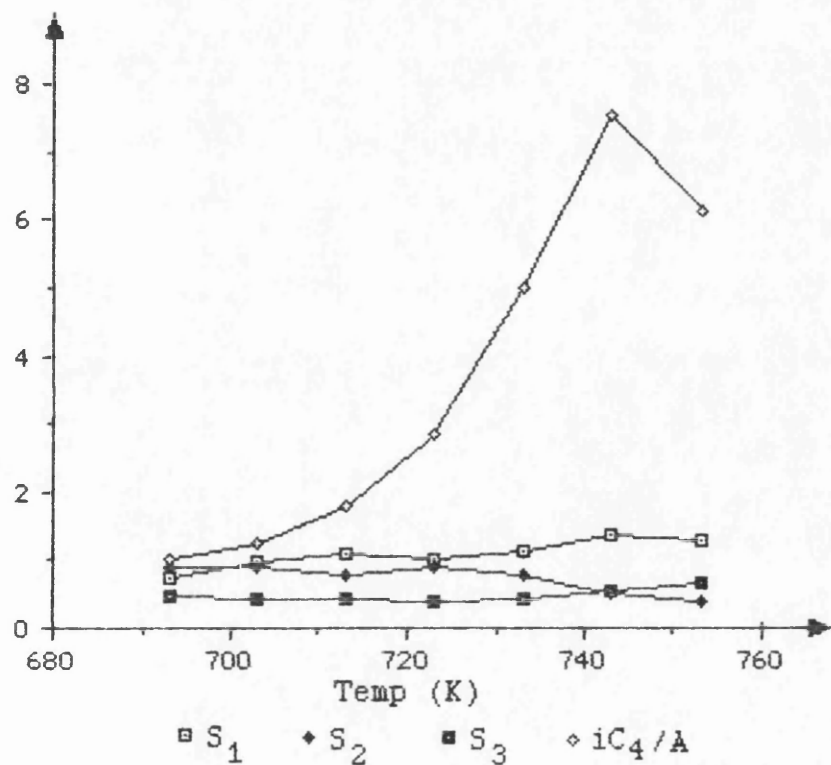


Table 17 - Hydrogenolysis of n-butane over Ni/Al<sub>2</sub>O<sub>3</sub>

Temp (K)	S <sub>1</sub>	S <sub>2</sub>	S <sub>3</sub>	$\frac{iC_4}{A}$	X <sub>H<sub>2</sub>D</sub>	X <sub>I<sub>2</sub>O</sub>	Turnover (hydrog)	Turnover (isom)
713	1.31	0.36	0.65	0.41	3.6x10 <sup>-3</sup>	1.5x10 <sup>-3</sup>	6.7x10 <sup>-3</sup>	2.7x10 <sup>-3</sup>
723	1.95	0.36	0.44	0.42	4.2x10 <sup>-3</sup>	1.8x10 <sup>-3</sup>	7.6x10 <sup>-3</sup>	3.3x10 <sup>-3</sup>
733	2.62	0.26	0.18	0.18	6.0x10 <sup>-3</sup>	1.1x10 <sup>-3</sup>	0.011	2.0x10 <sup>-3</sup>
743	2.87	0.22	0.23	0.11	8.6x10 <sup>-3</sup>	9.5x10 <sup>-4</sup>	0.015	1.6x10 <sup>-3</sup>
753	3.15	0.19	0.16	0.07	0.011	8.0x10 <sup>-4</sup>	0.021	1.5x10 <sup>-3</sup>
763	3.26	0.18	0.12	0.06	0.013	7.7x10 <sup>-4</sup>	0.025	1.4x10 <sup>-3</sup>

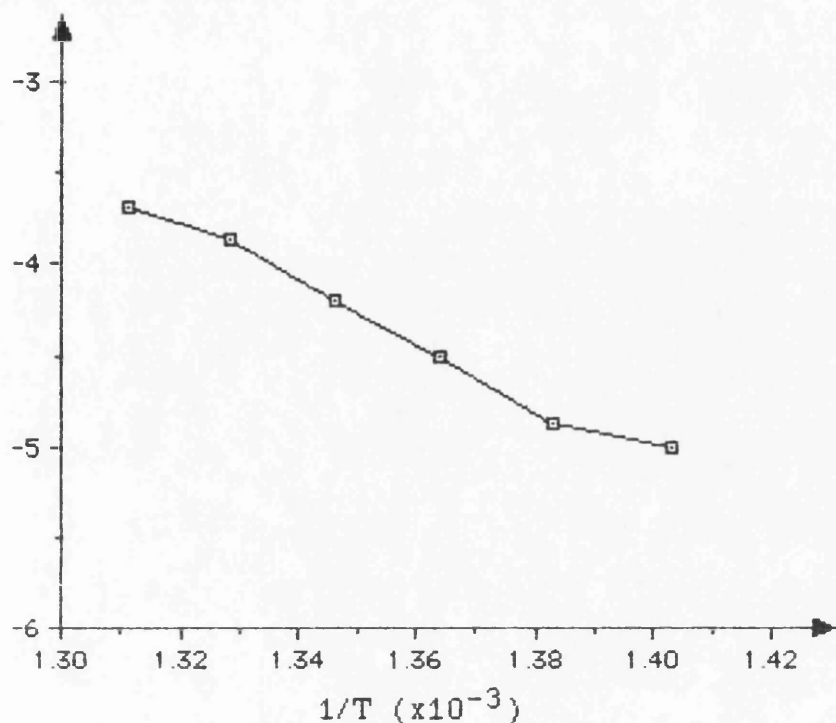
X<sub>H<sub>2</sub>D</sub> - Fractional hydrogenolysis conversion

X<sub>I<sub>2</sub>O</sub> - Fractional isomerisation conversion

Turnover - molecules s<sup>-1</sup> surface Ni atom<sup>-1</sup>

Graph 13 - Hydrogenolysis of n-butane over Ni/Al<sub>2</sub>O<sub>3</sub>

Ln Turnover



Graph 14 - Selectivity n-butane hydrogenolysis over Ni/Al<sub>2</sub>O<sub>3</sub>

Selectivity

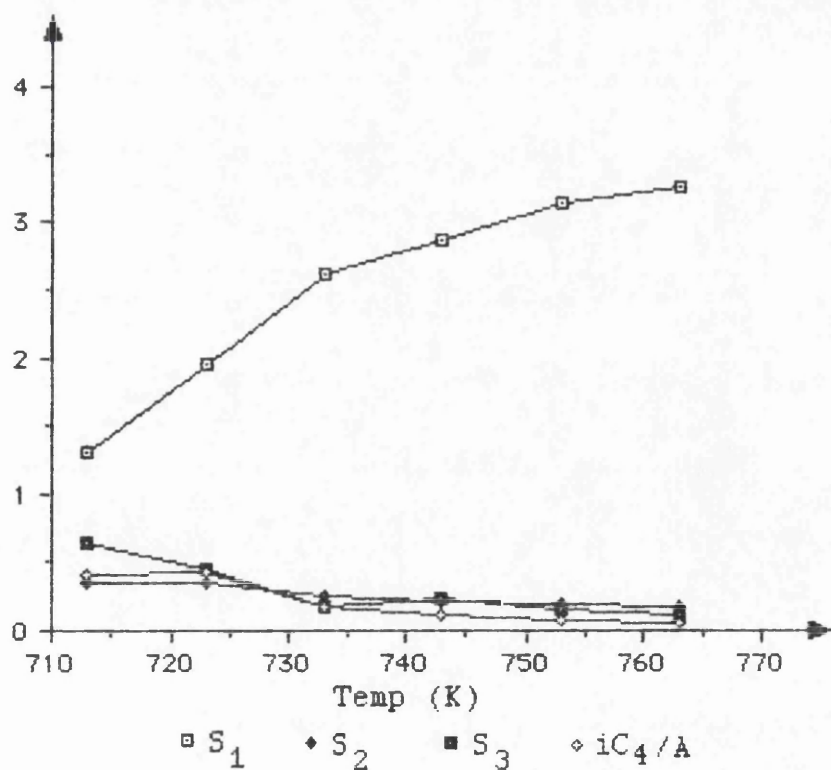


Table 18 - Hydrogenolysis of n-butane over Ni/SiO<sub>2</sub>

Temp (K)	S <sub>1</sub>	S <sub>2</sub>	S <sub>3</sub>	$\frac{iC_4}{A}$	X <sub>HYD</sub>	X <sub>ISO</sub>	Turnover (hydrog)	Turnover (isom)
583	1.27	0.17	0.80	0.042	0.017	6.9x10 <sup>-4</sup>	8.2x10 <sup>-3</sup>	3.5x10 <sup>-4</sup>
593	1.43	0.14	0.76	0.013	0.042	5.5x10 <sup>-4</sup>	0.021	2.7x10 <sup>-4</sup>
603	1.41	0.17	0.75	0.019	0.086	1.7x10 <sup>-3</sup>	0.043	8.2x10 <sup>-4</sup>
613	1.47	0.17	0.73	9.9x10 <sup>-3</sup>	0.18	1.7x10 <sup>-3</sup>	0.088	8.7x10 <sup>-4</sup>
623	1.64	0.20	0.65	8.5x10 <sup>-3</sup>	0.39	3.3x10 <sup>-3</sup>	0.20	1.7x10 <sup>-3</sup>
633	1.82	0.23	0.57	8.6x10 <sup>-3</sup>	0.58	5.0x10 <sup>-3</sup>	0.29	2.5x10 <sup>-3</sup>
643	2.03	0.26	0.48	0.010	0.75	7.6x10 <sup>-3</sup>	0.37	3.8x10 <sup>-3</sup>
653	2.34	0.28	0.37	5.2x10 <sup>-3</sup>	0.88	4.5x10 <sup>-3</sup>	0.44	2.3x10 <sup>-3</sup>
663	2.78	0.25	0.24	6.0x10 <sup>-3</sup>	0.86	5.2x10 <sup>-3</sup>	0.43	2.6x10 <sup>-3</sup>

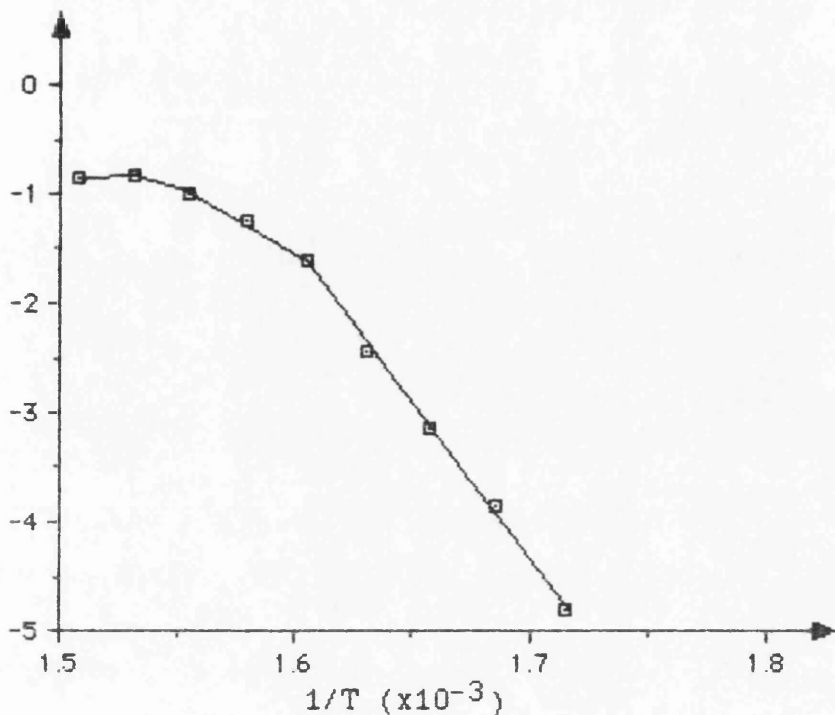
X<sub>HYD</sub> - Fractional hydrogenolysis conversion

X<sub>ISO</sub> - Fractional isomerisation conversion

Turnover - molecules s<sup>-1</sup> surface Ni atom<sup>-1</sup>

Graph 15 - Hydrogenolysis of n-butane over Ni/SiO<sub>2</sub>

Ln Turnover



Graph 16 - Selectivity for n-butane hydrogenolysis over Ni/SiO<sub>2</sub>

Selectivity

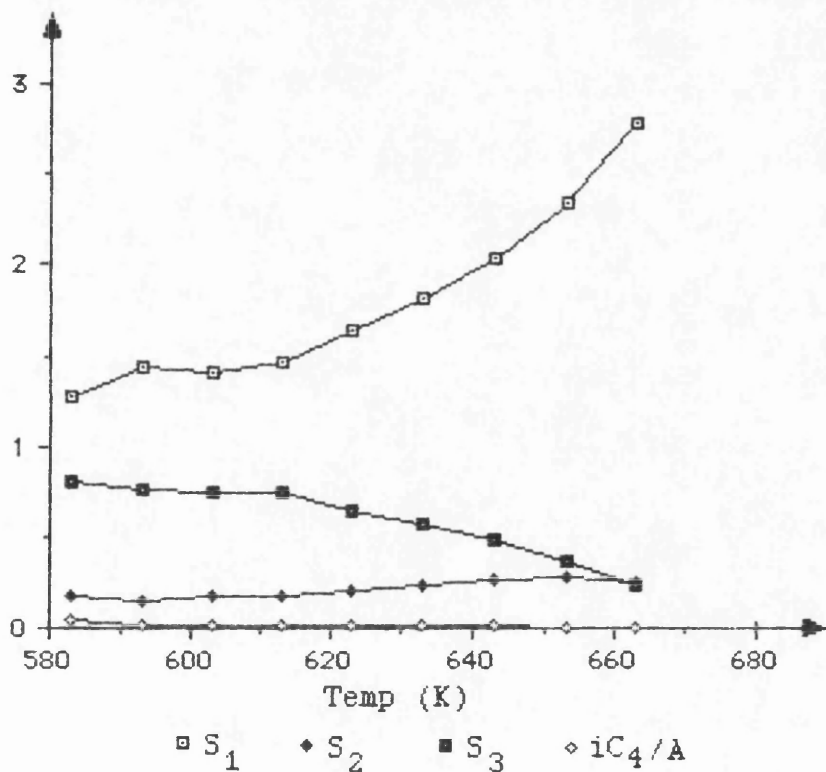


Table 19 - Hydrogenolysis of n-butane over Ni/MoO<sub>3</sub>

Temp (K)	S <sub>1</sub>	S <sub>2</sub>	S <sub>3</sub>	$\frac{iC_4}{A}$	X <sub>HYD</sub>	X <sub>ISO</sub>	Turnover (hydrog)	Turnover (isom)
693	2.41	0.14	0.43	0.75	$2.4 \times 10^{-3}$	$1.8 \times 10^{-3}$	$1.6 \times 10^{-3}$	$1.2 \times 10^{-3}$
703	1.51	0.59	0.44	0.79	$6.2 \times 10^{-3}$	$4.9 \times 10^{-3}$	$4.1 \times 10^{-3}$	$3.3 \times 10^{-3}$
713	1.71	0.37	0.52	0.15	0.012	$1.8 \times 10^{-3}$	$8.0 \times 10^{-3}$	$1.2 \times 10^{-3}$
723	1.75	0.21	0.60	0.18	0.016	$2.9 \times 10^{-3}$	0.011	$2.1 \times 10^{-3}$
733	1.52	0.26	0.61	0.52	0.012	$6.4 \times 10^{-3}$	$8.2 \times 10^{-3}$	$4.3 \times 10^{-3}$
743	1.84	0.38	0.46	1.25	0.010	0.013	$6.8 \times 10^{-3}$	$8.6 \times 10^{-3}$
753	1.79	0.42	0.46	1.68	0.010	0.017	$6.8 \times 10^{-3}$	0.011
763	1.58	0.69	0.35	1.42	0.014	0.020	$9.1 \times 10^{-3}$	0.013

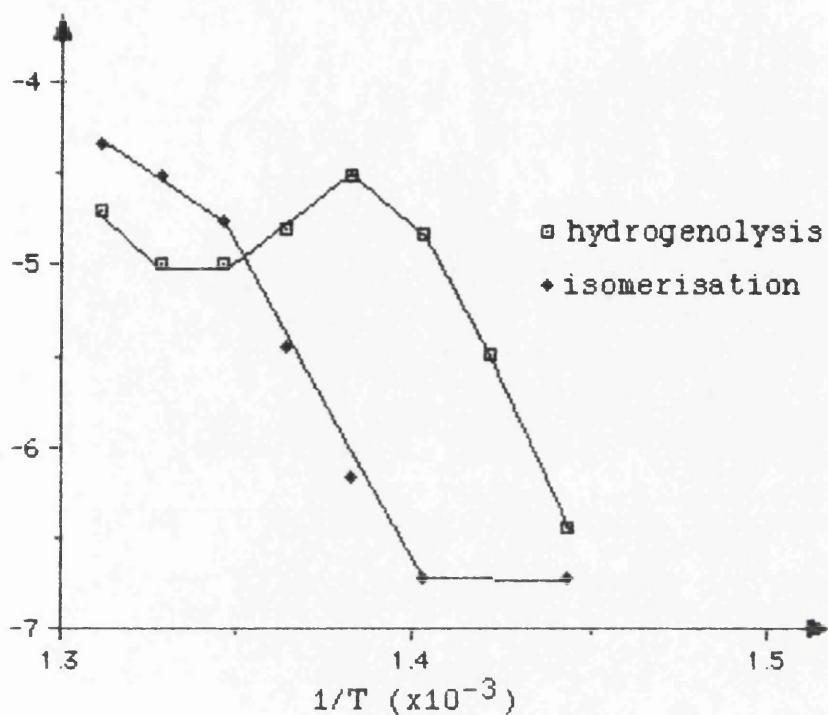
X<sub>HYD</sub> - Fractional hydrogenolysis conversion

X<sub>ISO</sub> - Fractional isomerisation conversion

Turnover - molecules s<sup>-1</sup> surface Ni atom<sup>-1</sup>

Graph 17 - Hydrogenolysis of n-butane over Ni/MoO<sub>3</sub>

Ln Turnover



Graph 18 - Selectivity for n-butane hydrogenolysis over Ni/MoO<sub>3</sub>

Selectivity

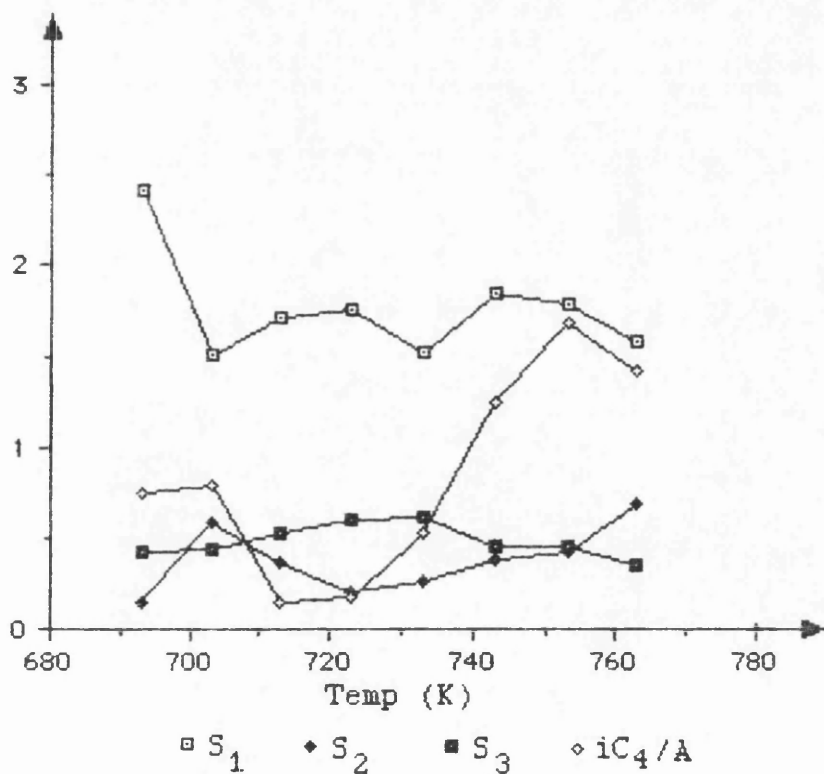


Table 20 - Hydrogenolysis of n-butane over Ni/WO<sub>3</sub>

Temp (K)	S <sub>1</sub>	S <sub>2</sub>	S <sub>3</sub>	$\frac{iC_4}{A}$	X <sub>H<sub>2</sub>D</sub>	X <sub>I<sub>2</sub>O</sub>	Turnover (hydrog)	Turnover (isom)
703	2.42	0.44	0.23	0.16	0.016	2.7x10 <sup>-3</sup>	4.2x10 <sup>-3</sup>	6.9x10 <sup>-4</sup>
713	2.72	0.29	0.23	0.33	0.011	3.7x10 <sup>-3</sup>	2.9x10 <sup>-3</sup>	9.5x10 <sup>-4</sup>
723	2.10	0.32	0.42	0.24	0.013	3.0x10 <sup>-3</sup>	3.3x10 <sup>-3</sup>	7.9x10 <sup>-4</sup>
733	2.16	0.27	0.43	0.14	0.017	2.8x10 <sup>-3</sup>	4.4x10 <sup>-3</sup>	7.2x10 <sup>-4</sup>
743	2.41	0.46	0.23	0.48	0.011	5.3x10 <sup>-3</sup>	2.8x10 <sup>-3</sup>	1.3x10 <sup>-3</sup>
753	1.85	0.81	0.18	0.36	0.010	3.8x10 <sup>-3</sup>	2.7x10 <sup>-3</sup>	9.8x10 <sup>-4</sup>

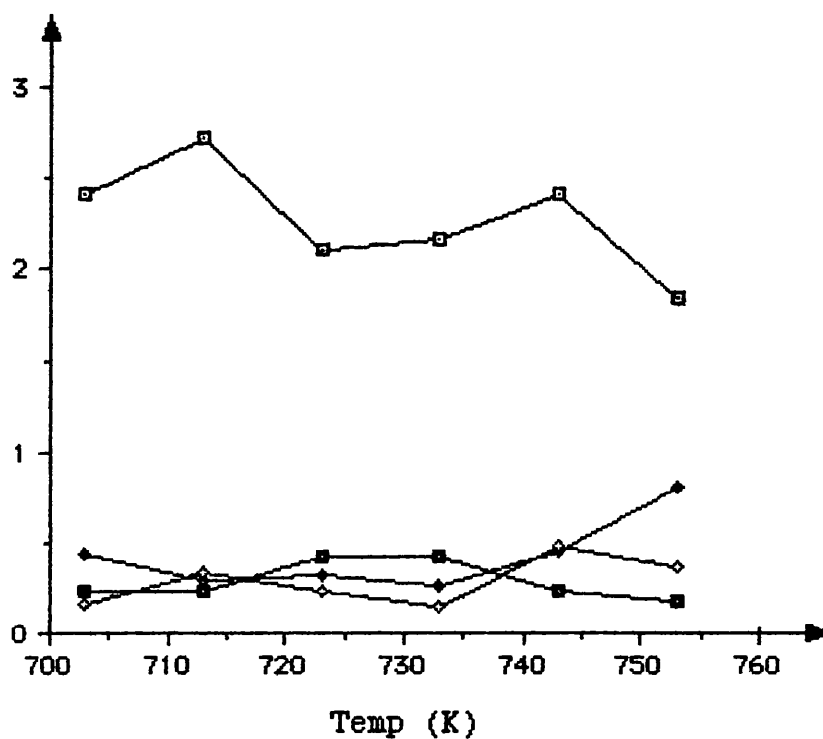
X<sub>H<sub>2</sub>D</sub> - Fractional hydrogenolysis conversion

X<sub>I<sub>2</sub>O</sub> - Fractional isomerisation conversion

Turnover - molecules s<sup>-1</sup> surface Ni atom<sup>-1</sup>

Graph 19 - Selectivity for n-butane hydrogenolysis  
over Ni/WO<sub>3</sub>

Selectivity



□ S<sub>1</sub>   ♦ S<sub>2</sub>   ■ S<sub>3</sub>   ◇ iC<sub>4</sub>/A

### 5.3.3.2 Activation energies for n-butane hydrogenolysis

The apparent activation energies in Table 21 below for the hydrogenolysis and isomerisation of n-butane over the supported catalysts were calculated where possible from the plots of  $\ln(\text{turnover})$  against  $1/T$  in a similar way to the hydrogenolysis of ethane (section 5.3.1.2).

Table 21(a) - Activation energies for n-butane hydrogenolysis

Catalyst	Temp (K)	Ea (kJmol <sup>-1</sup> )	ln A
Pt/Al <sub>2</sub> O <sub>3</sub>	693-763	130	22.3
Pt/SiO <sub>2</sub>	593-673	96	14.0
Pt/MoO <sub>3</sub>	693-763	53	7.7
-----			
Ni/Al <sub>2</sub> O <sub>3</sub>	713-763	154	23.5
Ni/SiO <sub>2</sub>	583-663	234	48.0
Ni/MoO <sub>3</sub>	693-768	271	44.7
Ni/WO <sub>3</sub>	703-753	-	-

Units of A - molecules s<sup>-1</sup> surface metal atom<sup>-1</sup>

Table 21(b) - Activation energies for n-butane isomerisation

Catalyst	Temp (K)	Ea (kJmol <sup>-1</sup> )	ln A
Pt/Al <sub>2</sub> O <sub>3</sub>	693-763	161	24.8
Pt/SiO <sub>2</sub>	593-673	102	15.1
Pt/MoO <sub>3</sub>	693-763	274	45.4
Ni/Al <sub>2</sub> O <sub>3</sub>	713-763	-	-
Ni/SiO <sub>2</sub>	583-663	-	-
Ni/MoO <sub>3</sub>	693-768	252	40.0
Ni/WO <sub>3</sub>	703-753	-	-

Units of A - molecules s<sup>-1</sup> surface metal atom<sup>-1</sup>

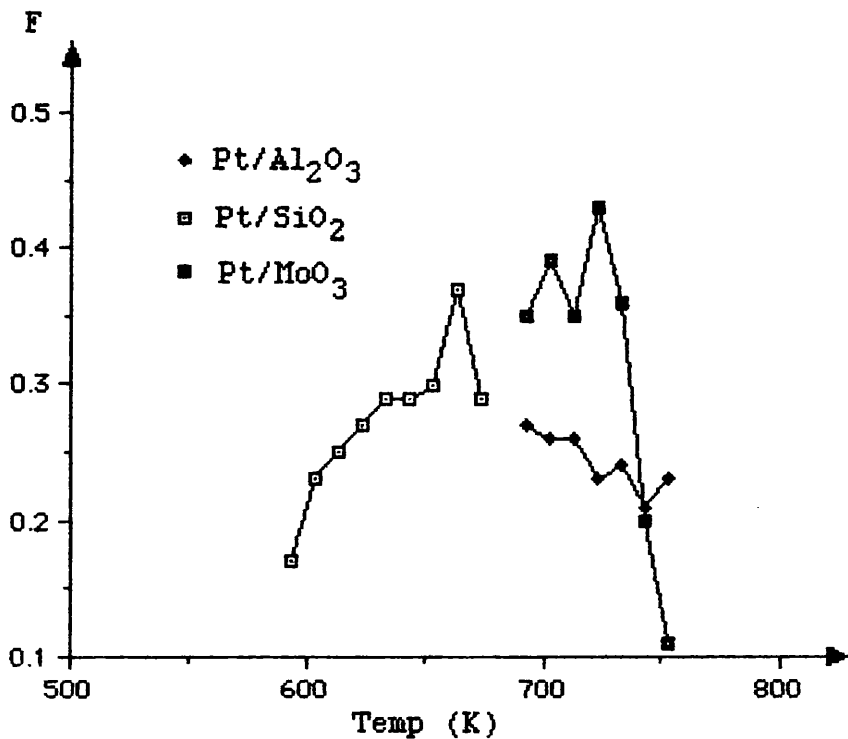
### 5.3.3.3 n-butane splitting factor (F)

Following the Kempling-Anderson reaction network, F, the probability of breaking the central C-C bond in n-butane was calculated for the platinum catalysts using the procedure given in section 4.3.8. These results are shown in Table 22 below and in Graph 20.

Table 22 - n-butane splitting factor (F)

Pt/Al <sub>2</sub> O <sub>3</sub>		Pt/SiO <sub>2</sub>		Pt/MoO <sub>3</sub>	
Temp (K)	F	Temp (K)	F	Temp (K)	F
693	0.27	593	0.17	693	0.35
703	0.26	603	0.23	703	0.39
713	0.26	613	0.25	713	0.35
723	0.23	623	0.27	723	0.43
733	0.24	633	0.29	733	0.36
743	0.21	643	0.29	743	0.20
753	0.23	653	0.30	753	0.11
		663	0.37		
		673	0.29		

Graph 20 - n-butane splitting factor (F)



#### 5.3.4 iso-butane hydrogenolysis

The hydrogenolysis of iso-butane was carried out over the series of supported catalysts, varying the reaction temperature to calculate activation energies. All the reactions were carried out with a He flow rate of 17.8 ml min<sup>-1</sup>, a H<sub>2</sub> flow rate of 22.0 ml min<sup>-1</sup> and a flow of iso-butane of 6.5 ml min<sup>-1</sup>. The forward gas pressures were held at 30 lb. in<sup>-2</sup>.

For each catalyst there is a table of results containing fractional conversions and turnover figures for hydrogenolysis and isomerisation reactions, selectivities for methane (S<sub>1</sub>), ethane (S<sub>2</sub>) and propane (S<sub>3</sub>) and selectivity for isomerisation over hydrogenolysis (n-C<sub>4</sub>/A).

Each table is accompanied by a graph of ln(turnover) against 1/T and selectivity against temperature.

Table 23 - Hydrogenolysis of iso-butane over Pt/Al<sub>2</sub>O<sub>3</sub>

Temp (K)	S <sub>1</sub>	S <sub>2</sub>	S <sub>3</sub>	$\frac{nC_4}{A}$	X <sub>HYD</sub>	X <sub>ISO</sub>	Turnover (hydrog)	Turnover (isom)
643	0.96	0.29	0.82	0.13	0.016	2.1x10 <sup>-3</sup>	0.015	1.9x10 <sup>-3</sup>
653	0.99	0.14	0.91	0.11	0.029	3.2x10 <sup>-3</sup>	0.027	2.9x10 <sup>-3</sup>
663	1.03	0.09	0.93	0.11	0.040	4.4x10 <sup>-3</sup>	0.036	4.1x10 <sup>-3</sup>
683	1.06	0.03	0.96	0.13	0.065	8.0x10 <sup>-3</sup>	0.058	7.5x10 <sup>-3</sup>
693	1.08	0.03	0.95	0.12	0.095	0.011	0.089	0.011
703	1.09	0.03	0.95	0.13	0.098	0.013	0.091	0.012
713	1.08	0.04	0.95	0.16	0.12	0.019	0.11	0.018

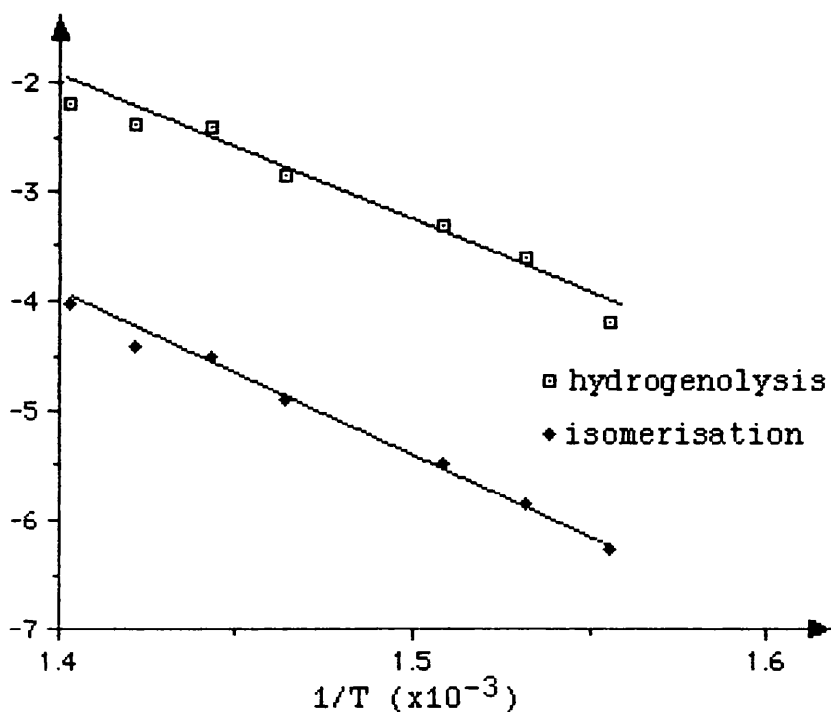
X<sub>HYD</sub> - Fractional hydrogenolysis conversion

X<sub>ISO</sub> - Fractional isomerisation conversion

Turnover - molecules s<sup>-1</sup> surface Pt atom<sup>-1</sup>

Graph 21 - Hydrogenolysis of iso-butane over Pt/Al<sub>2</sub>O<sub>3</sub>

Ln Turnover



Graph 22 - Selectivity for iso-butane hydrogenolysis over Pt/Al<sub>2</sub>O<sub>3</sub>

Selectivity

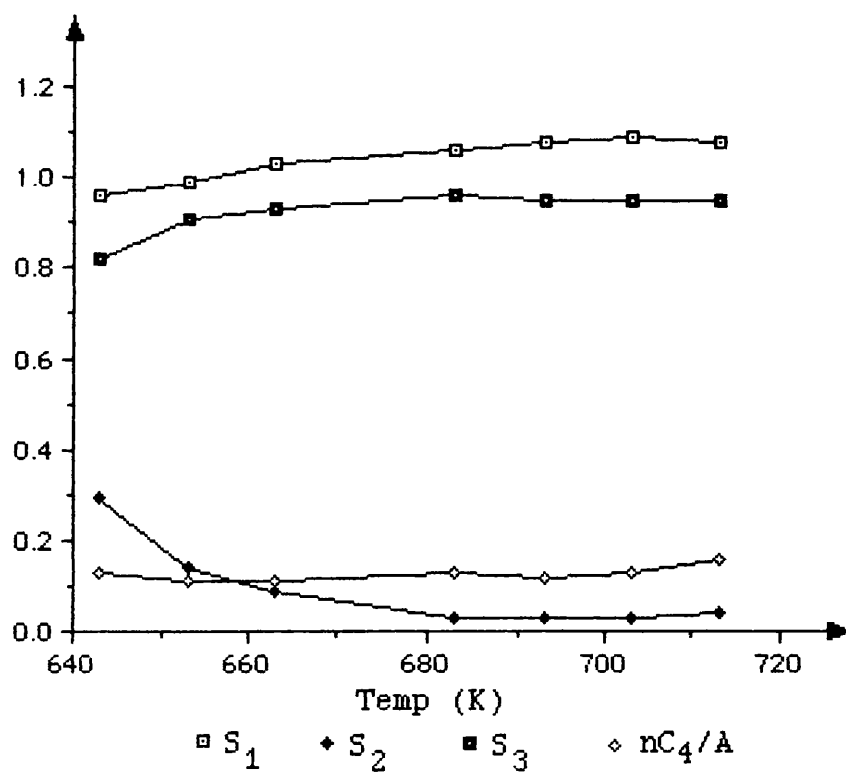


Table 24 - Hydrogenolysis of iso-butane over Pt/SiO<sub>2</sub>

Temp (K)	S <sub>1</sub>	S <sub>2</sub>	S <sub>3</sub>	$\frac{nC_4}{A}$	X <sub>H<sub>2</sub>D</sub>	X <sub>I<sub>2</sub>O</sub>	Turnover (hydrog)	Turnover (isom)
653	1.01	0.34	0.77	1.44	5.1x10 <sup>-3</sup>	7.3x10 <sup>-3</sup>	8.1x10 <sup>-3</sup>	0.012
663	1.10	0.16	0.86	2.00	6.9x10 <sup>-3</sup>	0.014	0.011	0.022
673	1.11	0.10	0.90	2.28	7.7x10 <sup>-3</sup>	0.018	0.012	0.028
683	1.06	0.10	0.91	2.24	0.012	0.026	0.019	0.042
703	1.06	0.18	0.86	2.67	0.021	0.057	0.034	0.085
713	1.09	0.21	0.84	2.16	0.035	0.074	0.056	0.12
723	1.10	0.26	0.79	1.83	0.046	0.083	0.073	0.13
733	1.07	0.25	0.81	1.67	0.051	0.085	0.082	0.14

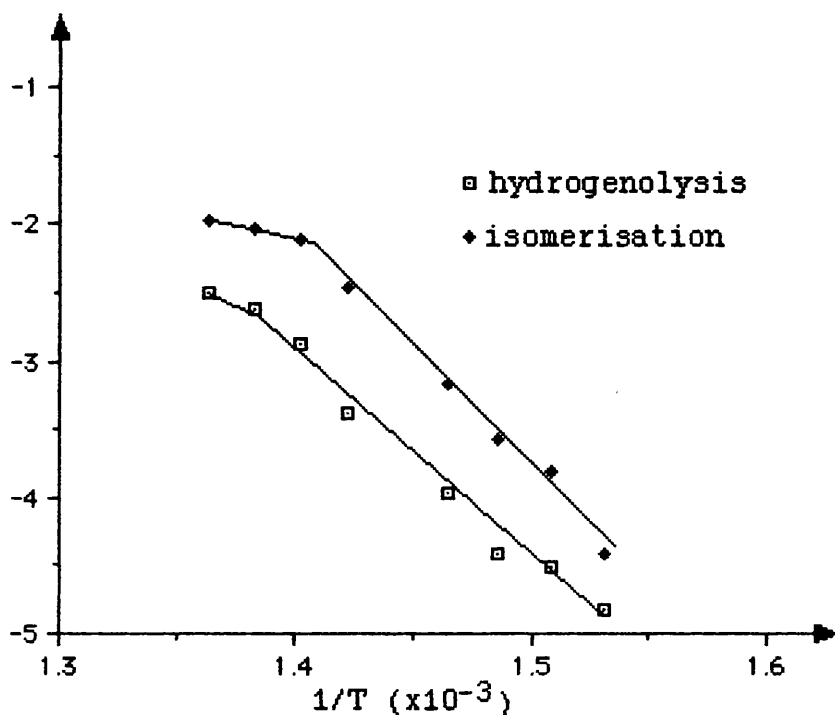
X<sub>H<sub>2</sub>D</sub> - Fractional hydrogenolysis conversion

X<sub>I<sub>2</sub>O</sub> - Fractional isomerisation conversion

Turnover - molecules s<sup>-1</sup> surface Pt atom<sup>-1</sup>

Graph 23 - Hydrogenolysis of iso-butane over Pt/SiO<sub>2</sub>

Ln Turnover



Graph 24 - Selectivity for iso-butane hydrogenolysis Over Pt/SiO<sub>2</sub>

Selectivity

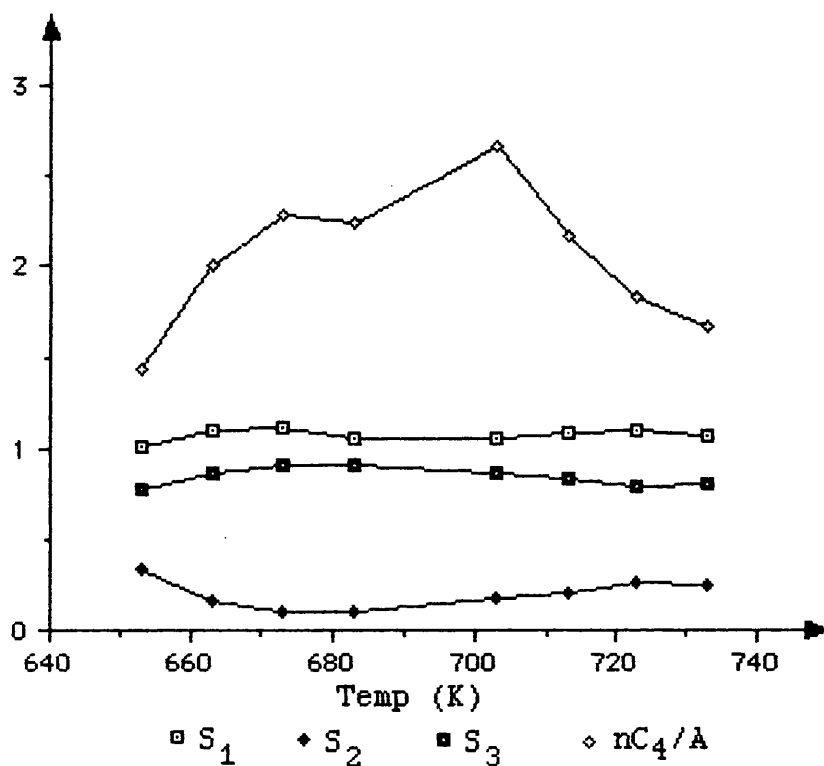


Table 25 - Hydrogenolysis of iso-butane over Pt/MoO<sub>3</sub>

Temp (K)	S <sub>1</sub>	S <sub>2</sub>	S <sub>3</sub>	$\frac{nC_4}{A}$	X <sub>H<sub>2</sub>D</sub>	X <sub>ISO</sub>	Turnover (hydrog)	Turnover (isom)
633	0.43	1.42	0.24	1.19	5.6x10 <sup>-3</sup>	6.7x10 <sup>-3</sup>	0.017	0.012
643	0.32	1.16	0.45	2.35	4.5x10 <sup>-3</sup>	0.010	0.014	0.019
653	0.55	0.94	0.62	4.68	3.2x10 <sup>-3</sup>	0.015	0.010	0.028
663	0.93	0.56	0.65	6.95	3.9x10 <sup>-3</sup>	0.021	0.012	0.039
673	0.98	0.55	0.65	8.01	6.9x10 <sup>-3</sup>	0.048	0.022	0.086
683	1.01	0.62	0.58	7.93	9.5x10 <sup>-3</sup>	0.076	0.030	0.14
693	0.90	0.42	0.75	8.99	0.015	0.12	0.045	0.21
703	1.01	0.35	0.76	9.10	0.019	0.17	0.058	0.30
723	0.95	0.31	0.81	7.44	0.025	0.19	0.079	0.34
733	1.04	0.32	0.77	6.52	0.030	0.20	0.093	0.35

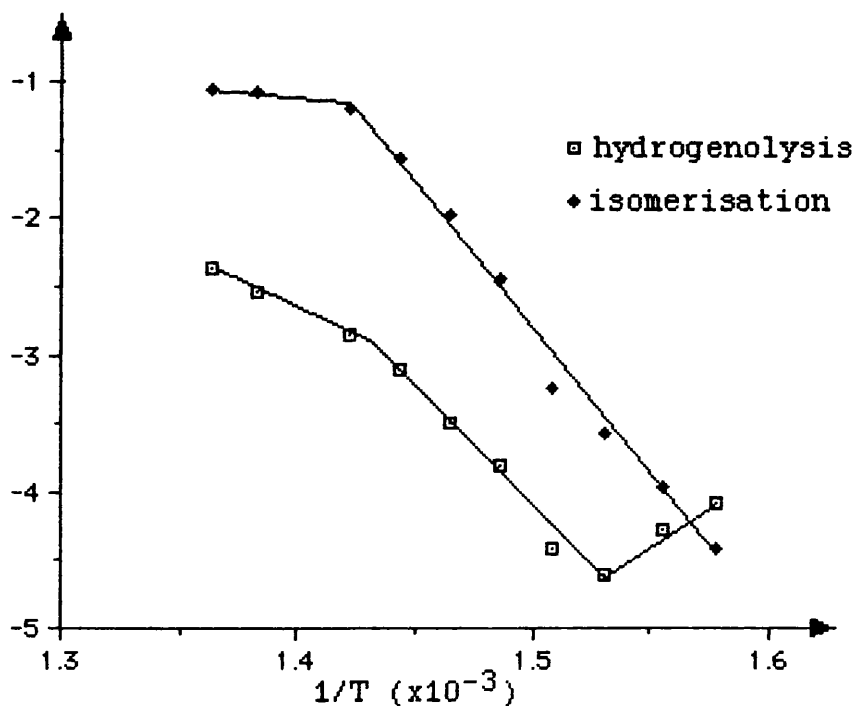
X<sub>H<sub>2</sub>D</sub> - Fractional hydrogenolysis conversion

X<sub>ISO</sub> - Fractional isomerisation conversion

Turnover - molecules s<sup>-1</sup> surface Pt atom<sup>-1</sup>

Graph 25 - Hydrogenolysis of iso-butane over Pt/MoO<sub>3</sub>

Ln Turnover



Graph 26 - Selectivity for iso-butane hydrogenolysis over Pt/MoO<sub>3</sub>

Selectivity

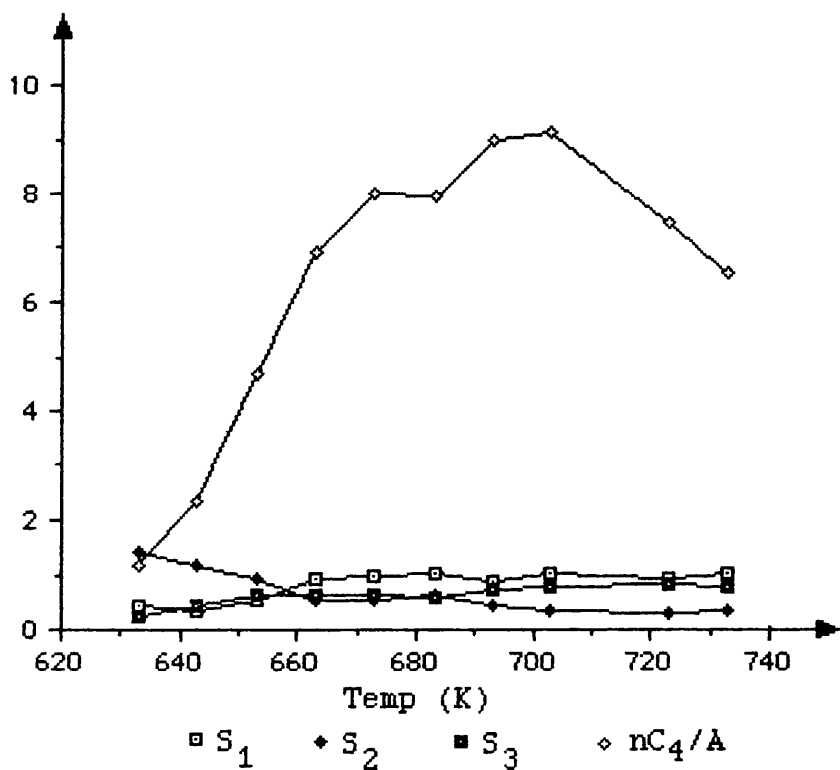


Table 26 - Hydrogenolysis of iso-butane over Ni/Al<sub>2</sub>O<sub>3</sub>

Temp (K)	S <sub>1</sub>	S <sub>2</sub>	S <sub>3</sub>	$\frac{nC_4}{A}$	X <sub>HYD</sub>	X <sub>ISO</sub>	Turnover (hydrog)	Turnover (isom)
593	1.78	0.15	0.64	0.34	5.1x10 <sup>-3</sup>	1.8x10 <sup>-3</sup>	9.4x10 <sup>-3</sup>	3.2x10 <sup>-3</sup>
603	1.97	0.51	0.34	0.04	7.2x10 <sup>-3</sup>	3.0x10 <sup>-3</sup>	0.013	5.4x10 <sup>-4</sup>
613	2.91	0.15	0.26	0.04	0.015	5.6x10 <sup>-3</sup>	0.028	1.0x10 <sup>-3</sup>
623	3.17	0.14	0.18	0.02	0.028	5.7x10 <sup>-3</sup>	0.052	1.0x10 <sup>-3</sup>
643	3.56	0.08	0.09	-	0.062	-	0.11	-
653	3.59	0.09	0.08	4.4x10 <sup>-3</sup>	0.084	3.7x10 <sup>-3</sup>	0.15	6.7x10 <sup>-3</sup>
673	3.79	0.06	0.03	3.6x10 <sup>-3</sup>	0.22	8.0x10 <sup>-4</sup>	0.40	1.5x10 <sup>-3</sup>
683	3.83	0.05	0.02	2.7x10 <sup>-3</sup>	0.29	7.9x10 <sup>-4</sup>	0.53	1.4x10 <sup>-3</sup>

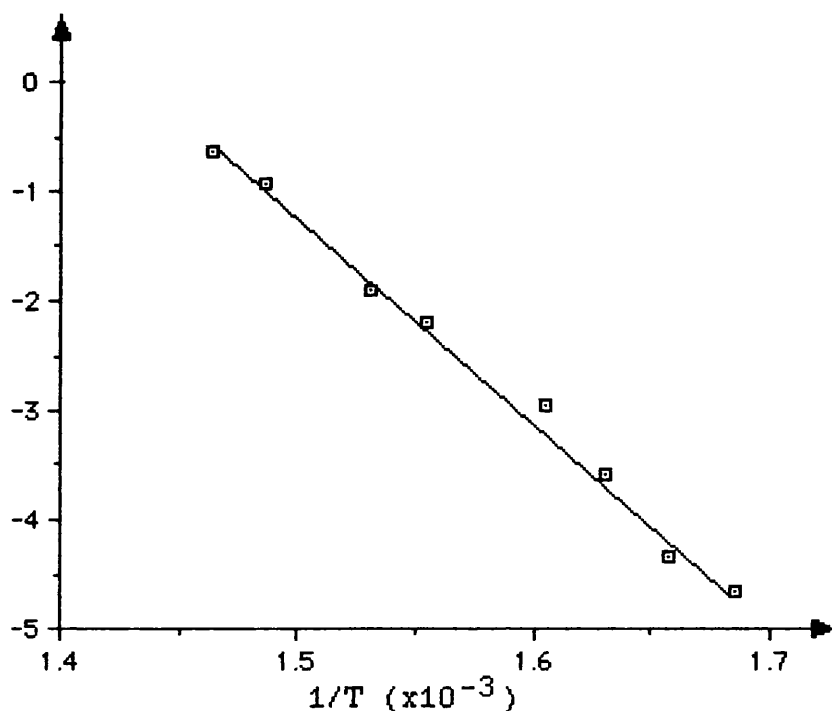
X<sub>HYD</sub> - Fractional hydrogenolysis conversion

X<sub>ISO</sub> - Fractional isomerisation conversion

Turnover - molecules s<sup>-1</sup> surface Ni atom<sup>-1</sup>

Graph 27 - Hydrogenolysis of iso-butane over Ni/Al<sub>2</sub>O<sub>3</sub>

Ln Turnover



Graph 28 - Selectivity for iso-butane hydrogenolysis over Ni/Al<sub>2</sub>O<sub>3</sub>

Selectivity

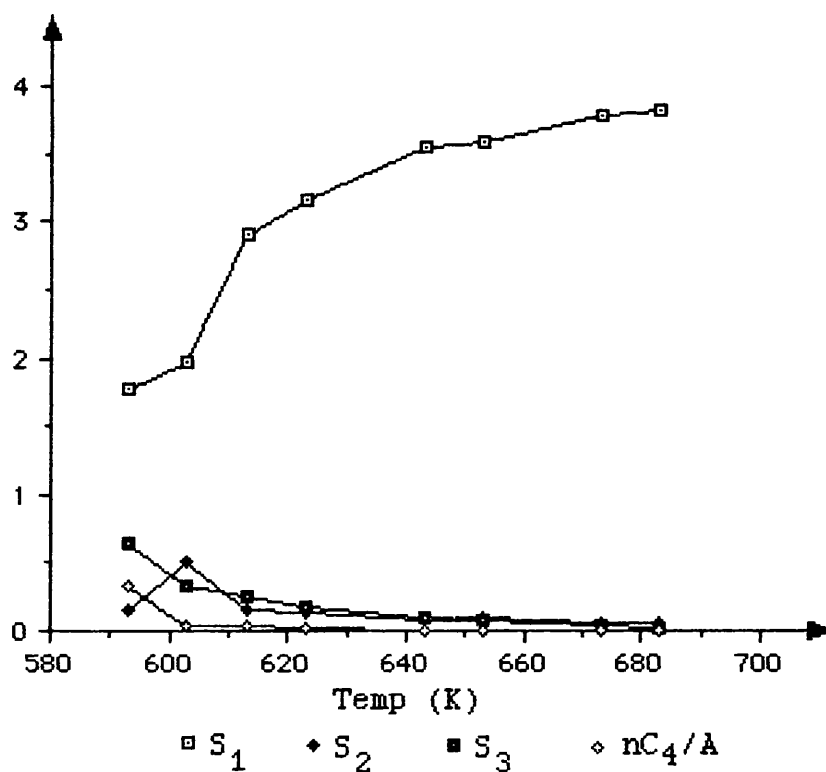


Table 27 - Hydrogenolysis of iso-butane over Ni/SiO<sub>2</sub>

Temp (K)	S <sub>1</sub>	S <sub>2</sub>	S <sub>3</sub>	$\frac{nC_4}{A}$	X <sub>HYD</sub>	X <sub>ISO</sub>	Turnover (hydrog)	Turnover (isom)
503	1.15	0.12	0.87	0.085	0.010	8.6x10 <sup>-4</sup>	5.0x10 <sup>-3</sup>	4.4x10 <sup>-4</sup>
513	1.18	0.12	0.86	0.046	0.017	7.6x10 <sup>-4</sup>	8.2x10 <sup>-3</sup>	3.8x10 <sup>-4</sup>
523	1.31	0.12	0.81	0.018	0.058	1.1x10 <sup>-3</sup>	0.029	5.5x10 <sup>-4</sup>
533	1.34	0.13	0.80	0.014	0.13	1.8x10 <sup>-3</sup>	0.064	8.8x10 <sup>-4</sup>
643	1.39	0.13	0.78	0.010	0.19	2.1x10 <sup>-3</sup>	0.096	1.0x10 <sup>-3</sup>
553	2.87	0.24	0.22	1.6x10 <sup>-3</sup>	0.62	1.0x10 <sup>-3</sup>	0.31	4.9x10 <sup>-4</sup>
563	3.43	0.25	0.02	-	1.00	-	0.50	-
573	3.34	0.28	0.04	-	1.00	-	0.49	-

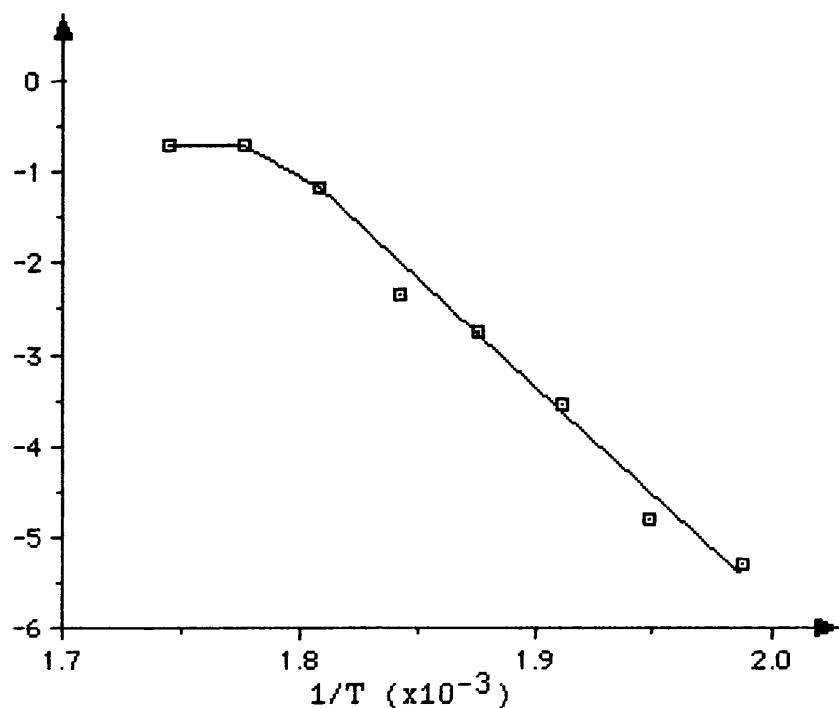
X<sub>HYD</sub> - Fractional hydrogenolysis conversion

X<sub>ISO</sub> - Fractional isomerisation conversion

Turnover - molecules s<sup>-1</sup> surface Ni atom<sup>-1</sup>

Graph 29 - Hydrogenolysis of iso-butane over Ni/SiO<sub>2</sub>

Ln Turnover



Graph 30 - Selectivity for iso-butane hydrogenolysis over Ni/SiO<sub>2</sub>

Selectivity

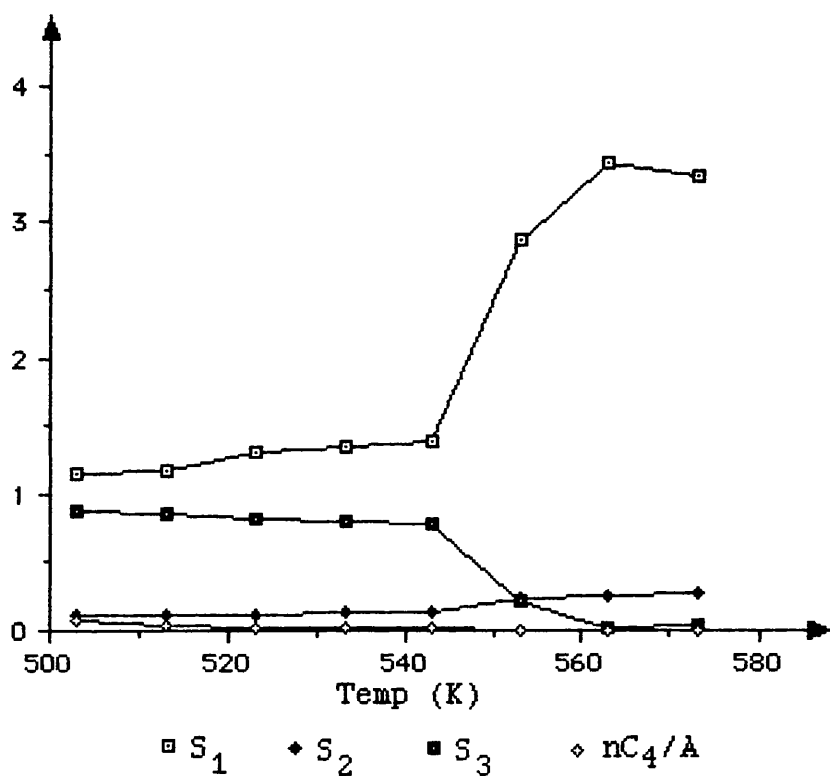


Table 28 - Hydrogenolysis of iso-butane over Ni/MoO<sub>3</sub>

Temp (K)	S <sub>1</sub>	S <sub>2</sub>	S <sub>3</sub>	$\frac{nC_4}{A}$	X <sub>H<sub>2</sub>D</sub>	X <sub>I<sub>2</sub>O</sub>	Turnover (hydrog)	Turnover (isom)
603	-	-	1.33	0.66	1.6x10 <sup>-3</sup>	1.0x10 <sup>-3</sup>	1.0x10 <sup>-3</sup>	6.8x10 <sup>-4</sup>
613	0.95	0.38	0.76	2.22	1.2x10 <sup>-3</sup>	2.8x10 <sup>-3</sup>	8.4x10 <sup>-4</sup>	1.9x10 <sup>-3</sup>
623	0.89	0.46	0.73	1.87	1.2x10 <sup>-3</sup>	2.2x10 <sup>-3</sup>	7.7x10 <sup>-4</sup>	1.5x10 <sup>-3</sup>
643	1.15	0.40	0.68	0.31	4.8x10 <sup>-3</sup>	1.5x10 <sup>-3</sup>	3.3x10 <sup>-3</sup>	9.9x10 <sup>-4</sup>
653	1.68	0.21	0.63	0.05	0.010	6.0x10 <sup>-4</sup>	7.0x10 <sup>-3</sup>	3.9x10 <sup>-4</sup>
663	1.85	0.21	0.58	0.05	0.018	8.4x10 <sup>-4</sup>	0.012	5.6x10 <sup>-4</sup>
673	1.87	0.28	0.53	0.11	0.028	3.1x10 <sup>-3</sup>	0.019	2.1x10 <sup>-3</sup>
683	1.83	0.20	0.59	0.15	0.020	3.0x10 <sup>-3</sup>	0.014	2.1x10 <sup>-3</sup>
693	2.02	0.19	0.53	0.66	0.014	9.5x10 <sup>-3</sup>	9.8x10 <sup>-3</sup>	6.3x10 <sup>-3</sup>
703	1.62	0.21	0.66	1.27	0.012	0.016	0.011	0.011
718	1.96	0.20	0.55	2.39	0.014	0.034	9.5x10 <sup>-3</sup>	0.023

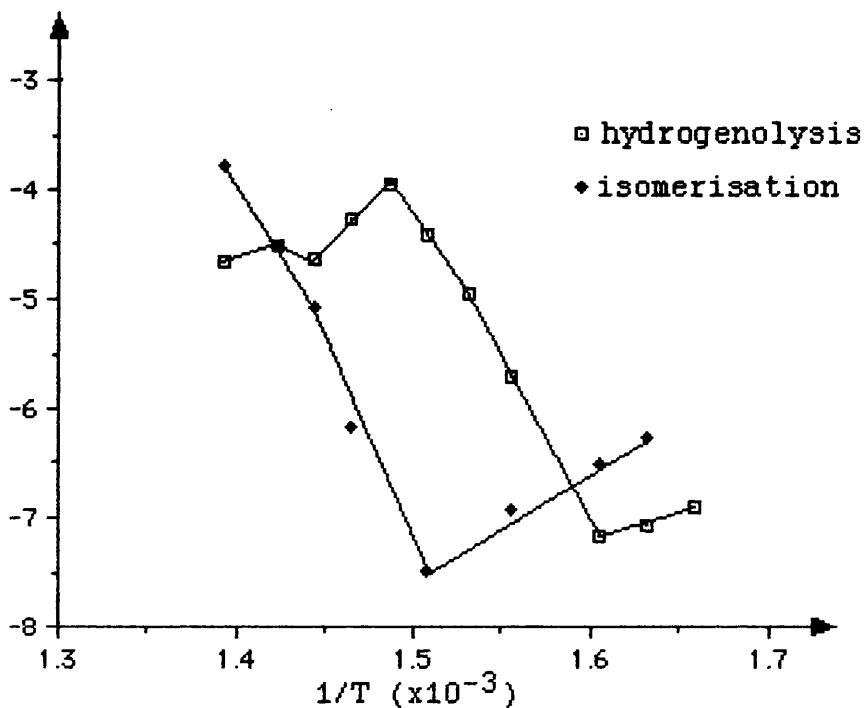
X<sub>H<sub>2</sub>D</sub> - Fractional hydrogenolysis conversion

X<sub>I<sub>2</sub>O</sub> - Fractional isomerisation conversion

Turnover - molecules s<sup>-1</sup> surface Ni atom<sup>-1</sup>

Graph 31 - Hydrogenolysis of iso-butane over Ni/MoO<sub>3</sub>

Ln Turnover



Graph 32 - Selectivity for iso-butane hydrogenolysis over Ni/MoO<sub>3</sub>

Selectivity

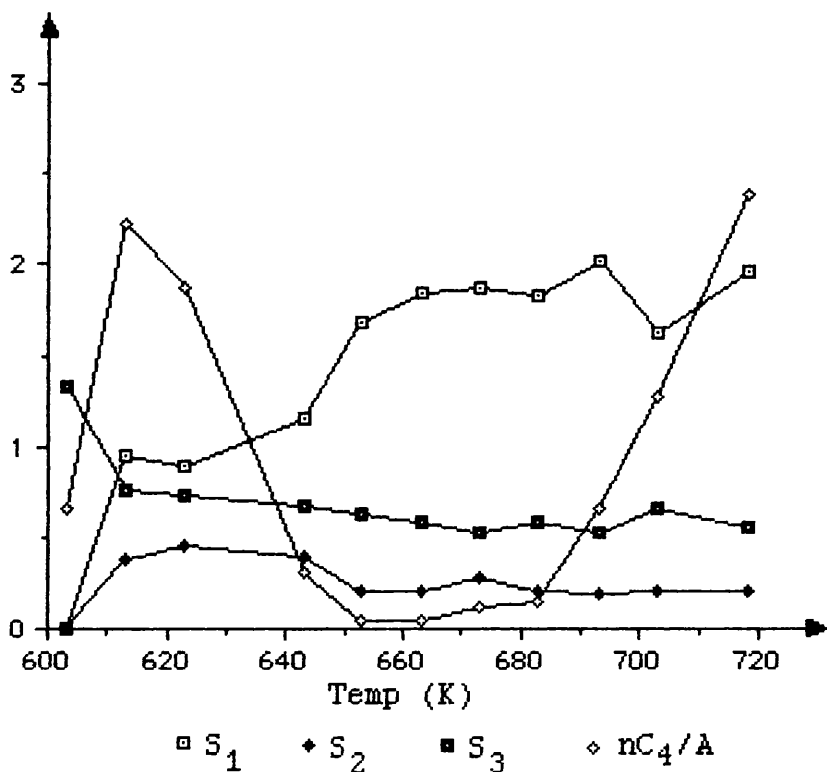


Table 29 - Hydrogenolysis of iso-butane over Ni/WO<sub>3</sub>

Temp (K)	S <sub>1</sub>	S <sub>2</sub>	S <sub>3</sub>	$\frac{nC_4}{A}$	X <sub>HYD</sub>	X <sub>ISO</sub>	Turnover (hydrog)	Turnover (isom)
643	2.66	0.36	0.21	0.07	0.019	1.4x10 <sup>-3</sup>	8.5x10 <sup>-3</sup>	6.4x10 <sup>-4</sup>
653	2.69	0.41	0.16	0.19	0.017	3.3x10 <sup>-3</sup>	8.0x10 <sup>-3</sup>	1.4x10 <sup>-3</sup>
663	2.42	0.34	0.30	0.26	0.016	3.9x10 <sup>-3</sup>	7.1x10 <sup>-3</sup>	1.8x10 <sup>-3</sup>
673	2.62	0.34	0.23	0.32	0.013	4.2x10 <sup>-3</sup>	6.1x10 <sup>-3</sup>	1.9x10 <sup>-3</sup>
683	2.21	0.44	0.30	0.33	8.0x10 <sup>-3</sup>	2.6x10 <sup>-3</sup>	3.7x10 <sup>-3</sup>	1.2x10 <sup>-3</sup>
693	1.35	0.69	0.43	0.81	3.4x10 <sup>-3</sup>	2.7x10 <sup>-3</sup>	1.6x10 <sup>-3</sup>	1.2x10 <sup>-3</sup>

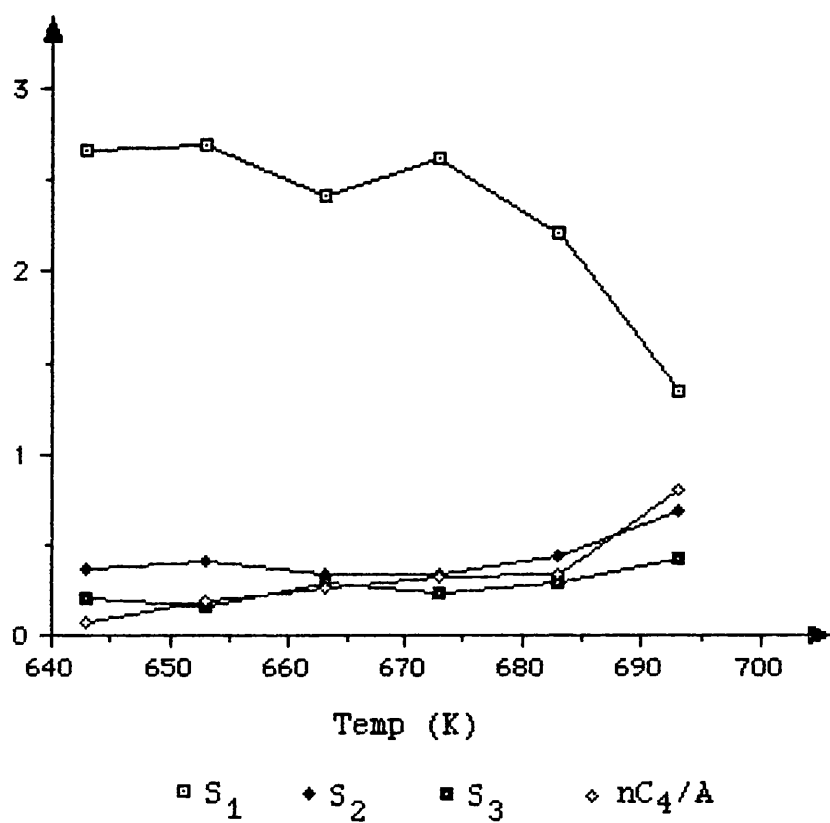
X<sub>HYD</sub> - Fractional hydrogenolysis conversion

X<sub>ISO</sub> - Fractional isomerisation conversion

Turnover - molecules s<sup>-1</sup> surface Ni atom<sup>-1</sup>

Graph 33 - Selectivity for iso-butane hydrogenolysis  
over Ni/WO<sub>3</sub>

Selectivity



### 5.3.4.2 Activation energies for hydrogenolysis of iso-butane

The apparent activation energies for the hydrogenolysis and isomerisation of iso-butane over the supported catalysts are shown in Table 30 below. They were calculated, where possible, from the plots of  $\ln(\text{turnover})$  against  $1/T$  in a similar fashion to the reactions of ethane, propane and n-butane earlier.

Table 30(a) - Activation energies for iso-butane hydrogenolysis

Catalyst	Temp (K)	Ea (kJmol <sup>-1</sup> )	ln A
Pt/Al <sub>2</sub> O <sub>3</sub>	643-713	92	17.1
Pt/SiO <sub>2</sub>	653-733	125	21.4
Pt/MoO <sub>3</sub>	633-733	136	22.8
Ni/Al <sub>2</sub> O <sub>3</sub>	593-683	152	29.4
Ni/SiO <sub>2</sub>	503-573	183	42.9
Ni/MoO <sub>3</sub>	603-718	228	41.7
Ni/WO <sub>3</sub>	643-693	-	-

Units of A - molecules s<sup>-1</sup> surface metal atom<sup>-1</sup>

Table 30(b)- Activation energies for iso-butane isomerisation

Catalyst	Temp (K)	Ea (kJmol <sup>-1</sup> )	ln A
Pt/Al <sub>2</sub> O <sub>3</sub>	643-713	116	19.4
Pt/SiO <sub>2</sub>	653-733	148	26.3
Pt/MoO <sub>3</sub>	633-733	176	31.3
Ni/Al <sub>2</sub> O <sub>3</sub>	593-683	-	-
Ni/SiO <sub>2</sub>	503-573	-	-
Ni/MoO <sub>3</sub>	603-718	274	46.3
Ni/WO <sub>3</sub>	643-693	-	-

Units of A - molecules s<sup>-1</sup> surface metal atom<sup>-1</sup>

#### 5.4 HYDROGEN PRESSURE RATE COEFFICIENT

One of the most important kinetic features of alkane hydrogenolysis is the strong inverse dependence of hydrogen pressure on the reaction rate, at high hydrogen pressures (section 1.4).

Following the procedure given in section 3.5.2 the hydrogenolysis of ethane, ethene, propane, propene

was carried out over the Pt/Al<sub>2</sub>O<sub>3</sub> and the Ni/Al<sub>2</sub>O<sub>3</sub> catalysts, varying the H<sub>2</sub> pressure to derive m, the order of the reaction with respect to hydrogen.

For the reactions of ethene and propene the fractional conversions towards hydrogenolysis and hydrogenated products were calculated from the following equations,

$$\text{For ethene} \quad X_{\text{Hydrogenolysis}} = \frac{A}{A + C_2H_6 + C_2H_4}$$

$$X_{\text{Hydrogenation}} = \frac{C_2H_6}{A + C_2H_6 + C_2H_4}$$

where A = moles of ethene transformed by hydrogenolysis  
 (=  $\frac{C_1}{2}$ )

C<sub>2</sub>H<sub>6</sub> = moles of ethane produced

C<sub>2</sub>H<sub>4</sub> = moles of unreacted ethene

$$\text{For propene} \quad X_{\text{Hydrogenolysis}} = \frac{A}{A + C_3H_8 + C_3H_6}$$

$$X_{\text{Hydrogenation}} = \frac{C_3H_8}{A + C_3H_8 + C_3H_6}$$

where A = moles of propene transformed by hydrogenolysis  
 (=  $\frac{C_1 + 2C_2}{3}$ )

C<sub>3</sub>H<sub>8</sub> = moles of propane produced

C<sub>3</sub>H<sub>6</sub> = moles of unreacted propene

All the reactions were carried out at 703K. The results of these reactions are shown in Tables 32, 32, 33 and 34. Graphs 34 and 35 plot  $\log(\text{turnover})$  against  $\log(\text{hydrogen pressure})$  for all the reactant gases over the  $\text{Pt}/\text{Al}_2\text{O}_3$  and  $\text{Ni}/\text{Al}_2\text{O}_3$  catalysts respectively. Graph 36 plots the selectivity for methane ( $S_1$ ) against hydrogen pressure for the hydrogenolysis of propane and propene over the  $\text{Pt}/\text{Al}_2\text{O}_3$  and  $\text{Ni}/\text{Al}_2\text{O}_3$  catalysts.

Table 31 - Ethane hydrogenolysis over Pt/Al<sub>2</sub>O<sub>3</sub> and Ni/Al<sub>2</sub>O<sub>3</sub>

Pt/Al <sub>2</sub> O <sub>3</sub>			Ni/Al <sub>2</sub> O <sub>3</sub>		
H <sub>2</sub> pressure (atm)	X <sub>HYD</sub>	Turnover	H <sub>2</sub> pressure (atm)	X <sub>HYD</sub>	Turnover
0.68	0.079	0.104	1.02	0.028	0.088
1.02	0.056	0.074	1.36	0.021	0.066
1.36	0.043	0.056	1.70	0.018	0.056
1.70	0.035	0.046	2.21	0.014	0.044
2.04	0.035	0.046	2.72	0.012	0.037
2.38	0.029	0.038	3.40	0.010	0.031
2.72	0.027	0.035			
3.06	0.025	0.033			
3.40	0.024	0.031			

X<sub>HYD</sub> - Fractional hydrogenolysis activity

Turnover - molecules s<sup>-1</sup> surface Pt atom<sup>-1</sup>

Table 32 - Ethene hydrogenolysis over Pt/Al<sub>2</sub>O<sub>3</sub> and Ni/Al<sub>2</sub>O<sub>3</sub>

Pt/Al <sub>2</sub> O <sub>3</sub>						Ni/Al <sub>2</sub> O <sub>3</sub>								
H <sub>2</sub> pressure (atm)	X <sub>1</sub>	X <sub>2</sub>	Turnover (1)	Turnover (2)	H <sub>2</sub> pressure (atm)	X <sub>1</sub>	X <sub>2</sub>	Turnover (1)	Turnover (2)	H <sub>2</sub> pressure (atm)	X <sub>1</sub>	X <sub>2</sub>	Turnover (1)	Turnover (2)
1.02	0.064	0.936	0.101	1.48	1.02	0.021	0.998	0.007	3.14	1.70	0.047	0.995	0.015	3.13
1.36	0.054	0.946	0.086	1.50	1.70	0.019	0.981	0.059	3.09	2.04	0.060	0.941	0.187	2.96
1.70	0.046	0.054	0.073	1.51	2.04	0.046	0.954	0.144	3.00	2.38	0.040	0.960	0.127	3.02
2.04	0.040	0.960	0.063	1.52	2.38	0.033	0.967	0.052	3.02	2.72	0.028	0.972	0.104	3.04
2.38	0.036	0.964	0.057	1.53	2.72	0.044	0.972	0.044	1.54	3.06	0.044	0.972	0.044	1.54
2.72	0.033	0.967	0.052	1.53	3.06	0.044	0.972	0.044	1.54	3.40	0.044	0.972	0.044	1.54
3.40	0.028	0.972	0.044	1.54	3.40	0.044	0.972	0.044	1.54					

X<sub>1</sub> - Fractional hydrogenolysis conversion      Turnover (1) - hydrogenolysis turnover

X<sub>2</sub> - Fractional hydrogenation conversion      (2) - hydrogenation turnover

(molecules s<sup>-1</sup> surface metal atom<sup>-1</sup>)

Table 33 - Hydrogenolysis of propane over Pt/Al<sub>2</sub>O<sub>3</sub> and Ni/Al<sub>2</sub>O<sub>3</sub>

Pt/Al <sub>2</sub> O <sub>3</sub>				Ni/Al <sub>2</sub> O <sub>3</sub>			
H <sub>2</sub> pressure (atm)	X <sub>HYD</sub>	Turnover	S <sub>1</sub>	H <sub>2</sub> pressure (atm)	X <sub>HYD</sub>	Turnover	S <sub>1</sub>
1.23	0.071	0.034	1.07	0.82	0.037	0.042	2.73
1.36	0.063	0.030	1.09	1.02	0.030	0.036	2.67
1.70	0.057	0.027	1.05	1.36	0.024	0.028	2.55
2.04	0.048	0.023	1.06	1.70	0.019	0.022	2.49
2.38	0.041	0.020	1.04	2.38	0.015	0.018	2.37
2.72	0.038	0.018	1.04	3.06	0.012	0.014	2.24
3.06	0.029	0.014	1.03				

X<sub>HYD</sub> - Fractional hydrogenolysis activity

Turnover - molecules s<sup>-1</sup> surface metal atom<sup>-1</sup>

Table 34 - Hydrogenolysis of propene over Pt/Al<sub>2</sub>O<sub>3</sub> and Ni/Al<sub>2</sub>O<sub>3</sub>

Pt/Al <sub>2</sub> O <sub>3</sub>						Ni/Al <sub>2</sub> O <sub>3</sub>					
H <sub>2</sub> pressure (atm)	X <sub>1</sub>	X <sub>2</sub>	Turnover (1)	Turnover (2)	S <sub>1</sub>	H <sub>2</sub> pressure (atm)	X <sub>1</sub>	X <sub>2</sub>	Turnover (1)	Turnover (2)	S <sub>1</sub>
0.68	0.079	0.92	0.095	1.11	1.25	1.36	0.054	0.944	0.047	0.82	2.06
1.02	0.084	0.91	0.102	1.09	1.37	2.04	0.035	0.963	0.031	0.84	1.92
1.70	0.10	0.89	0.122	1.07	1.49	2.38	0.028	0.970	0.025	0.84	1.81
2.04	0.13	0.86	0.159	1.03	1.78	3.06	0.023	0.976	0.020	0.85	1.88
2.38	0.18	0.82	0.211	0.99	1.90	3.40	0.019	0.980	0.017	0.86	1.77
2.72	0.22	0.78	0.259	0.94	1.96						
3.06	0.25	0.75	0.306	0.90	2.03						
3.40	0.28	0.72	0.339	0.87	2.05						

Turnover (1) - hydrogenolysis turnover

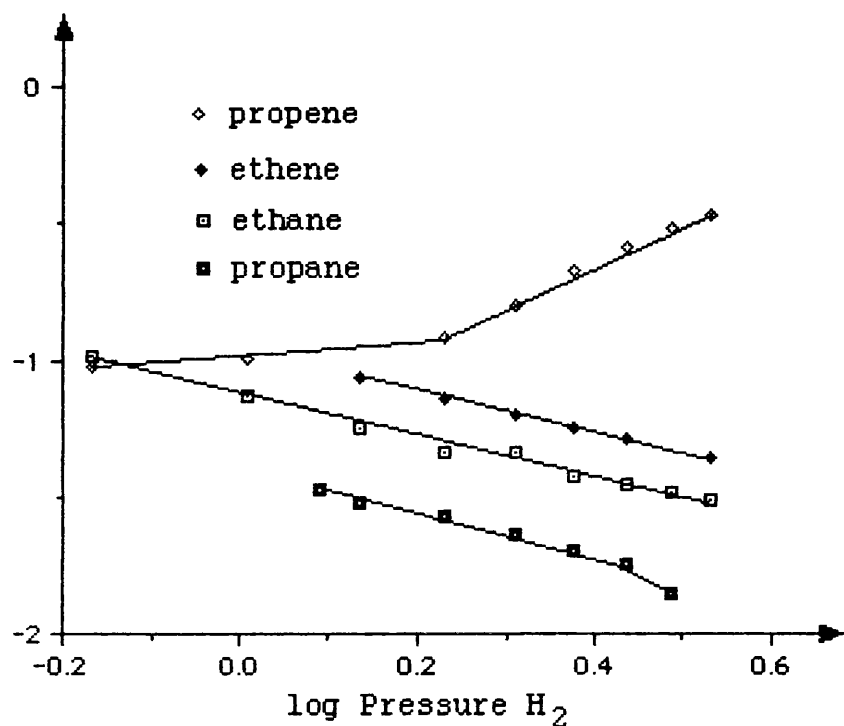
(2) - hydrogenation turnover

X<sub>1</sub> - Fractional hydrogenolysis conversion (molecules s<sup>-1</sup> surface metal atom<sup>-1</sup>)

X<sub>2</sub> - Fractional hydrogenation conversion

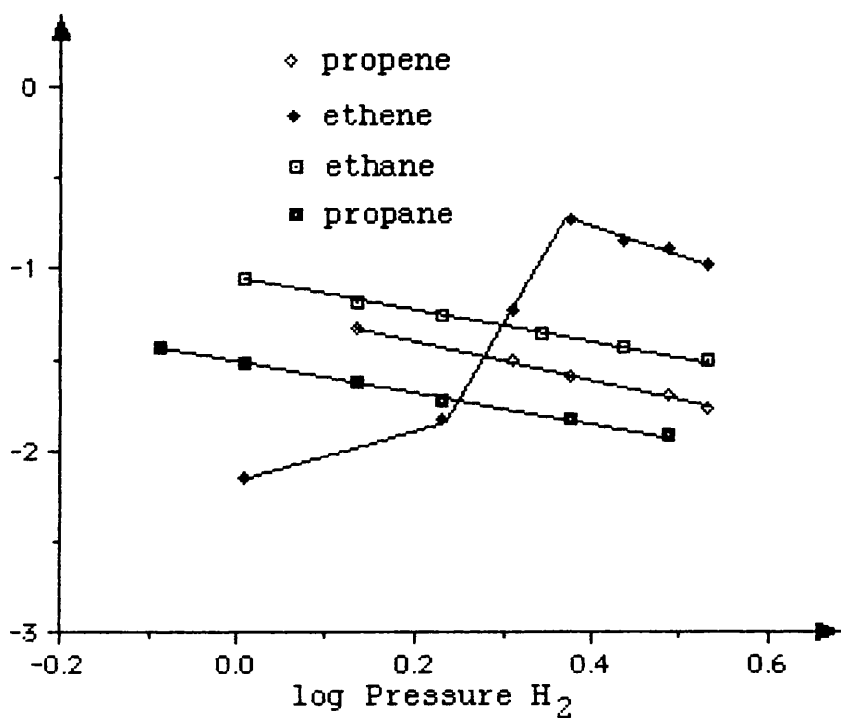
Graph 34 - Hydrogen pressure effect on hydrogenolysis of ethane, ethene, propane and propene over Pt/Al<sub>2</sub>O<sub>3</sub>

log turnover

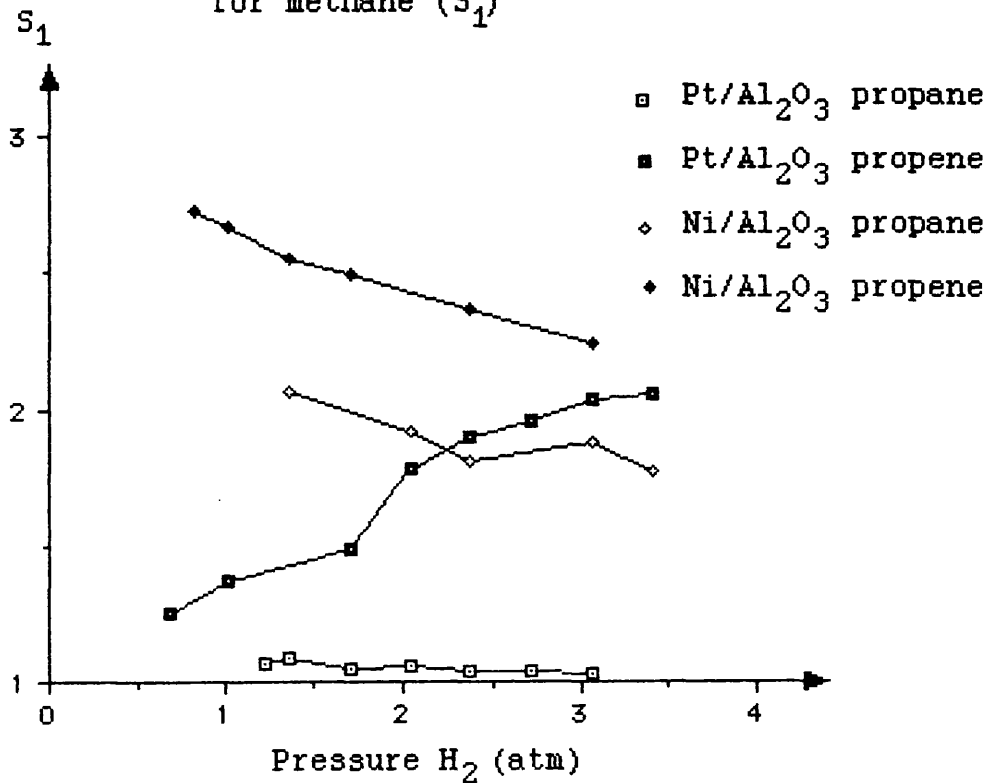


Graph 35 - Hydrogen pressure effect on hydrogenolysis of ethane, ethene, propane and propene over Ni/Al<sub>2</sub>O<sub>3</sub>

log turnover



Graph 36 - Hydrogenolysis of propane and propene over Pt/Al<sub>2</sub>O<sub>3</sub> and Ni/Al<sub>2</sub>O<sub>3</sub> selectivity for methane (S<sub>1</sub>)



#### 5.4.2 Values of m

From the best fit least squares lines through the linear portions of the graphs, the following values of  $m$  ( $\pm 3\%$ ), the order of the reactions of ethane, ethene, propane and propene over the Pt/Al<sub>2</sub>O<sub>3</sub> and Ni/Al<sub>2</sub>O<sub>3</sub> catalysts.

Table 35 - values of m

Feed Gas	Pt/Al <sub>2</sub> O <sub>3</sub> m values	Ni/Al <sub>2</sub> O <sub>3</sub> m values
C <sub>2</sub> H <sub>6</sub>	-0.71	-0.82
C <sub>2</sub> H <sub>4</sub>	-0.68	-1.59
C <sub>3</sub> H <sub>8</sub>	-0.79	-0.88
C <sub>3</sub> H <sub>6</sub>	+1.58	-1.09

### 5.5 REACTIONS ON THE MoO<sub>3</sub> SUPPORT

After on overnight reduction at 673K in a flow of H<sub>2</sub> of 60 ml min<sup>-1</sup> the hydrogenolysis of ethane, propane, iso-butane and n-butane was carried out over samples of the MoO<sub>3</sub> support material at 723K. These results are shown in Table 36 below.

By physically mixing the MoO<sub>3</sub> support material with the Pt/MoO<sub>3</sub> catalyst a series of platinum catalysts was prepared with platinum contents of 0.48%, 0.24%, 0.12%, 0.06%, 0.03% and 0% (MoO<sub>3</sub> support alone). These catalyst samples were reduced for two hours at 673K in a flow of H<sub>2</sub> of 60 ml min<sup>-1</sup> and reacted with iso-butane at 723K. These results are shown in Table 37 and Graph 37 below.

Table 36 - Hydrogenolysis over MoO<sub>3</sub> support at 723K

Feed gas	X <sub>HYD</sub>	X <sub>ISOM</sub>	Rate HYD	S <sub>1</sub>	S <sub>2</sub>	S <sub>3</sub>	<u>i</u> isom hyd
C <sub>2</sub> H <sub>6</sub>	0.027	-	1.66	-	-	-	-
C <sub>3</sub> H <sub>8</sub>	0.021	-	1.14	1.35	0.83	-	-
i-C <sub>4</sub> H <sub>10</sub>	0.020	0.012	0.85	2.47	0.59	0.74	0.60
n-C <sub>4</sub> H <sub>10</sub>	0.006	0.036	0.22	0.66	0.78	0.59	6.27

X<sub>HYD</sub> - Fractional hydrogenolysis conversion

X<sub>ISOM</sub> - Fractional isomerisation conversion

Rate HYD - Rate Hydrogenolysis (ml min<sup>-1</sup> g<sub>CAT</sub><sup>-1</sup>)

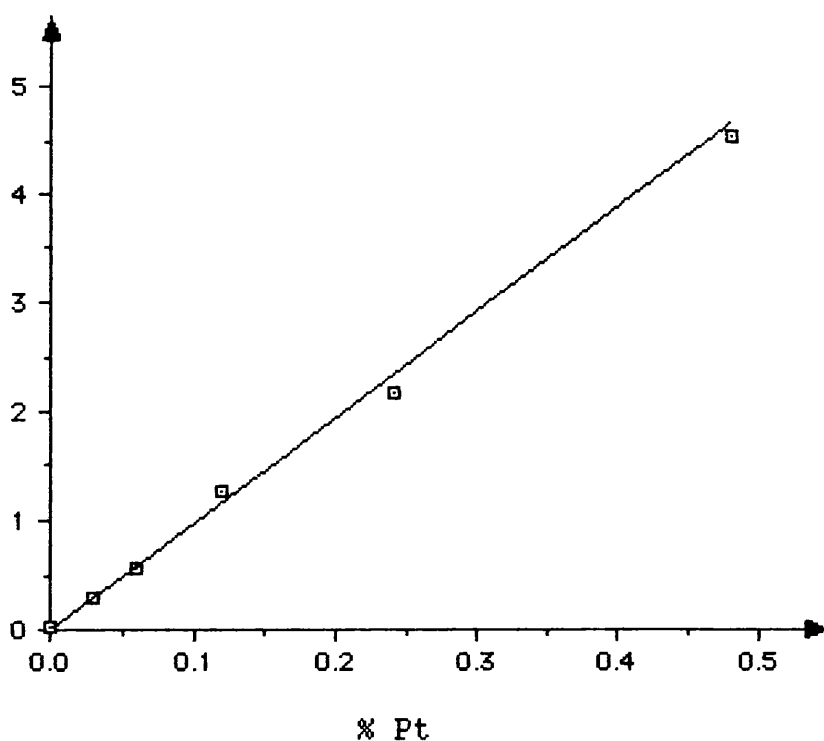
Table 37 - Isomerisation of iso-butane at 673K

%Pt	X <sub>ISO</sub>	X <sub>HYD</sub>	Rate iso
0.48	0.108	0.009	4.53
0.24	0.050	0.010	2.18
0.12	0.031	0.007	1.27
0.06	0.013	0.002	0.55
0.03	$7.0 \times 10^{-3}$	-	0.30
0	$7.0 \times 10^{-4}$	-	0.03

Rate iso -  $\text{ml min}^{-1} \text{g}_{\text{CAT}}^{-1}$

Graph 37 - Isomerisation of iso-butane over Pt/MoO<sub>3</sub> catalysts

Rate ( $\text{ml min}^{-1} \text{g}_{\text{CAT}}^{-1}$ )



## CHAPTER SIX

## CHAPTER 6

### DISCUSSION

#### 6.1 GHI CHARACTERISATIONS

The only significant impurity of potential catalytic significance found in the support materials was the chloride level in the Degussa alumina. Despite being prepared from a chloride precursor (hexachloroplatinic acid  $\text{H}_2\text{PtCl}_6$ ) the  $\text{Pt}/\text{SiO}_2$  and  $\text{Pt}/\text{MoO}_3$  catalysts had negligible chloride contents after reduction. In contrast, the  $\text{Pt}/\text{Al}_2\text{O}_3$  catalyst in its post-reduction state retained most of the chloride that was present in the initial stages of the preparation. From the chemisorption experiments it would appear that the chloride was associated with the support rather than the metal. As there was little isomerisation of n-butane or iso-butane over the  $\text{Pt}/\text{Al}_2\text{O}_3$  catalyst, compared with the other platinum catalysts, it would appear that the retained chloride did not greatly enhance the acidic nature of the support (section 5.3).

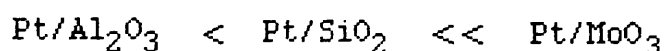
The value of  $x$  in  $\text{H}_x\text{MoO}_3$ , the hydrogen bronze formed from the  $\text{Pt}/\text{MoO}_3$  catalyst was variously calculated from TGA, TPR and XPS data. The TGA figure ( $x = 0.9$ ) was calculated from weight gains above 398K

during TGA using a 5% H<sub>2</sub>/N<sub>2</sub> mixture. The large hydrogen uptake during TPR was indicative of hydrogen bronze formation and produced a figure for x of x = 1.2. The XPS data estimated the x value (x = 0.8) from the ratio between surface Mo(VI) and Mo(IV) species. The existence of a range of bronze stoichiometries is well established (section 1.14) with the hydrogen bronze formed by hydrogen spillover having the composition H<sub>1.6</sub>MoO<sub>3</sub> (147).

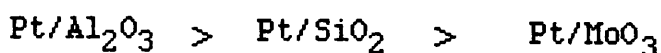
In contrast the TGA and TPR studies on the Ni/MoO<sub>3</sub> and Ni/WO<sub>3</sub> catalysts showed no evidence for significant bronze formations with the molybdena and tungstia supports. The uptake of hydrogen for the nickel catalysts during TPR was largely consistent with the stoichiometry required for the reduction of nickel nitrate. e.g.



The particle size distributions derived from HRTEM showed that the platinum crystallites were extremely highly dispersed on the Pt/Al<sub>2</sub>O<sub>3</sub> and Pt/SiO<sub>2</sub> catalysts with most particles less than 7Å in size, whereas the particle size distribution within the Pt/MoO<sub>3</sub> catalyst was very broad with large particles of up to 225Å in size. The average particle sizes in the samples lay in the order



From the gas chemisorption studies it was shown that the metal dispersions of the platinum catalysts lay in the order,



The mean surface average diameters calculated from HRTEM ( $\langle d \rangle_{\text{TEM}}$ ) were higher than those derived from the chemisorption experiments ( $\langle d \rangle_{\text{CHEM}}$ ) on the three platinum catalysts. This is not surprising as the smallest particles were likely to be missed by HRTEM.

## 6.2 NICKEL CATALYST CHARACTERISATIONS

The carbon monoxide chemisorption experiments on the nickel catalysts showed that the metal dispersions lay in the order,



The HRTEM studies were unsuccessful in producing particle size distributions for the nickel catalysts due to the low loadings, fairly high dispersions and the difficulty of contrasting the nickel particles from the support as compared with platinum particles.

## 6.3 HYDROGENOLYSIS REACTIONS

In the early reactions evidence was obtained to

indicate that, as the temperature was increased under continuous flow conditions, carbon was laid down on the surface. After passing through a temperature increase-decrease cycle it was found that the rate of reaction decreased. However, in the kinetic studies where the catalysts were subjected to pure hydrogen flow between determinations reproducibility of reaction rates was observed even after temperature cycling, which can be taken to indicate that under these conditions any carbon remaining on the surface did not influence the overall activity.

#### 6.4 ETHANE HYDROGENOLYSIS

The hydrogenolysis of ethane to produce methane is the simplest alkane hydrogenolysis reaction. i.e.



The results from the hydrogenolysis of ethane over the nickel and platinum catalysts (section 5.3.1.2) demonstrated that generally the nickel catalysts reacted at lower temperatures with lower activation energies and higher conversions than the platinum catalysts. This was as expected as nickel has a higher hydrogenolysis activity than platinum (14).

These results are comparable with the following

results from the literature, Table 1 below, apart from the Pt/MoO<sub>3</sub>, Ni/MoO<sub>3</sub> and Ni/SiO<sub>2</sub> catalysts which had considerably higher apparent activation energies.

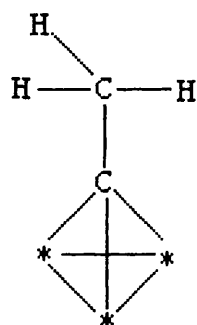
Table 1 - Ethane activation energies

catalyst	T(K)	Ea kJmol <sup>-1</sup>	ref
6.3% Pt/SiO <sub>2</sub>	613-633	210	(181)
5% Pt/SiO <sub>2</sub>	618-658	226	(14)
0.89% Pt/Al <sub>2</sub> O <sub>3</sub>	683-763	210	this work
0.75% Pt/SiO <sub>2</sub>	683-763	203	this work
0.48% Pt/MoO <sub>3</sub>	683-763	253	this work
5% Ni/SiO <sub>2</sub>	493-533	172	(14)
5% Ni/deluminated silica alumina	493	167	(42)
0.95% Ni/Al <sub>2</sub> O <sub>3</sub>	638-723	185	this work
0.97% Ni/SiO <sub>2</sub>	523-593	237	this work
0.54% Ni/MoO <sub>3</sub>	643-723	199	this work
0.50% Ni/WO <sub>3</sub>	642-723	175	this work

The high activation energies over the two molybdena supported catalysts may be due to reactions taking place on the support (see section 6.6).

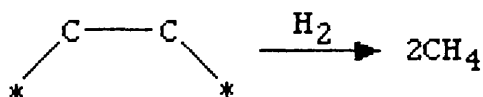
A common feature of the various kinetic analyses discussed in section 1.4 is the formation of a dehydrogenated surface complex C<sub>2</sub>H<sub>x</sub>(a). The mode of

adsorption of this dehydrogenated species is not, however, clear. Kristyan and Szamosi (45) assumed that only one carbon of the  $C_2H_x(a)$  surface compound participated in surface bonding. This agrees with the work of Somorjai (section 1.9) on  $C_2H_2$  and  $C_2H_4$  adsorbed on Pt[111] surfaces which both formed ethylidyne species above 310K in hydrogen,



ethylidyne

The breakage of C-C bonds, particularly the demethylation of nickel catalysts, is often explained, however, through the formation of 1,2 adsorbed species. i.e.



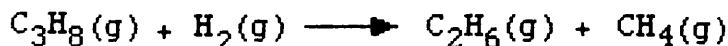
As there is only one reaction product from ethane hydrogenolysis there is no information available from selectivity, making differentiation between these two modes of adsorption to produce a reaction mechanism very difficult.

## 6.5 PROPANE HYDROGENOLYSIS

The hydrogenolysis of propane leads to two possible products, methane and ethane. e.g.



One of the major differences between platinum and nickel catalysts, the depth of hydrogenolysis, was demonstrated by the selectivity for methane ( $S_1$ ) during the hydrogenolysis of propane. For the Pt/Al<sub>2</sub>O<sub>3</sub> ( $S_1 = 1.06$ ) and Pt/SiO<sub>2</sub> ( $S_1 = 1.08$ ) catalysts the selectivities for methane were only slightly higher than unity, indicating that a single hydrogenolysis reaction was predominantly taking place. e.g.



The Ni/SiO<sub>2</sub>, Ni/Al<sub>2</sub>O<sub>3</sub> and Ni/MoO<sub>3</sub> catalysts all showed an almost linear increase in  $S_1$  with temperature. The sequential breakage of C-C bonds in the propane molecule was therefore an activated process.

When compared with the activation energies for ethane hydrogenolysis, the activation energies for propane hydrogenolysis over the Pt/Al<sub>2</sub>O<sub>3</sub> ( $E_a = 147 \text{ kJmol}^{-1}$ ) and Pt/SiO<sub>2</sub> ( $E_a = 157 \text{ kJmol}^{-1}$ ) were considerably lower. The nickel catalysts all showed an increase in activation energies from ethane hydrogenolysis apart from the Ni/Al<sub>2</sub>O<sub>3</sub> catalyst which had a slightly lower value. The conversion values for

the nickel catalysts were also much lower for propane than for ethane. The results can be compared with the following results from the literature,

Table 2 - Propane activation energies

catalyst	T(K)	Ea kJmol <sup>-1</sup>	ref
6.3% Pt/SiO <sub>2</sub>	588	189	(181)
0.6% Pt/Al <sub>2</sub> O <sub>3</sub>	551-573	205	(47)
0.89% Pt/Al <sub>2</sub> O <sub>3</sub>	603-673	147	this work
0.75% Pt/SiO <sub>2</sub>	653-733	157	this work
0.48% Pt/MoO <sub>3</sub>	683-763	310	this work
4.1% Ni/SiO <sub>2</sub>	523-573	176	(182)
5% Ni/deluminated silica alumina	493	150	(42)
0.95% Ni/Al <sub>2</sub> O <sub>3</sub>	683-733	171	this work
0.97% Ni/SiO <sub>2</sub>	563-613	243	this work
0.54% Ni/MoO <sub>3</sub>	683-743	257	this work
0.50% Ni/WO <sub>3</sub>	723-773	218	this work

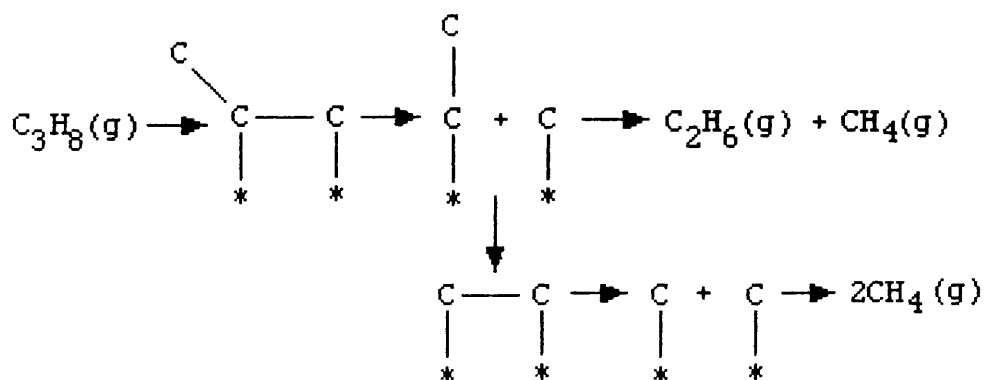
The extremely high activation energy for the Pt/MoO<sub>3</sub> catalyst (Ea = 310 kJmol<sup>-1</sup>) coupled with its increasing S<sub>1</sub> value with temperature suggests that the support greatly influenced the reaction over this catalyst. This can be compared with the reaction of propane over the Ni/MoO<sub>3</sub> catalyst and the MoO<sub>3</sub> support at 723K.

Table 3 - Hydrogenolysis of propane

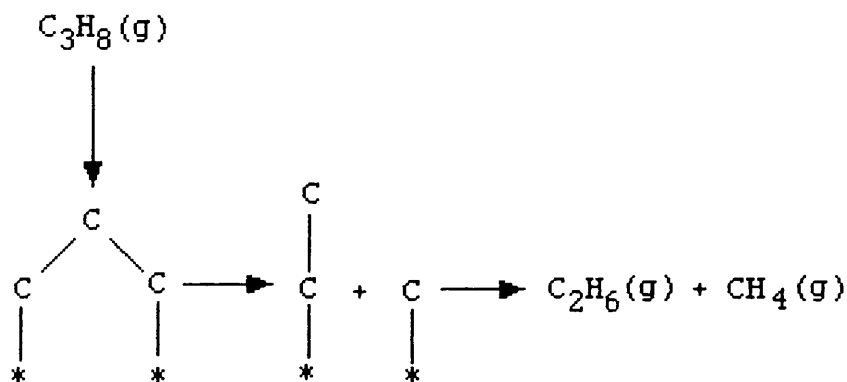
Pt/MoO <sub>3</sub>		Ni/MoO <sub>3</sub>		MoO <sub>3</sub>	
X <sub>HYD</sub>	S <sub>1</sub>	X <sub>HYD</sub>	S <sub>1</sub>	X <sub>HYD</sub>	S <sub>1</sub>
0.012	1.12	0.014	1.55	0.021	1.35

While the S<sub>1</sub> value over the Pt/MoO<sub>3</sub> catalyst was lower than for the Ni/MoO<sub>3</sub> catalyst or the MoO<sub>3</sub> support it would appear that some hydrogenolysis of the propane was occurring on support sites.

It is clear from the selectivity differences between the two metals that two different mechanisms of hydrogenolysis prevail on platinum and nickel catalysts. The increasing multiple hydrogenolysis with the nickel catalysts with rising temperature, coupled with the known propensity of nickel catalysts for demethylation (18), suggests a reaction mechanism which proceeds through a series of 1,2 adsorbed species. e.g.



Obviously successive hydrogenolysis of C-C bonds of this type does not occur on the Pt/Al<sub>2</sub>O<sub>3</sub> and Pt/SiO<sub>2</sub> catalysts, with their high selectivities for single hydrogenolysis. There was a marked decrease in activation energy from ethane to propane hydrogenolysis on these catalysts, but it is unclear whether this reflects the decreasing C-C bond energies between ethane and propane, the decreasing C-H bond energies or some other factor, for instance the formation of a 1,3-adsorbed species.

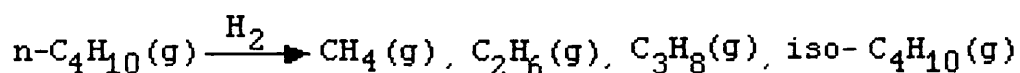


Regardless of the exact mechanism, the further hydrogenolysis of C<sub>2</sub> fragments on the platinum catalysts does not proceed to any great extent.

The metal function is therefore the deciding factor for the selectivity of the hydrogenolysis of propane. The support however can have a secondary effect on the reaction, as seen on the Pt/MoO<sub>3</sub> catalyst.

## 6.6 n-BUTANE HYDROGENOLYSIS

The hydrogenolysis of n-butane is altogether a far more complex and interesting reaction than the hydrogenolysis of either ethane or propane, with three hydrogenolysis products, methane, ethane and propane and also an isomerisation product, iso-butane. i.e.



The importance of the metal and the support for the selectivity for isomerisation over hydrogenolysis (iso-C<sub>4</sub>/A) was most apparent for both the platinum and nickel catalysts (Table 4 below).

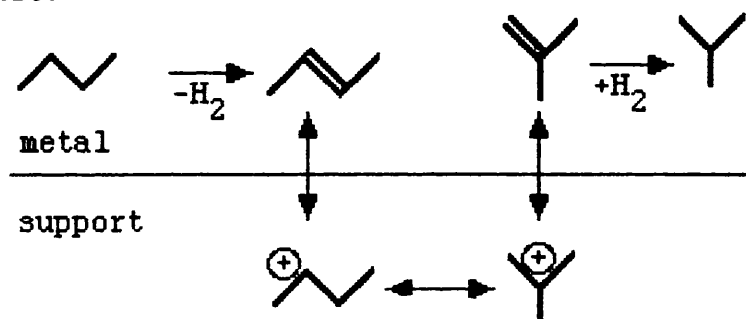
Table 4 - Isomerisation selectivity of n-butane

catalyst	iso-C <sub>4</sub> /A
Pt/Al <sub>2</sub> O <sub>3</sub>	0.09 → 0.07
Pt/SiO <sub>2</sub>	0.82 → 0.66
Pt/MoO <sub>3</sub>	7.55 → 1.01
Ni/Al <sub>2</sub> O <sub>3</sub>	0.41 → 0.06
Ni/SiO <sub>2</sub>	0.04 → 0.005
Ni/MoO <sub>3</sub>	1.68 → 0.15
Ni/WO <sub>3</sub>	0.48 → 0.14

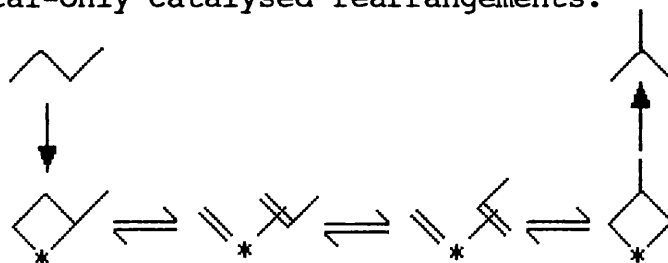
Three possible isomerisation mechanisms can be envisaged:

(i) a bifunctional mechanism involving acid sites on the

support.



(ii) metal-only catalysed rearrangements.



(iii) support only catalysed rearrangements.

The Arrhenius plots for hydrogenolysis and isomerisation of n-butane over the platinum and nickel catalysts produced the following activation energies for hydrogenolysis and isomerisation.

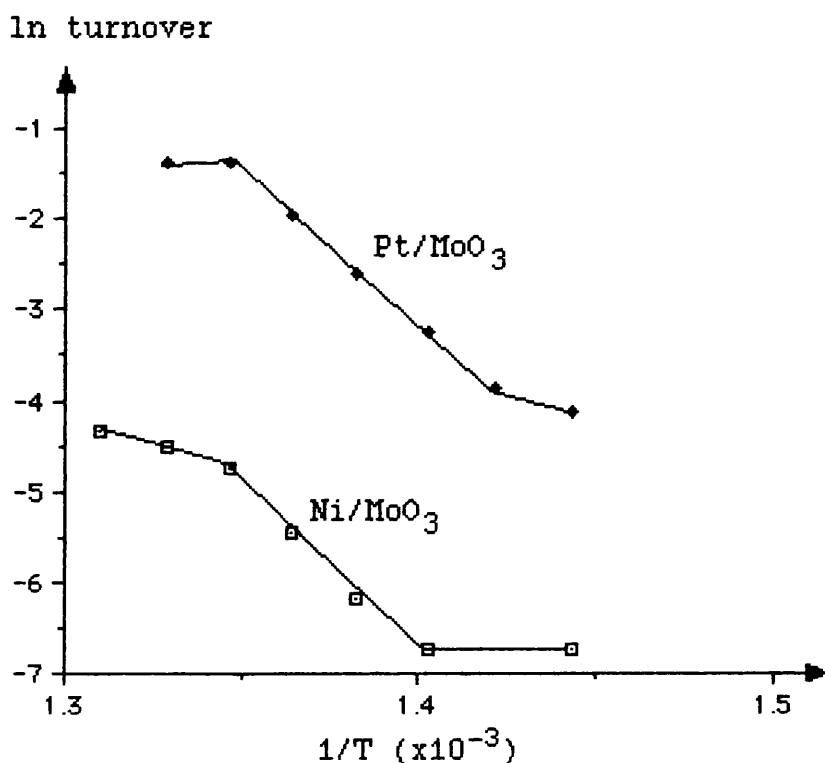
Table 5 - Hydrogenolysis of n-butane

catalyst	Ea hydrogenolysis kJ mol <sup>-1</sup>	Ea isomerisation kJ mol <sup>-1</sup>
Pt/Al <sub>2</sub> O <sub>3</sub>	130	161
Pt/SiO <sub>2</sub>	96	102
Pt/MoO <sub>3</sub>	53	274
Ni/Al <sub>2</sub> O <sub>3</sub>	154	-
Ni/SiO <sub>2</sub>	234	-
Ni/MoO <sub>3</sub>	271	252
Ni/WO <sub>3</sub>	-	-

The similarity between the activation energies for hydrogenolysis and isomerisation of n-butane over the Pt/Al<sub>2</sub>O<sub>3</sub> and Pt/SiO<sub>2</sub> catalysts suggests that metal-only catalysed rearrangements make the major contribution to isomerisation over these catalysts. Indeed, it is the only isomerisation route that is available to the Pt/SiO<sub>2</sub> catalyst.

If the Arrhenius plots for the isomerisation of n-butane over the Pt/MoO<sub>3</sub> and Ni/MoO<sub>3</sub> catalysts are compared, see Graph 1 below, the great similarity in activation energies and the shapes of the plots suggests that a common site is responsible for the isomerisation of n-butane over these two catalysts.

Graph 1 - Isomerisation of n-butane over Pt/MoO<sub>3</sub> and Ni/MoO<sub>3</sub>



A higher concentration of these sites is found on the platinum catalyst than on the nickel catalyst. Such a site could be the hydrogen bronzes which are readily formed on the Pt/MoO<sub>3</sub> catalyst.

Values of x in H<sub>x</sub>MoO<sub>3</sub>, the hydrogen bronze formed by the Pt/MoO<sub>3</sub> catalyst were derived from TPR (x = 1.2), TGA (x = 0.9) and XPS (x=0.8) measurements. However, as the TGA and TPR studies on the Ni/MoO<sub>3</sub> (and the Ni/WO<sub>3</sub> catalyst) showed no evidence for significant hydrogen bronze formation, it seems unlikely that hydrogen bronzes are the reaction sites.

At 723K the Pt/MoO<sub>3</sub>, Ni/MoO<sub>3</sub> and MoO<sub>3</sub> support had the following fractional conversions for hydrogenolysis and isomerisation.

Table 6 - Hydrogenolysis of n-butane

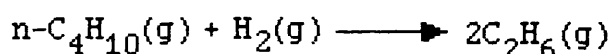
Pt/MoO <sub>3</sub>		Ni/MoO <sub>3</sub>		MoO <sub>3</sub>	
X <sub>HYD</sub>	X <sub>ISO</sub>	X <sub>HYD</sub>	X <sub>ISO</sub>	X <sub>HYD</sub>	X <sub>ISO</sub>
0.013	0.038	0.016	0.003	0.006	0.036

The fractional conversion for the isomerisation of n-butane over the MoO<sub>3</sub> support was comparable to that of the Pt/MoO<sub>3</sub> catalyst. The hydrogenolysis

activity of the  $\text{MoO}_3$  support was much less than that of the  $\text{Ni/MoO}_3$  and  $\text{Pt/MoO}_3$  catalysts. This supports the idea that the isomerisation of n-butane takes place on support sites without the need for an initial dehydrogenation step on a metal function on the  $\text{Ni/MoO}_3$  and  $\text{Pt/MoO}_3$  catalysts.

The activation energy for the hydrogenolysis reaction over the  $\text{Ni/MoO}_3$  catalyst had an extremely high value, similar to that for the isomerisation reaction. This indicates that the cracking of n-butane also takes place on the  $\text{MoO}_3$  support. In contrast, the hydrogenolysis of n-butane over the  $\text{Pt/MoO}_3$  catalyst had an extremely low activation energy ( $E_a = 53 \text{ kJmol}^{-1}$ ) as compared with the other platinum catalysts. This suggests that a different reaction site is responsible for the hydrogenolysis of n-butane over this catalyst.

The single hydrogenolysis activity of n-butane can be expressed by the two reactions,



The selectivity towards single hydrogenolysis can be followed from the  $\text{C}_1/\text{C}_3$  ratio; if  $\text{C}_1/\text{C}_3 = 1$  then only single hydrogenolysis is taking place, if





In contrast, the Ni/MoO<sub>3</sub> and Ni/WO<sub>3</sub> catalysts had S<sub>1</sub> values which decreased with increasing temperature. With the Ni/WO<sub>3</sub> catalyst there was also a fall in the overall hydrogenolysis activity with increasing temperature.

### 6.7 iso-BUTANE HYDROGENOLYSIS

The hydrogenolysis of iso-butane showed many similarities to the hydrogenolysis of n-butane, for instance the isomerisation selectivities were again associated with the metal and the support.

Table 7 - Isomerisation selectivity of iso-butane

catalyst	n-C <sub>4</sub> /A
Pt/Al <sub>2</sub> O <sub>3</sub>	0.16 → 0.11
Pt/SiO <sub>2</sub>	2.67 → 1.44
Pt/MoO <sub>3</sub>	9.10 → 1.19
Ni/Al <sub>2</sub> O <sub>3</sub>	0.34 → 0
Ni/SiO <sub>2</sub>	0.09 → 0
Ni/MoO <sub>3</sub>	2.22 → 0.05
Ni/WO <sub>3</sub>	0.81 → 0.07

The platinum and nickel catalysts had activation energies for the hydrogenolysis and isomerisation of iso-butane as follows.

Table 8 - Hydrogenolysis of iso-butane

catalyst	Ea hydrogenolysis kJ mol <sup>-1</sup>	Ea isomerisation kJ mol <sup>-1</sup>
Pt/Al <sub>2</sub> O <sub>3</sub>	92	116
Pt/SiO <sub>2</sub>	125	148
Pt/MoO <sub>3</sub>	136	176
Ni/Al <sub>2</sub> O <sub>3</sub>	152	-
Ni/SiO <sub>2</sub>	183	-
Ni/MoO <sub>3</sub>	228	274
Ni/WO <sub>3</sub>	-	-

Again, the similarity between the activation energies for the hydrogenolysis and isomerisation of iso-butane over the Pt/Al<sub>2</sub>O<sub>3</sub> and Pt/SiO<sub>2</sub>, and in this case the Pt/MoO<sub>3</sub> catalyst, are consistent with a mechanism of metal-only catalysed rearrangements over these catalysts. Unusually, the Pt/Al<sub>2</sub>O<sub>3</sub> catalyst had a lower activation energy for the hydrogenolysis of iso-butane than for n-butane. With the molecular wt. held constant the activation energy usually increases with substitution (47).

Although there was still a great deal of isomerisation over the Pt/MoO<sub>3</sub> catalyst, this activity, in this case, seemed to be associated with either a metal-only rearrangement or a bifunctional mechanism. For example the Pt/MoO<sub>3</sub> catalyst had a much higher

isomerisation activity than the Ni/MoO<sub>3</sub> catalyst or the MoO<sub>3</sub> support at 723K.

Table 9 - Hydrogenolysis of iso-butane

Pt/MoO <sub>3</sub>		Ni/MoO <sub>3</sub>		MoO <sub>3</sub>	
X <sub>HYD</sub>	X <sub>ISO</sub>	X <sub>HYD</sub>	X <sub>ISO</sub>	X <sub>HYD</sub>	X <sub>ISO</sub>
0.025	0.19	0.010	0.023	0.020	0.012

To further investigate the reaction of iso-butane over the Pt/MoO<sub>3</sub> catalyst a series of catalysts was prepared by mixing the Pt/MoO<sub>3</sub> catalyst with the MoO<sub>3</sub> support (section 5.5). These catalysts demonstrated that the isomerisation activity was dependent on the platinum content of the catalyst. In contrast, then, to the reaction of n-butane, the isomerisation of iso-butane over the Pt/MoO<sub>3</sub> catalyst takes place by either a metal-only rearrangement or a bifunctional mechanism, rather than a support only reaction.

The hydrogenolysis and isomerisation reactions of iso-butane over the Ni/MoO<sub>3</sub> catalyst both had very high activation energies, again indicating that both the reactions were occurring on the support.

Unlike the hydrogenolysis of n-butane there is only one single hydrogenolysis of iso-butane.



Therefore any  $\text{C}_2\text{H}_6(\text{g})$  that is produced, must be produced by a multiple hydrogenolysis reaction. For the platinum catalysts the  $S_2$  values fell in the ranges as follows.

	$\frac{\text{Pt/MoO}_3}{\quad}$	>	$\frac{\text{Pt/SiO}_2}{\quad}$	>	$\frac{\text{Pt/Al}_2\text{O}_3}{\quad}$
$S_2$ values	1.42 → 0.31		0.34 → 0.10		0.29 → 0.03

This follows the order of decreasing isomerisation on these catalysts and suggests a relation between isomerisation and multiple hydrogenolysis.

Another measure of multiple hydrogenolysis, the  $C_1/C_3$  values, for the three catalysts were as follows.

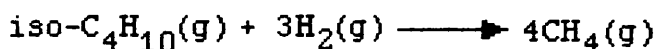
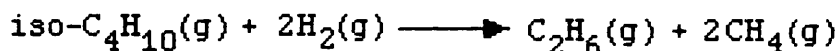
	$\frac{\text{Pt/MoO}_3}{\quad}$	>	$\frac{\text{Pt/SiO}_2}{\quad}$	>	$\frac{\text{Pt/Al}_2\text{O}_3}{\quad}$
$C_1/C_3$ values	1.79 → 0.71		1.39 → 1.16		1.17 → 1.07

These  $C_1/C_3$  ratios demonstrate that the  $\text{Pt/MoO}_3$  catalyst has a much greater selectivity towards single hydrogenolysis with iso-butane than with n-butane (where  $C_1/C_3 = 2.56$ ).

The Ni/Al<sub>2</sub>O<sub>3</sub> catalyst again showed a rising selectivity for methane with temperature during iso-butane hydrogenolysis. Under 543K the Ni/SiO<sub>2</sub> catalyst showed a very high selectivity towards single hydrogenolysis corresponding to the equation,



Above this temperature the S<sub>1</sub> value rose rapidly and the S<sub>3</sub> value fell steeply. The S<sub>2</sub> value also rose slightly. This corresponds to an increase in the multiple hydrogenolysis reactions and successive C-C bond breakages corresponding to the equations,



The Ni/WO<sub>3</sub> catalyst again showed a fall in both the overall hydrogenolysis activity and S<sub>1</sub> with increasing temperature similar to the reaction with n-butane.

The hydrogenolysis activity of iso-butane over the Ni/MoO<sub>3</sub> passed through a maximum at 673K as the temperature was increased. This effect was also seen with the reaction of n-butane over Ni/MoO<sub>3</sub>, the maximum in this case occurring at 723K. The high activation energies for these reactions suggested that these two reactions occurred on the MoO<sub>3</sub> support. Such a steep

decrease in activity in catalysis is consistent with a rapid desorption of reactants. This does not seem likely in this case as the isomerisation activity is unaffected. For the same reasoning the poisoning of the reaction sites, probably on the support, is unlikely. At these higher reaction temperatures hydrogen spillover from the nickel to the support increases, as shown from the TPR studies (171). Carbon present on the surface of the catalyst can act as a bridge between the metal and the support, facilitating hydrogen spillover (141). This spillover hydrogen may have an adverse effect on the hydrogenolysis reaction, if this takes place on the support via dehydrogenated intermediates.

This effect may also explain the decreasing hydrogenolysis activity with temperature for iso-butane and n-butane over the Ni/WO<sub>3</sub> catalyst where the hydrogenolysis activity is affected more severely than the isomerisation activity.

## 6.8 HYDROGEN PRESSURE EFFECT

One of the most important kinetic features of the hydrogenolysis reaction is the strong inverse dependence of the reaction rate on hydrogen pressure. Many of the reaction mechanisms discussed in section 1.4 relate this inverse dependence to the formation of

dehydrogenated intermediates on the surface of the catalyst.

For the reactions of ethane and propane over the Pt/Al<sub>2</sub>O<sub>3</sub> and Ni/Al<sub>2</sub>O<sub>3</sub> catalysts the hydrogen pressure had the following orders of reaction (m) with respect to hydrogen.

Table 10 - Hydrogenolysis of ethane and propane

catalyst	$C_2H_6$ m	$C_3H_8$ m
Pt/Al <sub>2</sub> O <sub>3</sub>	-0.71	-0.79
Ni/Al <sub>2</sub> O <sub>3</sub>	-0.82	-0.88

If a dehydrogenated alkene is used as a feedstock, this inverse dependence should then be effected. Using ethene and propene as reactant gases the following hydrogen orders (m) were found for the Pt/Al<sub>2</sub>O<sub>3</sub> and Ni/Al<sub>2</sub>O<sub>3</sub> catalysts.

Table 11 - Hydrogenolysis of ethene and propene

catalyst	$C_2H_4$ m	$C_3H_6$ m
Pt/Al <sub>2</sub> O <sub>3</sub>	-0.68	+1.59
Ni/Al <sub>2</sub> O <sub>3</sub>	-1.59	-1.09

Surprisingly the orders for the Ni/Al<sub>2</sub>O<sub>3</sub> catalyst were more negative than for the saturated

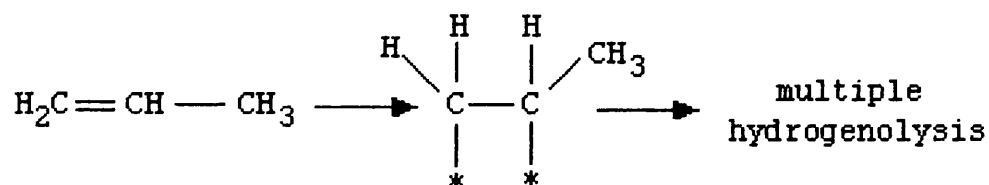
alkanes.

The reaction of ethene over the Pt/Al<sub>2</sub>O<sub>3</sub> catalyst produced a very similar hydrogen order to the reactions of ethane and propane. The reaction of propene over the Pt/Al<sub>2</sub>O<sub>3</sub> catalyst, in contrast, had a positive order with respect to hydrogen. This positive order suggests that further dehydrogenation is not required for the hydrogenolysis of propene over the Pt/Al<sub>2</sub>O<sub>3</sub> catalyst.

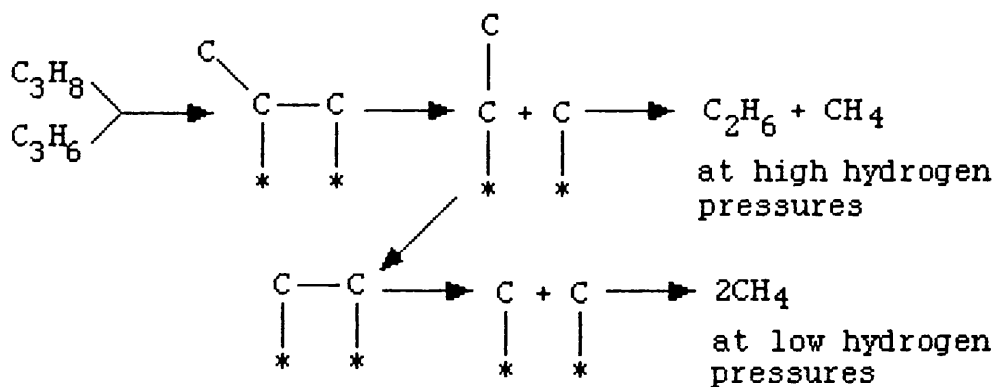
The selectivity plots for the reactions of the C<sub>3</sub>'s over the Pt/Al<sub>2</sub>O<sub>3</sub> and Ni/Al<sub>2</sub>O<sub>3</sub> catalysts also showed some interesting trends. The selectivity for methane fell for both propane and propene over the Ni/Al<sub>2</sub>O<sub>3</sub> catalyst with increasing hydrogen pressure. The hydrogen pressure had virtually no effect on the selectivity for the reaction of propane over the Pt/Al<sub>2</sub>O<sub>3</sub> catalyst, with very high selectivity for single hydrogenolysis. The reaction of propene over the Pt/Al<sub>2</sub>O<sub>3</sub> catalyst showed an increasing selectivity for methane with increasing hydrogen pressure.

Even at lower hydrogen pressures the reaction of propene over the Pt/Al<sub>2</sub>O<sub>3</sub> catalyst produced a substantial amount of multiple hydrogenolysis. As Pt/Al<sub>2</sub>O<sub>3</sub> is the most selective of the platinum catalysts for single hydrogenolysis during alkane

hydrogenolysis, this suggests that the mechanism of alkene hydrogenolysis proceeds via a different mechanism to alkanes, for instance 1,2 adsorption of the alkene,



The selectivity for methane fell with increasing hydrogen pressure for both propane and propene over the Ni/Al<sub>2</sub>O<sub>3</sub> catalyst. As the multiple hydrogenolysis reaction over the nickel catalysts appears to be related to a sequential breakage of C-C bonds this is not surprising as raising the hydrogen pressure would lead to increased desorption of C<sub>2</sub> fragments rather than further C-C bond breakage after the initial C-C bond cleavage. e.g.



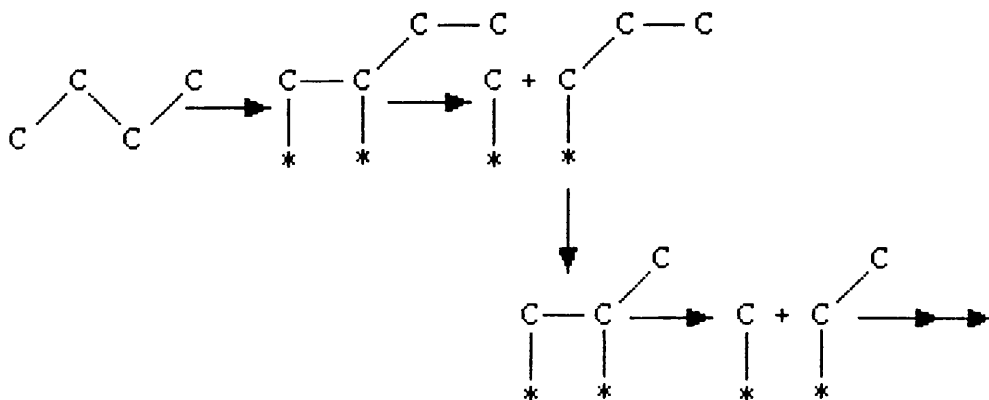
As the Ni/Al<sub>2</sub>O<sub>3</sub> catalyst had a negative hydrogen order with propene it suggests that further dehydrogenation takes place on the nickel catalyst

compared to the platinum catalyst during hydrogenolysis. This agrees with the known capacity of nickel to form metallocarbenes (53).

## 6.9 CONCLUSIONS

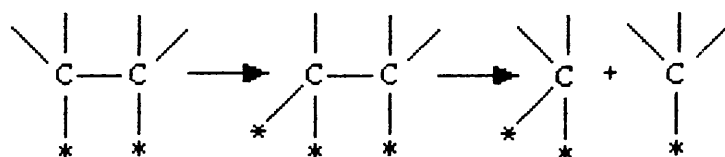
The determining factor for the selectivity of the hydrogenolysis reactions of propane, n-butane and iso-butane over the series of supported catalysts was the metal function of the catalysts. Over the nickel catalysts multiple hydrogenolysis was strongly favoured whereas the platinum catalysts had a high selectivity towards single hydrogenolysis.

The multiple hydrogenolysis over the nickel catalysts was shown to increase with increasing temperature. As nickel also has a high selectivity for demethylation (18) a reaction mechanism which proceeds through sequential C-C bond breakage of 1,2 adsorbed species is likely. e.g.



This sort of mechanism does not appear to occur over the platinum catalysts. Indeed the multiple hydrogenolysis of propene over the Pt/Al<sub>2</sub>O<sub>3</sub> catalyst suggests that 1,2- adsorption leads to multiple hydrogenolysis over platinum catalysts.

The breakage of the C-C bonds over the nickel catalysts may be induced by the formation of multiple bonds between the attached carbon and the metal and the subsequent strain produced on the C-C bond. e.g.



This 1,2- adsorption would also explain the difficulty of rupturing C-C bonds containing a quaternary atom over nickel catalysts (15). The smaller ionic radius of nickel (1.24Å) compared to platinum (1.38Å) may make 1,2- adsorptions more favourable on the nickel catalysts compared to the platinum catalysts.

The bifunctional mechanism of isomerisation can only operate where there are suitable acid sites available on the support and cannot operate on inert supports such as SiO<sub>2</sub>. The metal-only catalysed rearrangements are likely to make a higher contribution on the platinum catalysts than on the nickel catalysts (18). The formation of strongly adsorbed metallocarbene

species on nickel would also prevent the transfer of dehydrogenated hydrocarbons to acid sites on the support as required for a bifunctional mechanism. Not surprisingly then, the Ni/SiO<sub>2</sub> catalyst demonstrated the lowest selectivity for isomerisation of iso-butane and n-butane of any of the catalysts.

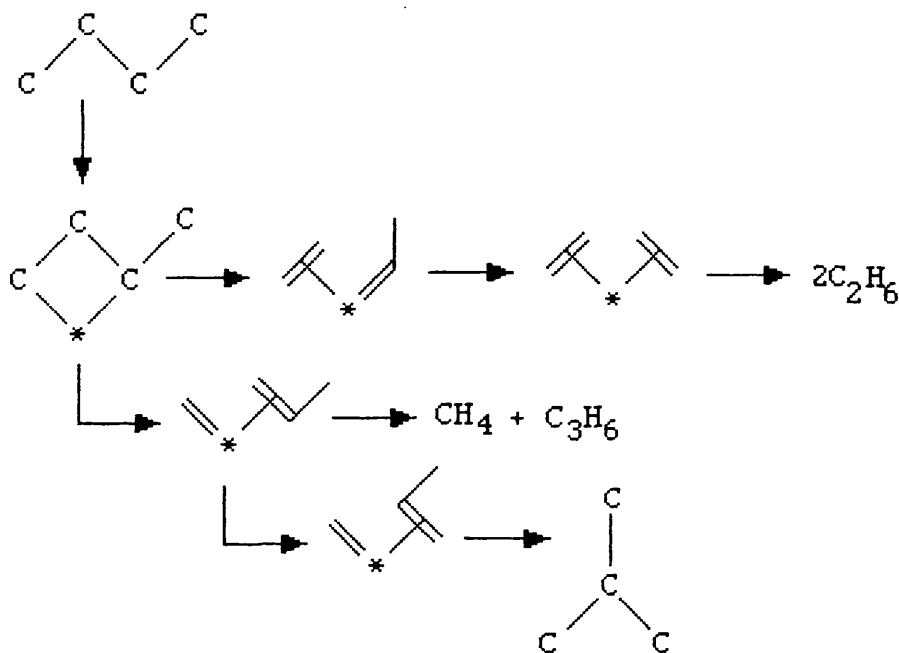
The nickel catalysts which showed an appreciable isomerisation activity were the Ni/MoO<sub>3</sub> and Ni/WO<sub>3</sub> catalysts. The high activation energies for the isomerisation reactions of n-butane and iso-butane over the Ni/MoO<sub>3</sub> catalyst suggested that the reactions took place directly on support sites.

The platinum catalysts, particularly the Pt/SiO<sub>2</sub> and Pt/Al<sub>2</sub>O<sub>3</sub> catalysts, demonstrated very high selectivities for single hydrogenolysis. The similarity between the hydrogenolysis and isomerisation activation energies for the reactions of n-butane over the Pt/SiO<sub>2</sub> and Pt/Al<sub>2</sub>O<sub>3</sub> catalysts and iso-butane over all three platinum catalysts suggests that these isomerisation reactions are metal-only catalysed reactions.

The metal-only catalysed skeletal rearrangements discussed in section 1.7 strongly suggested the involvement of 1,3- adsorbed intermediates for reactions where isomerisation and hydrogenolysis were related. The bond breakage of the 1,3-

intermediates has been suggested to follow the formation of a strained  $\alpha,\alpha,\gamma$ -intermediate (72).

Although no conclusive proof could be offered for any of the mechanisms, Garin's and Gault's metallocyclobutane mechanism best explained many of the reactions over platinum catalysts. i.e.

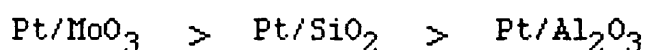


The isomerisation activity appeared to be related to the multiple hydrogenolysis activity of the platinum catalysts; the higher the isomerisation activity the higher the multiple hydrogenolysis for the reactions of both n-butane and iso-butane.

The isomerisation reaction of n-butane over the Pt/MoO<sub>3</sub> catalyst appeared to be a direct reaction on the support sites. This agreed with the reactions over the

reduced  $\text{MoO}_3$  support where n-butane was readily isomerised compared to iso-butane. This suggests that support sites can readily isomerise n-butane to iso-butane but not iso-butane to n-butane.

The isomerisation activities for the reactions of both n-butane and iso-butane over the platinum catalysts lie in the order,



This may be related to the particle sizes of the platinum crystallites, as shown by HRTEM (171), which also lie in the same order for these catalysts.

## References

1. H.M. Leicester, "The Historical Background of Chemistry", Dover Publications Inc., New York, 1971
2. C.B. Désormes and N. Clément, *Ann. Chim. Phys.*, 59, 329 (1806)
3. J.W. Döbereiner, *Scweigers, J. Chem. Phys.*, 38, 321 (1823)
4. W. Ostwald, *Z. Physik. Chem.*, 15, 705 (1894)
5. S.J. Thompson and G. Webb, "Heterogeneous Catalysis", Oliver and Boyd, 1967
6. P. Sabatier, *Ber. Dtsch. Chem. Ges.*, 44, 2001 (1911)
7. G.C. Bond, "Catalysis by Metals", Academic Press, London, 1962
8. B.A. Kazanskii, A.F. Platé and N.D. Zelinskii, *Chem. Ber.*, 66B, 1415 (1933)
9. W.S. Benedict, K. Morikawa and H.S. Taylor, *J. Amer. Chem. Soc.*, 58, 1795 (1936)
10. K. Morikawa, H.S. Taylor and N.R. Trenner, *J. Amer. Chem. Soc.*, 59, 1103 (1937)
11. V. Haensel and V.N. Ipatieff, *J. Amer. Chem. Soc.*, 68, 345 (1946)
12. E.H. Taylor and H.S. Taylor, *J. Amer. Chem. Soc.*, 61, 503 (1939)
13. R.C. Archibald, B.S. Greenfelder, G. Holzman and D.H. Rowe, *Ind. Eng. Chem.*, 52, 745 (1960)
14. J.H. Sinfelt, *Adv. Catal.*, 23, 91 (1973)
15. J.R. Anderson *Adv. Catal.*, 23, 1 (1973)

16. F.G. Gault, *Adv. Catal.*, 30, 1 (1981)
17. F.G. Garin and G. Maire, "Catalysis Science and Technology", ed. J.R. Anderson and M. Boudart, Springer-Verlag, Vol.6, p.162 (1984)
18. S.M. Davis and G.A. Somorjai, "The Chemical Physics of Solid Surfaces and Heterogeneous Catalysts", ed. D.A. King and D.P. Woodruff, Elsevier, Vol.4, p.217 (1982)
19. M. Boudart, *Adv. Catal.*, 20, 153 (1969)
20. M. Boudart, A. Cimino and H.S. Taylor, *J. Phys. Chem.*, 58, 796 (1954)
21. C.N. Satterfield, "Heterogeneous Catalysis in Industrial Practice", 2nd Edition, p.120, 1991
22. J.N. Beltramini and J.M. Parera, *J. Catal.*, 112, 357 (1988)
23. G.F. Berndt, Ph.D. Thesis, Glasgow University, 1980
24. J.L. Carter, G.B. McVicker, W.S. Kmack, J.H. Sinfelt, W. Weisman, *Appl. Cat.*, 3, 327 (1982)
25. P.G. Ashmore, C. Kemball and P.G. Wright, *Trans. Faraday Soc.*, 54, 1692 (1958)
26. C. Kemball, *Catal. Rev.*, 5, 33 (1972)
27. J. Addy and G.C. Bond, *Trans. Faraday Soc.*, 53, 388 (1957)
28. A. Crucq, L. Degols, A. Frennet and G. lienard, *J. Catal.*, 35, 18 (1974)
29. J.R. Anderson and C. Kemball, *Proc. Roy. Soc.*, A 233, 361 (1954)
30. R. Coekelbergs, Y. Delannois, A. Frennet and G. Lienard, *J. Chim. Phys.*, 61, 1167 (1964)
31. A. Frennet and G. Lienard, *Proc. Int. Congr. Catal.*, 4th,

Vol.II, p.65, paper 51, 1971

32. A. Frennet and G. lienard, J. Chim. Phys., 68, 1526 (1971)
33. J.H. Sinfelt, J. Catal., 27, 468 (1972)
34. J.H. Sinfelt, Catal. Rev., 3, 175 (1969)
35. J.P. Candy, J.A. Dalmon and G.A. Martin, Proc. Int. Congr. Catal., 6th (London) ed. G.C. Bond, P.B. Wells and F.C. Tompkins, Chemical Society London, p.903, 1977
36. G. Leclercq, L. Leclercq and R. Maurel, J. Catal., 44, 68 (1976)
37. J.R. Anderson and N.R. Avery, J.Catal., 5, 446 (1966)
38. F. Luck, Thèse Spécialité, Strasbourg, 1976
39. F. Garin, Thèse d'Etat, Strasbourg, 1978
40. F. Garin and F.G. Gault, J. Amer. Chem. Soc., 97, 4466 (1975)
41. J.H. Sinfelt, W. Taylor and D.J.C. Yates, J. Amer. Chem. Soc., 86, 2996 (1964)
42. C.M. Bouleau, G. Leclercq, L. Leclercq, S. Pietrzyk and R. Maurel, J. Catal., 88, 8 (1984)
43. A. Crucq, L. Degols, A. Frennet and G. lienard, J. Catal., 53, 150 (1978)
44. S. Kristyan and J. Szamosi, J. Chem. Soc. Faraday Trans I, 80, 1645 (1984)
45. S. Kristyan and J. Szamosi, J. Chem. Soc. Faraday Trans I, 84, 917 (1988)
46. G.A. Martin, J. Catal., 60, 345 (1979)
47. G.C. Bond and M.R. Gelsthorpe, J. Chem. Soc. Faraday Trans. I, 85, 3767 (1989)
48. J.R. Anderson and B.G. Baker, Proc. Roy. Soc. Ser. A, 271,

402 (1963)

49. G.A. Somorjai and I. Toyoshima, *Catal. Rev.*, 19, 550 (1979)
50. L. Pauling, *Proc. Roy. Soc. (London) Ser. A*, 196, 343  
(1949)
51. J.R. Anderson and B.G. Baker, *Nature*, 187, 937 (1960)
52. Z. Karpinski, *Nouv. J. Chim.*, 4, 561 (1980)
53. C. Kemball, *Proc. Roy. Soc. (London) Ser. A*, 207, 539  
(1951), 217, 376 (1953)
54. J. Newham, *J. Chem. Rev.*, 63, 123 (1963)
55. S.G. Hindin, G.A. Mill and A.G. Oblad, *J. Amer. Chem. Soc.*, 77, 535 (1955)
56. D. Beeck, J.W. Otvos, D.P. Stevenson and C.P. Wagner, *J. Amer. Chem. Soc.*, 74, 3269 (1952)
57. F.E. Condon, "Catalysis", Riehold, New York, 6, 141 (1958)
58. H.S. Bloch, H. Pines and L. Schmerling, *J. Amer. Chem. Soc.*, 68, 153 (1946)
59. C.D. Prater and P.B. Weisz, *Adv. Catal.*, 6, 143 (1954)
60. H. Heinemann, A.G. Oblad, T.H. Milliken and G.A. Mills, *Ind. Eng. Chem.*, 45, 134 (1953)
61. P.B. Weisz, *Adv. Catal.*, 13, 137 (1962)
62. G.C. Bond, "Heterogeneous Catalysis", Oxford, 1977
63. E.P. Parry, *J. Catal.*, 2, 371 (1963)
64. B.C. Gates, J.R. Katzer and G.C.A. Schmit, "Chemistry of Catalytic Processes", New York, McGraw Hill, p.259, 1979
65. W.O. Haag and H. Pines, *J. Amer. Chem. Soc.*, 82, 2471 (1960)
66. O.V. Bragin, B.A. Kazanskii and A.L. Liberman, *Dokl. Akad. Nauk, SSSR*, 156, 1114 (1964)
67. A.F. Platé, B.A. Kazanskii and N.D. Zelinskii, *Ber. Dtsch.*

- Chem. Ges., 66, 1415 (1933)
68. T.F. Bulanova and B.A. Kazanskii, Dokl, Akad, Nauk, SSSR, 62, 83 (1948)
69. Y. Barron, D. Cornet, F.G. Gault and G. Maire, J. Catal., 2, 152 (1963)
70. Y. Barron, F.G. Gault, G. Maire and J.M. Muller , J. Catal., 5, 428 (1966)
71. M. Boudart and L.D. Ptak, J. Catal., 16, 90 (1970)
72. J.R. Anderson and Y. Shimoyama, Proc. Int. Congr. Catal., 5th (Miami), ed. J. Hightower, North-Holland, Amsterdam, p.695, 1973
73. F.G. Gault, C. Kemball and J.J. Rooney, J. Catal., 1, 255 (1962)
74. J.R. Anderson and N.R. Avery, J. Catal., 7, 315 (1967)
75. J.C. Kutz and K.F. Purcell, "Inorganic Chemistry", Saunders, Philadelphia, p.873, 1977
76. G. Leclercq, L. Leclercq and G. Maurel, J. Catal., 50, 87 (1977)
77. F. Garin, F.G. Gault and G. Maire, Nouv. J. Chim., 5, 553 (1981)
78. F. Garin, F.G. Gault and G. Maire, Nouv. J. Chim., 5, 563 (1981)
79. (a) S.E. Binns, R.H. Cragg, R.D. Gillard, B.T. Hearton and M.F. Pilbrow, J. Chem. Soc. A, 1227 (1969)
- (b) R.D. Gillard, M. Keeton, R. Mason, M.F. Pilbrow and R.D. Russel, J. Organometal. Chem., 33, 247 (1971)
- (c) J.A. McGinnety, J. Organometal. Chem., 59, 429 (1973)
- (d) F.J. McQuillin and K.G. Powell, J. Chem. Soc. Dalton,

- 2123 (1972)
- (e) J.A. Ibers and J. Rajaram, *J. Amer. Chem. Soc.*, 100, 829 (1978)
80. F.G. Gault, *Advan. Catal.*, 30, 1 (1981)
81. C.P. Casey, *Org. Chem. (N.Y.)*, 33-I, 189 (1976)
82. S. Mija and K. Saito, *Inorg. Chem.*, 20, 287 (1981)
83. F. Garin and F.G. Gault, *J. Amer. Chem. Soc.*, 97, 4466 (1975)
84. B. Aldag, M. Boudart and L.D. Ptak, *J. Catal.*, 11, 35 (1968)
85. V.S. Boronin, A.N. Mitrofanova and O.M. Poltorak, *Vestn. Mosk. Univ. Ser.II Khim.*, 5, 40 (1966)
86. V.S. Boronin, A.N. Mitrofanova and O.M. Poltorak, *Vestn. Mosk. Univ. Ser.II Khim.*, 1, 95 (1967)
87. V.S. Boronin, N.M. Dmitrienko and O.M. Poltorak, *Vestn. Mosk. Univ. Ser.II Khim.*, 6, 106 (1966)
88. V.S. Boronin and O.M. Poltorak, *Zh. Fiz. Khim.*, 40, 2671 (1966)
89. A. Aldag, M. Boudart, J.E. Benson, A.N. Dougharty and C. Harkins-Girvin, *J. Catal.*, 6, 92 (1966)
90. G. Leclercq, L. Leclercq and R. Maurel, *Bull. Soc. Chim. Fr.*, 491 (1972)
91. J.L. Carter, J.A. Cusumano and J.H. Sinfelt, *J. Phys. Chem.*, 70, 2257 (1966)
92. J.H. Sinfelt and D.J.C. Yates, *J. Catal.*, 8, 348 (1967)
93. K. Otto, H.C. Yau and Y.F. Yu Yau, *J. Catal.*, 56, 21 (1979)
94. J.P. Brunelle, R.E. Montarnal and A.A. Sugier, *Proc. Int. Congr. Catal.*, 6th (London), ed. G.C. Bond, F.C. Tompkins

- and P.B. Wells, The Chemical Society, p.844, 1977
95. R. Van Hardeveld and A. Van Montfoort, *Adv. Catal.*, 22, 75 (1972)
  96. H.J. Maat and L. Moscou, *Proc. Int. Congr. Catal.*, 3rd (Amsterdam), North Holland, 1965
  97. F.G. Gault, *Ann. Chim.*, (Paris) [13] 5, 645 (1960)
  98. D.W. Blakely and G.A. Somorjai, *Surf. Sci.*, 91, 73 (1980)
  99. D.W. Blakely and G.A. Somorjai, *Nature (London)* 258, 580 (1975)
  100. J.L. Carter, J.H. Sinfelt and D.J.C. Yates, *J. Catal.*, 24, 283 (1972)
  101. C.M. Castilla, J.D. López-González, F. Rodríguez-Reinoso, I. Rodríguez-Ramos and A. Guerrero-Ruiz, *J. Catal.*, 107, 1 (1987)
  102. V.S. Boronin and O.M. Poltorak, *Zh. Fiz. Khim.*, 39, 1476 (1965), 40, 2671 (1966)
  103. (a) R. Van Hardeveld and A. Van Montfoort, *Surf. Sci.*, 4, 396 (1966)  
(b) R. Van Hardeveld and F. Hartog, *Surf. Sci.*, 15, 189 (1969)
  104. J.J. Burton, *Catal. Rev. Sci. Eng.*, 9, 209 (1974)
  105. H.R. Hoare and P. Pal
    - (a) *Nature Phys. Sci.*, 230, 5 (1971)
    - (b) *Phys.*, 20, 161 (1971)
    - (c) *Nature Phys. Sci.* 236, 35 (1972)
    - (d) *J. Cryst. Growth*, 17, 77 (1972)
  106. M.C. Desjonquères, M.B. Gordon and F. Cryot-Lackmann, *Surf. Sci.*, 68, 359 (1977)

107. M.C. Desjonquères, M.B. Gordon and F. Cryot-Lackmann, 1st Europ. Conf. Surf. Sci., E.C.O.S.S. 1, p.294, 1978
108. C. Kemball, Adv. Catal., 11, 223 (1959)
109. L. Guzzi and P.C. Ujszaszi, React. Kinet. Catal. Lett., 8, 489 (1978)
110. A. Frennet, Catal. Rev., 10, 37 (1974)
111. L.H. Dubois, L.L. Kesmodel and G.A. Somorjai, Chem. Phys. Lett., 56, 267 (1978)
112. L.H. Dubois, L.L. Kesmodel and G.A. Somorjai, J. Chem. Phys., 70, 2180 (1979)
113. D.G. Castner, B.A. Sexton and G.A. Somorjai, Surf. Sci., 71, 519 (1978)
114. L.H. Dubois and G.A. Somorjai, "Vibrational Spectroscopies Applied to the Characterisation of Adsorbed Species on Catalysts", ed. A.T. Bell and M.L. Hair, A.C.S. Symp. Ser., Washington, 1980
115. C.M. Friend, Ph.D. Thesis, University of California, Berkeley, 1981
116. D.I. Hagen, D.E. Nieuwenhuys, G. Rovida and G.A. Somorjai, Surf. Sci., 59, 155 (1976)
117. C. de la Cruz and N. Sheppard, J. Chem. Soc. Chem. Commun., 1854 (1987)
118. G. Shahid and N. Sheppard, Spectrochimica Acta, Vol. 46A, No.6, 999 (1990)
119. T.J. Campione and J.G. Ekerdt, J. Catal., 102, 64 (1986)
120. J.M. Griffiths, University of California, unpublished results
121. V. Ponc, "The Chemical Physics of Solid Surfaces and

- Heterogeneous Catalysis", ed. D.A King and D.P. Woodruff, Elsevier, Vol.4, p.391, 1982
122. K. Foger, "Catalysis Science and Technology", ed. J.R. Anderson and M. Boudart, Springer-Verlag, Vol.6, p.227, 1984
123. D.L. Trimm, "Design of Industrial Catalysts", Elsevier, p.91, 1980
124. F.A. Cotton and G. Wilkinson, "Advanced Inorganic Chemistry", John Wiley and Sons, 5th edition, 1988
125. B.C. Lippens and J.J. Steggeron, "Physical and Chemical Aspects of Adsorbents and Catalysts", London, New York Academic Press, p.171, 1970
126. G.M. Bell and K. Wefer, Alcoa Technical Paper, No.19, 1972
127. H. Hattori, T. Kotanigawa, K. Tanabe, M. Utiyama and M. Yamamoto, Appl. Catal., 1, 185 (1981)
128. H. Kirschner, Ber. dt. Ceram. Gesellschaft, 43, 479 (1966)
129. J.J. Fripiat, A.J. Leonard and P.N. Semaille, Proc. Brit. Ceram. Soc., 103 (1969)
130. C.N. Cochran and A.S. Russel, Ind. Eng. Chem., 42, 1336 (1950)
131. C. Okkerse, "Physical and Chemical Aspects of Adsorbents and Catalysts", London, New York Academic Press, p.213, 1970
132. R.K. Iler, "The Chemistry of Silica", Wiley-Interscience Publication, 1979
133. A.F. Wells, "Structural Inorganic Chemistry", 5th edition, Oxford Science Publication, p.569, 1984
134. G.C. Bond and R. Burch, "Catalysis", ed. G.C. Bond and G.

- Webb (Specialist Periodical Reports), The Royal Society of Chemistry, London, Vol.6, p.27, 1983
135. J.C. Kuriacose, *Ind. J. Chem.*, 5, 646 (1967)
136. E.S. Taylor, *Actes. Congr. Int. Catal.* 2nd, Vol.1, p.159 (1961)
137. S. Khoobiar, *J. Phys. Chem.*, 68, 411 (1964)
138. P.J. Lucchesi and J.H. Sinfelt, *J. Amer. Chem. Soc.*, 85, 3365 (1963)
139. G.C. Bond and P.A. Sermon, *J. Chem. Soc. Faraday Trans. I*, 76, 889 (1980)
140. J.E. Benson, M. Boudart and H.W. Kohn, *J. Catal.*, 5, 307 (1966)
141. W.C. Conner, G.M. Pajonk and S.J. Teichner, *Adv. Catal.*, 34, 1 (1986)
142. D.A. Dowden, "Catalysis", Vol.VIII, chapter 6, Chem. Soc., London, 1980
143. G.C. Bond and P.A. Sermon, *Catal. Rev.*, 8, 211 (1973)
144. J.A. Altham and G. Webb, *J. Catal.*, 18, 133 (1970)
145. E.V. Ballou, M. Boudart and J.A. Robell, *J. Phys. Chem.*, 68, 2748 (1964)
146. R. Kramer and M. Andre, *J. Catal.*, 58, 287 (1979)
147. G.C. Bond and P.A. Sermon, *J. Chem. Soc. Faraday Trans. I*, 72, 730 (1976)
148. J.E. Benson, M. Boudart and M.A. Vannice, *Z. Phys. Chem. (N.F.)*, 64, 171 (1969)
149. A.W. Aldag, M. Boudart and M.A. Vannice, *J. Catal.*, 18, 46 (1970)
150. M. Boudart and R.B. Levy, *J. Catal.*, 32, 304 (1974)

151. W.J. Ambs and M.M. Mitchell, *J. Catal.*, 82, 226 (1983)
152. G.C. Bond, "Spillover of Adsorbed Species", ed. J.E. Germain, G.M. Pajonk and S.J. Teichner, Elsevier, Amsterdam, 1983
153. J.A. Dumesic, T.F. Hayden and X.Z. Jiang, *J. Catal.*, 83, 168 (1983)
154. T. Huizinga and R. Prins, *J. Phys. Chem.*, 85, 2156 (1981)
155. D. Bianchi, G.E.E. Gardes, G.M. Pajonk and S.J. Teichner, *J. Catal.*, 38, 135 (1975)
156. W.C. Conner and D.H. Lenz, *J. Catal.*, 104, 288 (1987)
157. M. Lacroix, G.M. Pajonk and S.J. Teichner, *Bull. Soc. Chim. Fr.*, p.101 (1980)
158. D. Bianchi, M. Lacroix, G.M. Pajonk and S.J. Teichner, *J. Catal.*, 59, 467 (1979)
159. F. Wohler, *Philos. Mag.*, 66, 263 (1825)
160. J.J. Fripiat, *NATO ASI SER., SER.C*, 105, 471 (1983)
161. K.M. Sancier, *J. Catal.*, 23, 298 (1971)
162. M. Greenblatt, *Chem. Rev.*, 88, 31 (1988)
163. J.J. Birtill, P.G. Dickens and C.J. Wright, *J. Solid State Chem.*, 28, 185 (1979)
164. P.G. Dickens, T.K. Halstead and R.C.T. Slade, *J. Solid State Chem.*, 34, 183 (1980)
165. C. Ritter, R. Schölthorn and W. Müller-Warmuth, *J. Chem. Phys.*, 83, 6130 (1985)
166. J.J. Fripiat, D. Keravis, J.P. Marcq, G. Poncelet and X. Wispenninckx, *J. Catal.*, 73, 309 (1982)
167. P.G. Dickens, J.H. Moore and D.J. Nield, *J. Solid State Chem.*, 7, 241 (1973)

168. M. Boudart and H.W. Kohn, *Science*, 145, 149 (1964)
169. M. Lacroix, G.M. Pajonk and S.J. Teichner, *Bull. Soc. Chim., France*, 1981, I-87-93 and I-94-100
170. R. Benali, L. Hoang-Van and P. Vergnon, *Bull. Soc. Chim., France*, 417 (1985)
171. B.M. Glanville, S.D. Jackson, G.D. McLellan, R.B. Moyes, S. Simpson, G. Webb, P.B. Wells, R. Whyman and J. Willis, "Supported Metal Catalysts", Parts I-V, *J. Catal.*, in press
172. G.M. Bickle, J. Biswas and D.D. Do, *Appl. Catal.*, 36, 259 (1988)
173. G.J. Haughey, Ph.D., Glasgow University, 1987
174. J.H. Sinfelt, *Chem. Eng. Sci.* 23, 1181 (1968)
175. R.B. Anderson and P.K. Tsjeng, *The Canadian Journal of Chemical Engineering*, 54, 101 (1978)
176. W. Romanowski, "Highly Dispersed Metals as Adsorbents", Habled Press, John Wiley and Sons, p.171, 1987
177. F. Delannay, "Characterisation of Heterogeneous Catalysts", Marcel Dekker Inc., Ch.7, 1984
178. P. Flynn, P. Turner and S. Wanke, *J. Catal.*, 33, 233 (1974)
179. J. Freel, *J. Catal.*, 25, 139 (1972)
180. R.B. Anderson and J.C. Kempling, *Ind. Eng. Chem. Process. Des. Dev.*, 11, 146 (1972)
181. G.C. Bond and X. Yide, *J. Chem. Soc. Faraday Trans. I*, 80, 969 (1984)
182. R.B. Anderson and C.M Machiels, *J. Catal.*, 58, 253 (1979)